Molecular function of SEP domain adapters in VCP/p97 mediated protein unfolding

Inaugural-Dissertation

zur

Erlangung des Doktorgrades

Dr. rer. nat.

der Fakultät für

Biologie

an der

Universität Duisburg-Essen

vorgelegt von

Matthias Kracht

aus Köln

Februar 2021

Die der vorliegenden Arbeit zugrundeliegenden Experimente wurden in der Abteilung für Molekularbiologie I am Zentrum für Medizinische Biotechnologie der Universität Duisburg-Essen durchgeführt.

1. Gutachter: Prof. Dr. Hemmo Meyer

2. Gutachter: Prof. Dr. Peter Bayer

Vorsitzender des Prüfungsausschusses: Prof. Dr. Michael Ehrmann

Tag der mündlichen Prüfung: 10.05.2021

DOI: 10.17185/duepublico/74503
URN: urn:nbn:de:hbz:464-20210728-071443-4

Table of contents

Table of contents 3
List of figures 6
List of tables 8
Summary 9
Zusammenfassung 11
1 Introduction 13
1.1 AAA+ ATPases 13
1.2 The p97 protein 14
1.3 The role of p97 in degradative pathways 14
1.3.1 The ubiquitin-proteasome system (UPS) 15
1.3.2 ER-associated degradation (ERAD) 18
1.3.3 Ribosomal quality control 19
1.3.4 Role of p97 for mitochondrial homeostasis 20
1.3.5 Role of p97 in the endolysosomal system 21
1.3.6 Degradation of cytosolic proteins 22
1.4 Regulatory functions of p97 23
1.4.1 Role of p97 in regulation of chromatin associated processes 23
1.4.2 Role of p97 in post-mitotic golgi reassembly 24
1.5 p97 associated multisystem proteinopathy 26
1.6 p97 as a potential target for cancer treatment 27
1.7 Role of p97 in viral infections 27
1.8 The structure of p97 28
1.9 Interaction of p97 with adapters and cofactors 30
1.10 Specific adapter proteins of p97 32
1.10.1 The Ufd1-Npl4 adapter and mechanism of ubiquitin substrate translocation 32
1.10.2 The SEP domain adapter family 36
1.11 Protein Phosphatase 1 39
1.11.1 The SDS22-PP1-I3 complex 42
1.11.2 The SDS22-PP1-I3 complex is a target of p97 44
1.12 Aims of this thesis 46
2 Results 47

2.1 Establishment of a p97 unfolding assay for a ubiquitinated model substrate ... 47
2.2 Establishment of a p97 unfolding assay for the SDS-PP1-I3 complex 50
2.2.1 Effect of p97 concentration on the unfolding rate 53
2.2.2 Differential unfolding rate of p97 expressed in bacteria vs insect cells 54
2.3 Effect of different SEP domain adapters on the unfolding reaction 55
2.3.1 Effect of the p47 brake motif on the ATPase activity of p97 56
2.3.2 Effect of adapter concentration on the unfolding rate 57
2.4 Detailed dissection of differences between p37 and p47 for I3 unfolding associated with SPI disassembly 58
2.4.1 Analysis of the SHP-UBX linker 61
2.4.2 Binding of the SPI complex by p37 is dependent on the SHP-UBX linker . 63
2.5 Analysis of the importance of the N-terminal adapter region for SPI unfolding. 64
2.5.1 Effect of N-terminal truncations of p37 on the p97 unfolding rate 64
2.5.2 Identification of a conserved N-terminal helix in p37 65
2.5.3 The N-terminal helix affects binding of the SPI complex 67
2.5.4 The influence of N-terminal p37 mutations on substrate insertion 68
2.6 Analysis of the spatial orientation of the critical domains of p37 via crosslinks and mass spec 70
3 Discussion 74
3.1 Disassembly of the SPI complex by p97 and p37 involves unfolding of I3 74
3.2 SPI disassembly and I3 unfolding is ubiquitin-independent 75
3.3 Substrate recognition by p37 is multivalent 77
3.4 Stoichiometry of p97 and adapter in the unfolding reaction 80
3.5 A function of the adapter in substrate insertion? 81
3.6 Comparison of SEP domain adapters 82
3.7 Regulation of p97 by p47 84
3.8 Implications of our findings for the interpretation of p97 function and physiology 85
4 Materials and Methods 87
4.1 Materials 87
4.2 Methods 99
4.2.1 Molecular Cloning 99
4.2.2 Protein expression 107
4.2.3 Protein purification 109

4.2.4 Determination of protein concentration 113
4.2.5 Photoconversion of Eos 114
4.2.6 Ubiquitination 114
4.2.7 ATPase assay 114
4.2.8 Fluorescence-based unfolding assay 115
4.2.9 Immunoprecipitation 115
4.2.10 SDS-PAGE and Western-blot 116
4.2.11 Generation of the p97-p37 model 116
4.2.12 Crosslinking 117
4.2.13 Mass spectrometry 117
References 118
Abbreviations 130
Acknowledgements 133
Curriculum Vitae 134
Erklärungen 136

List of figures

Figure 1 The role of p97 in the ubiquitin-proteasome system (UPS). 15
Figure 2 Structure of the 26S proteasome unfolding a substrate based on cryo-electron microscopy 17
Figure 3 Schematic overview of key steps in endoplasmic reticulum associated degradation of misfolded glycoproteins in the ER lumen (ERAD-L) 19
Figure 4 Role of p97 in mitochondrial homeostasis 20
Figure 5 The ELDR-complex (endolysosomal damage response) consisting of p97, UBXD1, PLAA and YOD1 is crucial for the clearance of damaged lysosomes through lysophagy. 22
Figure 6 Removal of Ku70/80 from repaired DNA depends on p97 24
Figure 7 Domain structure of p97 29
Figure 8 Binding sited of p97 adapter proteins on the p97 N domain 31
Figure 9 Binding sites of p97 adapters at the C-terminal tail of p97 32
Figure 10 Structure and interactions of the yeast Ufd1-Npl4 heterodimer 32
Figure 11 Cryo-electron microscopy based structure of the slowly translocating Cdc48 mutant E588Q (Walker B in D2) together with Ufd1-Np4l in the process of unfolding a ubiquitin chain 34
Figure 12 Translocation of ubiquitin-Eos model substrate by Cdc48 35
Figure 13 Domain architecture and function of the SEP domain adapter proteins 36
Figure 14 Overview of selected binding sites of PP1 interactors 40
Figure 15 Structure of SDS22 bound to PP1 43
Figure 16 Model for the disassembly of the SDS22-PP1-I3 complex by p97-p37 46
Figure 17 Design and photoconversion of the ubiquitin-Eos model substrate 48
Figure 18 Purification of polyubiquitinated Ub^{n}-Eos substrate via gel filtration 49
Figure 19 Unfolding of the ubiquitinated model substrate by p97 and Ufd1-Npl4 50
Figure 20 Schematic describing the fluorescence unfolding assay for the SDS22PP1-mEos3.2-I3 substrate (SPEosI) 51
Figure 21 Purification of SDS22-PP1-His-Eos-I3 (SPEosI) complex from Sf9 cells 52
Figure 22 p97 together with unfolds Eos-I3 during SPI disassembly 53
Figure 23 Effect of p97 concentration on the initial unfolding rate 54
Figure 24 Comparison of SPEosI unfolding by p97 purified from E.coli (BL21) and insect cells (Sf9) 55
Figure 25 Effect of different SEP domain adapters on p97 mediated unfolding of Eos-I3 56
Figure 26 Mutation of the brake motif reduces p97 inhibition but does not support unfolding 57
Figure 27 Titration of p37 and UBXN2A adapter concentration 58
Figure 28 Overview of adapter domain swapping between p37 and p47 and the effect on the relative unfolding rate of p97 59
Figure 29 Unfolding of SPEosI by p97 and the different p37/p47 transplantation mutants 60

Figure 30 The p37 Linker region between the SHP-box and the UBX-domain is critical for unfolding 61
Figure 31 Division of the Linker sequence into Link1 and Link2 62
Figure 32 Inserting the Linker1 sequence from p37 into p47 enables unfolding 62
Figure 33 The linker is crucial for binding of the SPI complex by p37 63
Figure 34 Comparison of the structures of p37, p47 and UBXD4 64
Figure 35 Effect of N-terminal truncations of p37 on unfolding activity 65
Figure 36 The N-termini of p37, p47 and UBXN2A contain a conserved α-helix 66
Figure 37 Effect of helix mutation on the unfolding of SPEosI by p97 67
Figure 38 Co-immunoprecipitation analysis of PP1 show that the N-terminal truncations and the helix mutations affect the binding by p37 68
Figure 39 Crosslining of I3 in the D1 pore of p97 69
Figure 40 Generation of ^{p37pBpA} crosslinker mutants 70
Figure 41 Crosslinking of p37 BPA mutants with parts of the SPI complex and p97 72
Figure 42 Crosslinking mass spec identified two peptides from PP1 that crosslinked to $p37^{234pBp}$ 73
Figure 43 Additionally identified peptides between $p37^{182pBpa}$ and I3, respectively other $p37^{182pBpa}$ molecules in crosslinking mass spec 73
Figure 44 Crosslinks between a pBpA at position 278 of p97, close to the entrance of the central pore and p37. 79
Figure 45 Model for the interaction between the SPI-complex, the p37 adapter and p97 79

List of tables

Table 1: Buffers 87
Table 2: Plasmids 89
Table 3: Cells and Bacterial Strains 89
Table 4: Proteins 90
Table 5: Antibodies 92
Table 6: Media 93
Table 7: Reagents and chemicals 93
Table 8: Protein purification columns 95
Table 9: Laboratory appliances 96
Table 10: Cloning Reagents from New England Biolabs (NEB) 97
Table 11: Kits 97
Table 12: Proteases 98
Table 13: Filters, concentrators and cuvettes 98
Table 14 Pipetting scheme for PCR 99
Table 15 Thermocycle steps for PCR 99
Table 16 Gibson-assembly pipetting scheme 100
Table 17 Construct cloned by Gibson-assembly 101
Table 18: Site directed mutagenesis pipetting scheme 103
Table 19: Constructs cloned by site directed mutagenesis 103
Table 20: Restriction digest pipetting scheme 104
Table 21: Ligation pipetting scheme 105
Table 22: Constructs cloned by restriction digestion 106

Summary

The ATPase p97 (also known as VCP) is a member of family of AAA+ ATPases, a group of enzymes that form hexameric rings and unfold substrate proteins by ATP powered translocation through the central channel. The protein is highly conserved in metazoans, with homologues found in yeast (Cdc48) and flies (Ter94) and represents up to 1% of the total protein mass in the cell. Its main function is the extraction and subsequent unfolding of mostly ubiquitinated substrate proteins from membranes and protein complexes. In this capacity, p97 is an important factor in many cellular processes, including proteasomal degradation of misfolded proteins, clearance of cellular organelles via autophagy, cell cycle regulation and DNA repair. Substrate specificity is controlled by adapter proteins and cofactors that control substrate recruitment and p97 activity. Although up to 30 different proteins that interact with p97 in this manner have been identified, the exact mechanism by which these adapters facilitate substrate processing by p97 is only sufficiently understood for the Ufd1-Npl4 pair, which is the major adapter for polyubiquitinated substrates. Recent discoveries had identified the SDS22-PP1-I3 (SPI) complex, which forms during biogenesis of the phosphatase PP1, as a new substrate, whose disassembly by p97 together with the adapter p37 was not dependent on ubiquitination.

This thesis focused on the elucidation of the mechanism by which adapter proteins from the family of SEP domain containing proteins (p37, p47, UBXN2A, UBXN11) facilitate this process. We established a new *in vitro* fluorescence-unfolding assay that allowed us to determine that I3 is being unfolded by p97 during SPI complex disassembly. Further investigation on the function of p37 and the differences with the other three SEP domain proteins revealed that only UBXN2A was equally capable to support the unfolding reaction, while p97 remained inactive in the presence of p47 or UBXN11. Systematic exchange of protein domains between p37 and p47 showed that the inability of p47 to support unfolding was caused by a divergence in the sequence of a C-terminal linker region, which was found to be critical for binding of the SPI complex by p37. Furthermore, p47 impeded unfolding through inhibition of the ATPase activity of p97 by a “brake” motif in its N-terminal region.

Additional investigations into the N-terminal structure of p37 led to the identification of an amphipathic helix that was important for efficient unfolding. Using genetically encoded crosslinkers and mass spectrometry we could show that p37 recruits the SPI complex through a multivalent interface, which includes the N-terminal helix, the SEP domain and the C-terminal linker. This interaction involves binding of I3 by the N-terminus and the SEP domain of p37 close to the pore of p97, while the C-terminal linker of p37 binds to PP1 and positions at a distance from the pore. This primes I3 as the unfolding substrate of p97 and prevents unfolding of PP1. These results demonstrate the mechanism by which the SEP domain adapters direct unfolding of a non-ubiquitinated substrate of p97.

Zusammenfassung

Die ATPase p97 (auch als VCP bekannt) ist ein Mitglied der Familie der AAA+ ATPasen, einer Gruppe von Enzymen welche ringförmige Hexamere bilden und Substratproteine durch von ATP Hydrolyse getriebene Translokation durch die zentrale Pore entfalten. Das Protein ist in Metazoen hochkonserviert, mit Homologen welche in Hefen (Cdc48) und Fliegen (Ter94) vorkommen und macht bis zu 1% der gesamten Proteinmasse in einer Zelle aus. Seine Hauptfunktion ist die Extraktion und darauffolgende Entfaltung von meistens ubiquitinierten Substratproteinen aus Membranen und Proteinkomplexen. In dieser Funktion spielt p97 eine bedeutende Rolle für viele Zelluläre Prozesse, darunter der Abbau von fehlgefalteten Proteinen durch das Proteasom, der Abbau von Zellorganellen durch Autophagie, die Regulation des Zellzyklus und die DNA-Reparatur. Substrate Spezifität wird durch Adapter Proteine und Kofaktoren vermittelt, welche die Substrate Rekrutierung und die Aktivität von p97 kontrollieren. Obwohl bis zu 30 verschiedene Proteine, die mit p97 auf diese Weise interagieren, identifiziert worden sind, ist der genaue Mechanismus, durch den diese Adapter zur Prozessierung der Substrate durch p97 beitragen nur für das Adapterpaar Ufd1-Npl4 ausreichend verstanden. Ufd1-Npl4 ist der hauptsächliche Adapter für die polyubiquitinierte Substrate. Neueste Entdeckungen haben den SDS22-PP1-I3 (SPI) Komplex, welcher sich während der Biogenese von PP1 formt, als ein Substrat identifiziert, das von p97 zusammen mit dem Adapter p37 auseinandergenommen wird. Dieser Vorgang ist unabhängig von Ubiquitinierung.

Diese Arbeit behandelt die Aufklärung des Mechanismus durch den Adapterproteine aus der Familie der SEP-Domänen Adapter (p37, p47, UBXN2A, UBXN11) diesen Vorgang ermöglichen. Wir entwickelten einen neuen *in vitro* Fluoreszenz-Entfaltungsassay, durch den wir bestimmen konnten, dass I3 während des Auseinandernehmens des SPI-Komplexes durch p97 entfaltet wird. Weitere Untersuchungen der Funktion von p37 and der Unterschiede zu den anderen drei SEP-Domänen Adaptern zeigten, dass nur UBXN2A ebenfalls in der Lage ist die Entfaltung zu ermöglichen, während p97 in Gegenwart von p47 oder UBXN11 inaktiv bleibt. Durch systematischen Austausch von Proteindomänen zwischen p37 und p47 konnten wir das Unvermögen von p47 die Entfaltung zu unterstützen auf den Unterschied in der Sequenz eines Linkers in der C-

terminalen Region der Adapter zurückführen. Es zeigte sich, dass dieser Linker von entscheidender Bedeutung für die Bindung des SPI-Komplexes durch p37 ist. Weiterhin erschwert p47 die Entfaltung durch Inhibition der ATPase Aktivität von p97 mittels eines „Brems“ Motivs in der N-terminalen Region.

Zusätzliche Untersuchungen der Struktur der N-terminalen Region von p37 führten zur Identifikation einer amphipathischen Helix, welche für die effiziente Entfaltung wichtig ist. Durch den Einsatz von genetisch kodierten Crosslinkern und Massenspektrometrie konnten wir zeigen, dass p37 den SPI-Komplex mittels einer multivalenten Oberfläche bindet, die aus der N-terminalen Helix, der SEP-Domäne und dem C-terminalen Linker besteht. Diese Interaktion involviert die Bindung von I3 durch den N-terminus und die SEP-Domäne von p37 in geringem Abstand zur zentralen Pore von p97, während der C-terminale Linker PP1 bindet und auf Distanz zur Pore positioniert. Dies fördert die Entfaltung von I3 als dem Substrat von p97 und verhindert ungewolltes Entfalten von PP1. Diese Ergebnisse geben Aufschluss über den Mechanismus durch den die SEP-Domänen Adapter die zur Entfaltung von nicht-ubiquitinierten Substraten von p97 beitragen.

1 Introduction

Disassembly of protein complexes is a fundamental cellular process that regulates protein function and homeostasis. This is facilitated by enzymes that use the energy generated by ATP hydrolysis to extract and unfold target proteins from complexes or membrane. One such enzyme is the AAA+ ATPase p97/VCP, which relies on adapter proteins and cofactors for substrate interaction and processing. This thesis examines the molecular function of members of the SEP domain adapter protein family in the p97-dependent disassembly of the SDS22-PP1-I3 complex. The following chapter will at first give a brief introduction into the general role of the AAA+ ATPase p97 in the cell. Next, the structure of p97 and its interaction with adapter proteins and cofactors will be discussed, with a focus on adapters that are directly involved in protein unfolding by p97. The final part of the introduction will introduce the SDS22-PP1-I3 complex and its connection to p97 and proteins from the family of SEP domain adapters.

1.1 AAA+ ATPases

AAA+ ATPases (**A**TPases **a**ssociated with diverse cellular **a**ctivities) are a class of enzymes, which unfold or remodel substrate proteins through force generated by ATP hydrolysis. These enzymes are found in bacteria, archaea and eukaryotes and fulfill important functions in a large number of cellular processes (Snider et al., 2008) (Puchades et al., 2019). All AAA+ ATPases share a number of common features. The proteins assemble into functional hexamers, where each protomer contains a regulatory N-terminal domain and at least one ATPase domain. This αβα nucleotide-binding domain contains a nucleotide-binding motif (Walker A, also known as P-loop) and a ATPs hydrolysis motif (Walker B) (Snider et al., 2008), which control ATPase activity. An additional feature are aromatic pore loop residues that face towards the interior of the hexamer and push substrates through the central channel. AAA+ ATPases can be divided into four subgroups with different characteristics. Type I ATPases contain only one ATPase domain per protomer. This group contains proteins like VPS4, which is involved in the disassembly of ESCRT III complexes (Monroe et al., 2017), ATAD1 (Msp1 in yeast), which extracts wrongly inserted proteins from membranes (Wang et al., 2020), or Spastin, which is involved in microtubule regulation (Lumb et al., 2012). Type II ATPases, which contain an additional ATPase domain, include member like the N-ethylmaleimide-sensitive-factor

(NSF) that disassembles SNARE protein complexes during membrane fusion (White et al., 2018), p97 (Cdc48 in yeast) which will be the focus of this thesis, the archaeal protein VAT, a homologue of p97 (Golbik et al., 1999), or the peroxisomal ATPase Pex1/Pex6 (Gardner et al., 2018). Members of the type III AAA+ ATPases function as heat shock proteins, like the bacterial protein ClpB or its eukaryotic homologue Hsp104 (DeSantis and Shorter, 2012). Finally, type IV AAA+ ATPases couple the ATPase activity with proteasomal activity. This group includes proteins such as the mitochondrial protein Yme1 (Puchades et al., 2017). A similar arrangement is also present in the 26S proteasome, where the 20S core particle contains the degradative proteases, while the 19S regulatory particle includes AAA+ ATPase domains that feed substrates into the core (Budenholzer et al., 2017).

1.2 The p97 protein

The AAA+ ATPase p97, which is also known as valosin containing protein (VCP), is a highly conserved protein, with homologues like Cdc48 in yeast, or TER94 (transition endoplasmic reticulum ATPase) in flies. Like other AAA+ ATPases, p97 functions as a molecular engine, powered by ATP hydrolysis, which applies force to substrates to extract them from protein complexes or membrane compartments and unfolds them in the process. Substrate recruitment is mediated by a number (~30) of different adapter proteins and cofactors proteins that control cellular localization, substrate binding and unfolding. The protein is important for several degradative and regulative processes in the cell, ranging from proteasomal degradation, autophagy, DNA repair and cell cycle regulation. Due to its role in protein homeostasis and DNA repair, p97 has been investigated as a potential drug target for cancer therapy. Disease mutations in p97 result in a number of muscular and neurological defects that are subsumed under the name Multisystem proteinopathy 1 (MSP1).

In the following section I will give an overview of the different functions of p97, starting with its role in degradative processes and then discussing its role in regulation.

1.3 The role of p97 in degradative pathways

The p97 protein plays a major role in processes that lead to the degradation misfolded proteins, stalled translation products or damaged organelles. The following paragraphs will give an overview of the role of p97 in the ubiquitin proteasome system (UPS), in ER-

associated degradation (ERAD), maintenance of mitochondrial homeostasis, ribosomal quality control (RQC) and the endolysosomal system.

1.3.1 The ubiquitin-proteasome system (UPS)

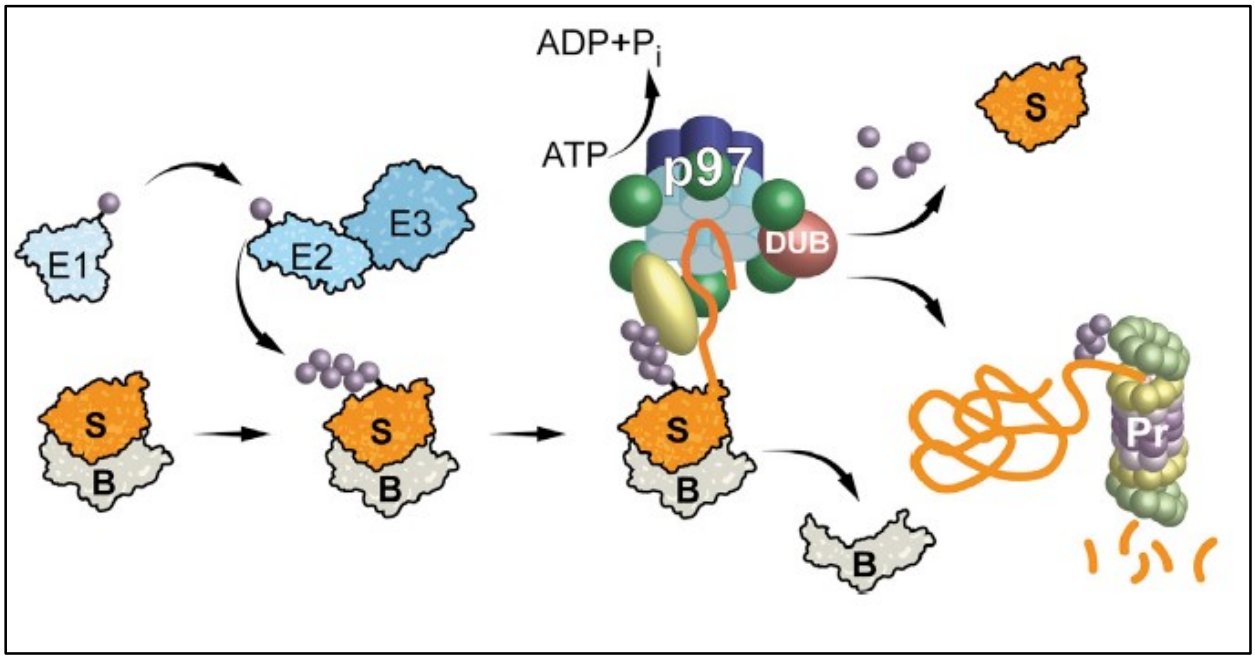

Figure 1: The role of p97 in the ubiquitin-proteasome system (UPS). Substrate proteins (S) are modified with ubiquitin by the interaction of E1 (ubiquitin activating enzymes), E2 (ubiquitin conjugating enzymes) and E3 (ubiquitin ligases) enzymes. The polyubiquitinated substrate is recognized by p97 via an adapter protein and unfolded, which leads to dissociation from its binding partner (B). After unfolding is complete, the ubiquitin chain can be removed by an deubiquitinating enzyme (DUB), which leads to refolding of the substrate or the unfolded substrate is further degraded by the proteasome (Pr) *(van den Boom and Meyer, 2017)*.

The majority of known substrates of p97 are ubiquitinated. Ubiquitin is the small 8.5 kDa large protein ubiquitin, serving as a universal marker for protein degradation. Substrates destined for degradation are modified the formation of a covalent peptide bond between the carboxyl group on the C-terminus of ubiquitin and a lysine residue on the substrate. The ubiquitin can in turn itself be modified by another ubiquitin on one of its 7 lysine residues (K6, K11, K27, K29, K33, K48, K63) or the N-terminal amino group (M1), which leads to the formation of long ubiquitin chains on the target, which are characterized by the specific lysine connection. The formation of the covalent peptide bond is the result of three different enzymes called E1-ubiquitin activation enzyme, E2-ubiquitin conjugating enzyme and E3-ubiquitin ligase. At first, the E1 enzyme forms catalyzes the adenylation

of the ubiquitin C-terminus by hydrolyzing ATP apart into AMP and pyrophosphate, which renders the C-terminus susceptible to a nucleophilic attack by a cysteine residue on the E1 enzyme, leading to the formation of a covalent thioester bond between ubiquitin and the E1. Next, the ubiquitin is transferred from the E1 onto the cysteine of an E2-ubiquiting conjugating enzyme. The E2 enzyme in turn in forms a complex with an E3-ubiquitin ligase, which recruits the target protein and transfers the ubiquitin onto a lysine residue on the target protein. This hierarchical system consists of only one type of E1, several dozen different E2 who control the type of ubiquitin linkage and hundreds of different E3 who are responsible for substrate selection (Komander and Rape, 2012). Chain specificity is the result of the interactions between E2, E3 and substrate that can be classified into three categories. In the case of RING-type E3 ligases, linkage specificity is controlled by the E2, while the E3 binds the E2 through its RING domain and serfs as substrate recruitment factor. HECT domain E3 ligases are charged by the E2 on a catalytic cysteine residue and then transfer this ubiquitin to the substrate, thereby controlling chain specificity. RBR (Ring-in-between-Ring) E3 ligases represent a hybrid between the other two cases, where the E3 binds an E2 via its RING domain, is charged with ubiquitin and then transfers the ubiquitin to the substrate (Komander and Rape, 2012). The resulting type of ubiquitin chain or mono-ubiquitination determines the fate of the substrate protein. While mixed or branched chains have been observed (Meyer and Rape, 2014), their function is not as well understood as that of pure linkage type chains. Mono-ubiquitination affects substrate localization, for example controlling the nuclear export of p53 (Li et al., 2003) or sorting of cargo proteins into multivesicular bodies (Stringer and Piper, 2011). The K63 linkage has regulatory functions, for example in the activation of Nf-κB (Chen and Chen, 2013). Substrates bearing K48 chains are destined to be degraded by the proteasome (Ye and Rape, 2009).

The 26S proteaseome is a large ~ 2.5 MDa multiprotein complex that is responsible for the degradation of the majority of proteins in eucaryotic cells (Budenholzer et al., 2017). It can be divided into the 20S degradative core particle (CP) that forms a barrel like structure and one or two 19S regulatory particles (RP) which can bind to either end of the core. The core particle consists of four stacked heptameric rings. The two adjacent inner rings are made up of seven β-subunits that are responsible for the proteolytic activity of the core (Kunjappu and Hochstrasser, 2014). These are flanked by two rings made up of

α-subunits that control acces to the central core (Groll et al., 2000). The regulatory particle can be further subdivided into a base and a lid. The base is stacked on top of the core particle and consist of three ubiquitin binding domains and a hexameric AAA+ ATPase complex that unfolds substrates and feeds them into the central chamber. Similar to other AAA+ ATPases, the proteasomal ATPase subunits (Rpt1-6) assume a staircase-conformation when unfolding a substrate (Peña et al., 2018). The lid contains a total of nine different subunits that control proteasome activity (Lasker et al., 2012). Importantly, the Rpn11 metalloprotease functions as a deubiquitinating enzyme (DUB) that trims the ubiquitin chain before the substrate is degraded.

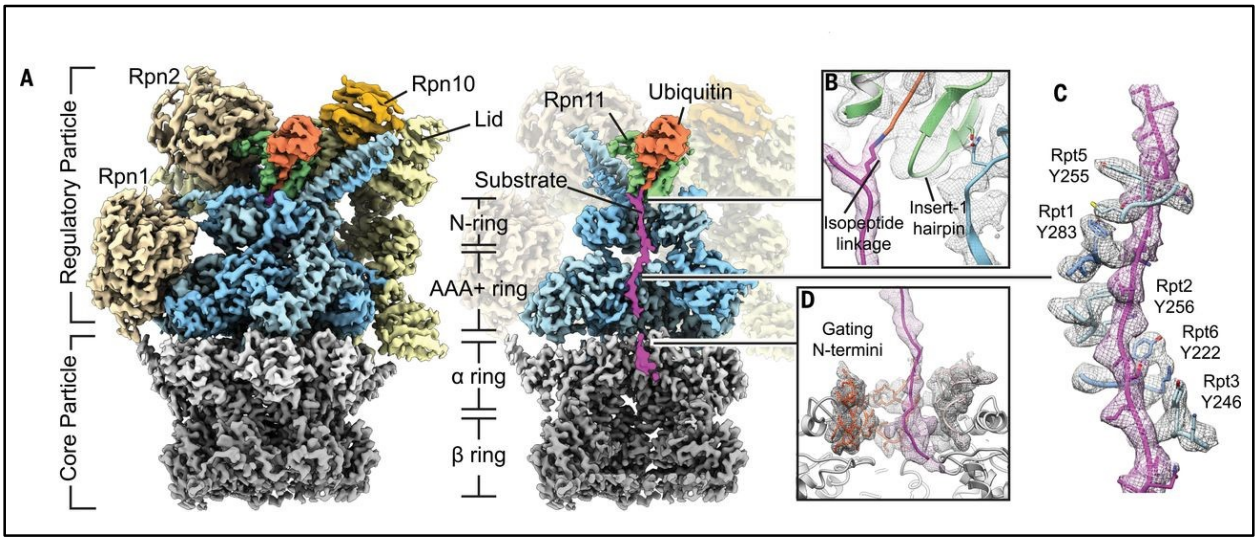

Figure 2: Structure of the 26S proteasome unfolding a substrate based on cryo-electron microscopy *(Peña et al., 2018)*. Only one half of the entire proteasome complex is shown. **A** Overview of the core particle (in grey) and the regulatory particle (in color), consisting of the base (blue) including the ATPase domains, the lid (yellow/light brown) and the DUB Rpn11 (green). The complex is in the process of unfolding a ubiquitinated substrate (purple). One still folded ubiquitin (orange) is bound by Rpn11. **B** Zoom on the isopeptide linkage connecting the substrate and its ubiquitin chain, which is bound by Rpn11. **C** Staircase arrangement of the Rpt1-6 ATPase subunits around the substrate. **D** Zoom on the entry of the substrate into the α-ring of the core particle.

Although the proteasome includes its own AAA+ ATPase, it is dependent on p97 to process a subset of its substrates, (van den Boom and Meyer, 2017). A primary reason for the necessity of p97 for proteasomal function is the need to extract substrates from complex structures that are not directly accessible by the proteasome. This includes the retrotranslocation of misfolded ER proteins during endoplasmic reticulum associated degradation (ERAD) (Olzmann et al., 2013), the extraction of aberrant translation products

from stalled ribosomes (Brandman and Hegde, 2016) or the removal of DNA binding proteins after successful DNA repair (van den Boom et al., 2016). In addition, unfolding by p97 generates unstructured tails which are required for substrate recognition by the proteasome. This was demonstrated by Beskow et al. *in vivo* and by Olszewski et al. *in vitro* using polyubiquitinated fluorescent reporter proteins (Beskow et al., 2009), (Olszewski et al., 2019). Permanent quenching of the substrate fluorescent caused by proteasomal degradation was dependent on either the activity of p97 or the addition of an unstructured region to the substrate sequence.

1.3.2 ER-associated degradation (ERAD)

One of the major and best studied functions of p97 is its role in maintaining ER homeostasis by contributing to the degradation of misfolded ER proteins. The lack of UPS components in the lumen of the ER necessitates the retrotranslocation into the cytosol for subsequent degradation by the proteasome. This process has been mostly studied in yeast, but most of the components have been found to also exist in higher eukaryotes (Wu and Rapoport, 2018). Depending on the type of ER substrate, the following steps can be classified as ERAD-L, ERAD-M or ERAD-C. ERAD-L describes the extraction of proteins that are misfolded inside the ER lumen. ERAD-M deals with ER membrane bound substrates that are misfolded inside the membrane. ERAD-C deals with substrates that stretch across the ER membrane and are misfolded at the cytosolic side. The degradation of ERAD-L substrates is described in the following paragraph. After being directly released into the ER from ribosomes during biosynthesis, most of these proteins are heavily glycosylated with mannose, glucose and N-acetyl glucosamine (Olzmann et al., 2013). Failure to fold, results in the binding of the misfolded protein by the lectin Os9 (Yos9 in yeast) and the chaperone BiP. This leads to association of the misfolded substrate a translocon complex at the ER membrane consisting of multiple proteins including, Derlin1, HERP and the E3 ligase complex Hrd1 (Christianson and Ye, 2014). Alternative E3 ligases are gp78 in mammals or Doa10 for ERAD-M and ERAD-C substrates in yeast (Schmidt et al., 2020). Once the misfolded substrate is ubiquitinated it needs to be removed from the ER membrane. The p97 (Cdc48 in yeast) protein is recruited to the ER membrane by several cofactors including UBXD8 (Suzuki et al., 2012) and VIMP (Ye et

al., 2005). The AAA+ ATPase then extracts the ubiquitinated substrate from the ER membrane into the cytosol with the help of the adapter proteins Ufd1-Npl4 (Ye et al., 2003). This process is thought to involve translocation of the substrate through the p97 pore and concomitant trimming of the substrate ubiquitination by a p97 bound deubiquitinating enzyme (DUB), based on data from *in vitro* experiments (Bodnar and Rapoport, 2017). Post extraction, the misfolded protein is bound by the BAG6 chaperone and reubiquitinated by the E3 ligase RNF126, followed by its final degradation by the proteasome (Hu et al., 2020).

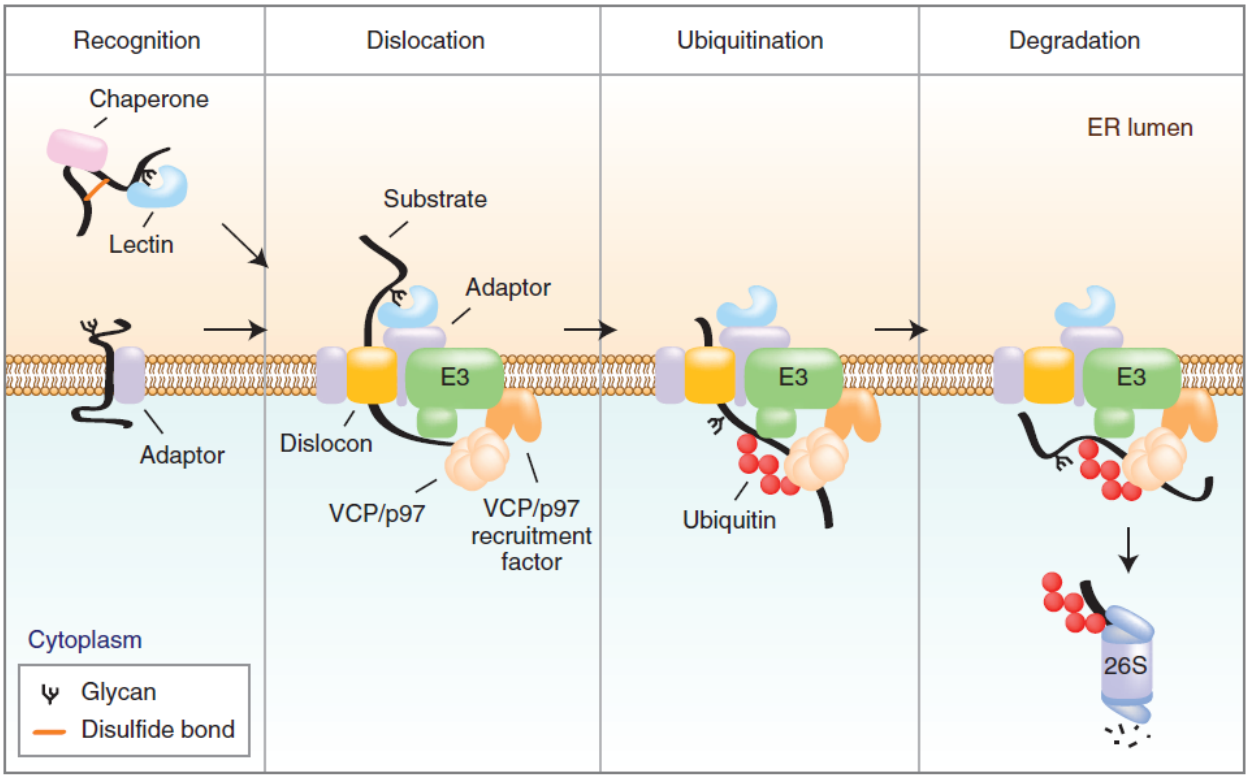

Figure 3: Schematic overview of key steps in endoplasmic reticulum associated degradation of misfolded glycoproteins in the ER lumen (ERAD-L) *(Olzmann et al., 2013)*. Substrates are first recognized by lectins and chaperones and recruited to the dislocon complex at the ER membrane. There, the substrate is ubiquitinated by E3 ligases and subsequently extracted from the ER by the AAA+ ATPase p97. The substrate is finally degraded by the 26S proteasome in the cytosol.

1.3.3 Ribosomal quality control

In addition to the clearance of misfolded proteins, p97 is also involved in the removal of stalled ribosomes. These defective complexes can arise through missing stop codons that

lead to stalling of the polypeptide chain, either because the mRNA sequence reaches its end or because of an accumulation of polylysine caused by translation of the poly-A tail that interacts with the negatively charged exit tunnel of the ribosome (Lu and Deutsch, 2008). The stalling is detected by the GTPase Hbs1 and the endonuclease Pelota (Dom34 in yeast) that recruit the ATPase ABCE1 (Rli1 in yeast), which leads to disassembly of the ribosome into it 40s and 60s subunits and the release of the mRNA (Brandman and Hegde, 2016). The exposed interior interface of the 60s ribosomal subunit is bound by NEMF (Rqc2 in yeast) that recruits the E3 ligase Listerin (Ltn1 in yeast), which ubiquitinates the stalled peptide (Bengtson and Joazeiro, 2010). The peptide chain is then extracted from the 60s ribosomal subunit by p97 together with the adapters Ufd1-Npl4 (Verma et al., 2013).

1.3.4 Role of p97 for mitochondrial homeostasis

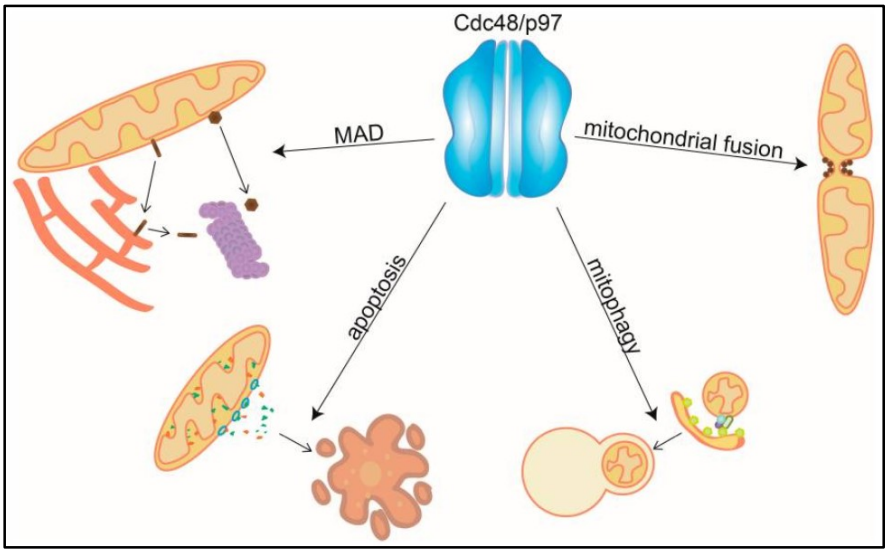

Figure 4: Role of p97 in mitochondrial homeostasis (Escobar-Henriques and Anton, 2020).

Mitochondria are vital for cellular survival, providing essential metabolic functions through oxidative phosphorylation and the citric acid cycle. In addition, they form storage hubs for signaling factors such as reactive oxygen species (ROS) and calcium ions. Mitochondrial homeostasis is affected by p97 through several mechanisms. Misfolded mitochondrial proteins in the outer mitochondrial membrane (OMM) are ubiquitinated and extracted by p97-Ufd1-Npl4 in a process called mitochondria associated degradation (MAD) that

shares similarities to ERAD (Heo et al., 2010). In addition, p97 is involved in the regulation of mitochondrial fusion, which is controlled by mitofusin GTPases (Mfn1/Mfn2 in mammals, Fzo1 in yeast). In yeast, fusion activity of Fzo1 is regulated by the opposing activity of the two deubiquitinating enzymes (DUBs) Ubp2 and Ubp12, which are themselves targets of E3 ligases and thereby subject to p97 dependent degradation (Simões et al., 2018). Mitofusins are also direct targets of p97 during autophagic clearance of damaged mitochondria. Damage to the mitochondria causes membrane depolarization, which leads to ubiquitination of Mfn1 and Mfn2 by the E3 ligase Parkin that is activated by the kinase PINK1 (Escobar-Henriques and Anton, 2020). Extraction from the OMM by p97-Ufd1-Npl4 and subsequent degradation of the Mfn1 and Mfn2 is required for mitophagy to proceed (McLelland et al., 2018).

1.3.5 Role of p97 in the endolysosomal system

The endolysosomal system facilitates the uptake and transport of extracellular cargo, as well as degradation of cellular organelles through the autophagic machinery (Repnik et al., 2013). Molecules and particles are taken into the cell through vesicles called endosomes that fuse with lysosomes, which leads to degradation or release of their cargo. The p97 ATPase has been identified as a factor that functions in several parts of this system. One specific type of endocytosis, caveolae-mediated endocytosis, involves the internalization of cargo through lipid raft rich invaginations in the plasma membrane that are called caveolae, which contain the protein caveolin-1 (Pelkmans et al., 2004). Sorting of caveolin-1 into endosomes is dependent on ubiquitination, as well as p97 and its cofactor UBXD1 (Ritz et al., 2011), (Kirchner et al., 2013).

In addition, p97 has been shown to play a role in the clearance of damaged lysosomes. Lysosomes that are damaged by exogenous chemicals, reactive oxygen species (ROS), protein aggregates or pathogens, can be repaired by the ESCRT machinery (Skowyra et al., 2018),(Radulovic et al., 2018). However, if the damage to the lysosomal membrane is too severe, the organelles can be resolved by the autophagic machinery of the cell, a process called lysophagy (Papadopoulos et al., 2017). The damaged lysosome is decorated with K63 and K48 ubiquitin chains, which leads to the recruitment of p97 together with the adapters UBXD1 and PLAA and the deubiquitinase YOD1, the so called

ELDR-complex (**E**ndo**l**ysosomal **d**amage **r**esponse). This complex removes K48 modified substrates from the damaged lysosomes, which is a necessary step before autophagosome formation and engulfment of the damaged lysosome.

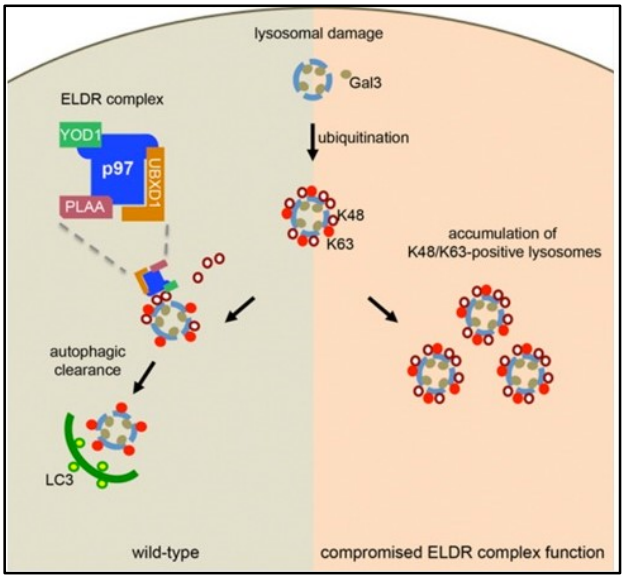

Figure 5: The ELDR-complex (endolysosomal damage response) consisting of p97, UBXD1, PLAA and YOD1 is crucial for the clearance of damaged lysosomes through lysophagy. Ruptures in the lyosomal membrane induced by chemicals or pathogens lead to ubiquitination of substrates on lysosomes with K48 and K63 chains. The ELDR-complex is recruited to the damaged lysosomes and removes K48 ubiquitinated substrates. If this removal is successful, the damaged lysosome is engulfed by a phagophore and cleared by autophagy. A defective ELDR-complex causes accumulation of damaged lysosomes. *(Papadopoulos et al., 2017)*.

1.3.6 Degradation of cytosolic proteins

In addition to organelle specific degradation, p97 is also involved in the clearance of cytosolic targets. For example, unassembled soluble proteins that contain exposed hydrophobic residues are ubiquitinated by the E3 ligase HUWE1, which leads to the recruitment of p97 through Ufd1-Npl4 followed by proteasomal degradation (Xu et al., 2016). Aggregation of cytosolic proteins, which can be caused by an overflow of the UPS or through proteins with polyglutamine tracts, is cleared through aggresome formation, which is dependent on p97 and HDAC6 (Ju et al., 2008).

1.4 Regulatory functions of p97

In addition to its role in the clearance of damaged and misfolded substrates, p97 is also involved in the regulation of signaling pathways, by facilitating the unfolding and subsequent degradation of specific substrates. For example, activation of the Nf-κB pathway, a key regulator of inflammation and immune response, depends on the degradation of the IκBα, which binds Nf-κB in the cytosol and prevents its translocation to the nucleus. Upon ubiquitination by the E3 ligase $SCF^{\beta Trcp}$, IκBα is unfolded by p97 and degraded by the proteasome, which allows Nf-κB to translocate to the nucleus and function as a transcription factor (Li et al., 2014). Another regulatory function of p97 is the turnover of constitutive repressor of eIF2α phosphorylation (CReP), a regulator of the integrated stress response (Hülsmann et al., 2018). CReP (also PPP1R15B) is a regulatory subunit of the protein phosphatase γ (PP1C) that dephosphorylates eIF2α under basal conditions and prevents activation of the ISR. Under specific stress conditions (UV light, arsenite) CReP is ubiquitinated by $SCF^{\beta Trcp}$, unfolded by p97 and degraded by the proteasome, which leads to accumulation of phosphorylated eIF2α and activation of the ISR (Hülsmann et al., 2018). Another substrate of p97 is the enzyme glutamine synthase, which is ubiquitinated by the E3 ligase $CRL4^{CRBN}$ (cereblon) in a glutamine dependent feedback mechanism (Nguyen et al., 2017). Glutamine synthase is then unfolded by p97 together with Ufd1-Npl4 and degraded by the proteasome.

1.4.1 Role of p97 in regulation of chromatin associated processes

Several proteins that are involved in cell cycle progression are also regulated by p97. DNA damage induces phosphorylation of Cdc25a by the Chk1 kinase, which causes ubiquitination of Cdc25a by $SCF^{\beta Trcp}$. Unfolding by p97-Ufd1-Npl4 and degradation by the proteasome causes G2/M arrest of the cell cycle (Riemer et al., 2014). Another factor involved in regulation of mitosis that is a target of p97 is the kinase Aurora B, which together with surviving and INCENP regulates chromosome segregation and cytokinesis. At the end of mitosis, p97-Ufd1-Npl4 extracts ubiquitinated Aurora B from chromatin, which results in chromatin decondensation and nuclear envelope formation (Ramadan et al., 2007), (Dobrynin et al., 2011).

Other regulatory functions of p97 include the extraction of DNA bound proteins that are involved in DNA replication or DNA repair. After replication termination, the CMG helicase

complex needs to be removed from chromatin. This process is initiated by the extraction of the MCM7 subunit by p97-Ufd1-Npl4, after K48 ubiquitination by the E3 ligase $CRL2^{Lrr1}$ (Dewar et al., 2017), (Moreno et al., 2014). Extraction of MCM7 by p97 is also found in the repair of interstrand crosslinks (ICLs) which block replication, in a process that unlike replication termination is dependent on BRCA1 (Fullbright et al., 2016), (Semlow et al., 2016). A substrate of p97 during DNA double strand repair is the Ku70/Ku80 protein. Upon fragmentation of DNA strands by ionizing irradiation, the loose ends are bound by the Ku70/Ku80 heterodimer, which forms a double ring structure that wraps around the exposed ends of the DNA double strand break and locks the repair pathway into non-homologous end joining (NHEJ) and precludes homologous recombination (HR). After strand repair the Ku70/Ku80 rings can no longer dissociate from the DNA by themselves and are ubiquitinated and removed by p97 together with Ufd1-Npl4 (van den Boom et al., 2016).

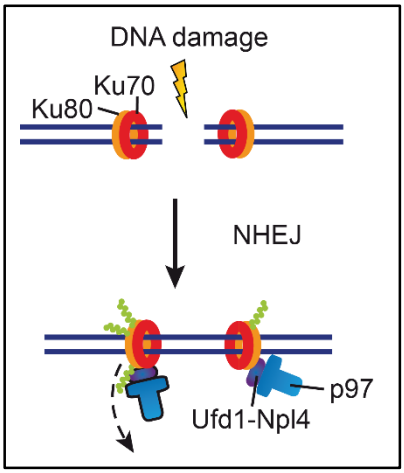

Figure 6: Removal of Ku70/80 from repaired DNA depends on p97. After a DNA double strand break (for example caused by UV light) the exposed ends are bound by the Ku70/80 heterodimer. p97 together with the adapter pair Ufd1-Npl4 removes polyubiquitinated Ku 70/80 from repaired DNA after DNA repair through non-homologous end joining (NHEJ) (adapted from van den Boom et al., 2016).

1.4.2 Role of p97 in post-mitotic golgi reassembly

At the beginning of mitosis, the golgi apparatus is broken down and reassembled after separation into two daughter cells. The reassembly of the golgi membrane has been shown to depend on the activity of p97 and several of its cofactors (Meyer, 2005). Both

the p47 and the p37 adapter are involved in this process, albeit with different functions. While the p97-p47 dependent mechanisms in golgi reassembly requires the activity of the p97 cofactor and deubiquitinating enzyme VCIP135, the p97-p37 mechanisms seems to function independent of ubiquitination (Meyer et al., 1998), (Zhang and Wang, 2015). The p97-p37 complex is also important for the reassembly of the ER (Uchiyama et al., 2006)

1.5 p97 associated multisystem proteinopathy

Several mutations in the *vcp* gene have been shown to be connected to a number of different pathologies, which are collectively called IBMPFD/ALS, short for inclusion body myopathy, paget's disease of the bone, frontotemporal dementia and amytrophic lateral sclerosis (Watts et al., 2004). The majority of the mutations responsible for these effects are located in close proximity to the linker that connects the N-domain with the D1 domain(Meyer and Weihl, 2014). How these mutations lead to the aforementioned pathologies is not clearly understood. In vitro experiments with p97 disease mutants have shown higher ATPase activity for most of the disease mutants as well as slightly higher unfolding rates for some of them (Blythe et al., 2019). The increase in unfolding activity points to a gain of function as the cause of the disease, which is supported by the observation that p97 inhibitors alleviate disease symptoms in *Drosophila*, such as mitochondrial defects caused by dysregulation of mitofusins by hyperactive p97 (Zhang et al., 2017). However, it is unclear if the increase in unfolding rate is solely responsible for the disease phenotype. The in vitro experiments used homomeric hexamers, where every protomer carries the same mutation. While in vitro studies with mixed hexamers (resembling heterozygous patients) also showed an increase in the ATPase rate compared to fully wild type p97, the effect was significantly weaker than with fully mutated hexamers (Blythe et al., 2019). NMR studies have shown that disease mutant protomers have a higher propensity to have the N-domain in the up-conformation independent of the nucleotide state, compared to the wild type (Huang et al., 2019a). In addition, they showed that neighboring protomers influence each other's N-domain state. Using methyl TROSY they could also show that the binding of the UBXD1 adapter to p97 is reduced in R95G protomers due to the change in N-domain conformation. Based on these findings, Huang et al. speculated that the disease mutants cause a dysregulation in the ability of adapters to bind to p97, where some adapters bind significantly tighter compared to p97 wild type, while the interaction with other adapters is significantly weakened. Thereby, the pathologies would be a result of perturbed adapter interactions.

1.6 p97 as a potential target for cancer treatment

Cancer cells experience an upregulation in pathways regulating protein homeostasis in order to cope with the increase in unregulated protein synthesis. This presents a potential target for cancer therapy, because inhibition of said pathways, would affect cancer cells more strongly than healthy cells. An example of this strategy is the proteasome inhibitor bortezomib, which is used to treat multiple myeloma. Since p97 is an important part of the protein homeostasis system of the cell upstream of the proteasome, it represents an additional target for this strategy. Several p97 inhibitors haven been developed that impede its function. These inhibitors can be separated into those that directly inhibit the ATPase activity of the D2 domain, such as DBeQ and CB-5083, those that inhibit p97 via an allosteric mechanism, such as NMS-873, UPCDC30245 and MSC1094308. Additionally, there are covalent inhibitors like Eeyarestatin I and NMS-859. Out of these inhibitors, CB-5083 came furthest in clinical trials, but had to be abandoned due to severe offtarget effects (Tang et al., 2019). Recently, the anti-alcohol abuse medication disulfiram has come into focus as a cancer treatment (Skrott et al., 2017). This effect was traced back to a copper binding metabolite of disulfiram that shuttled copper ions preferably into cancer cells. Further studies showed that copper ions (Cu^{+2}) bound to the zinc-finger domain of Npl4 and blocked interaction with p97, thereby severely compromising p97 dependent protein homeostasis (Pan et al., 2021).

1.7 Role of p97 in viral infections

Studies have found evidence that p97 is important for replication of several viruses (Arita et al., 2012) (Lin et al., 2017),. (Carissimo et al., 2019). While inhibiton of p97 with a chemical inhibitor did not prevent viral entry, it appeared to compromise replication of the viral genome and membrane trafficking. In addition, p97 is known to be utilized by viruses to degrade MHC class I molecules through ERAD, before they can reach the cell membrane and trigger an immune response (Ye et al., 2001). The outbreak of the novel coronavirus SARS-CoV-2/COVID-19 has renewed interest in p97 as a factor in viral infections, since previous work on related coronaviruses had shown that p97 inhibition compromised maturation of virus-loaded endosomes (Wong et al., 2015). A recent study showed that the p97 inhibitor NMS-873 inhibited Sars-CoV-2 replication at low nanomolar concentration (Bojkova et al., 2020).

1.8 The structure of p97

The p97 protomer has a length of 806 amino acids and contains three distinct domains. These are the N-, D1- and D2-domain from N- to C-terminus. The N-domain (aa 1-187) serves as the major interaction site for most adapters and interactors of p97. It can be further divided into two subdomains, one double Ψ β-barrel (Nn, residues 21–106) and a four-stranded β-barrel (Nc, residues 107–187). The D1 domain is connected to the N-domain though a short linker (188-207) (Xia et al., 2016), (Buchberger et al., 2015). Both ATPase domains (D1 and D2) contain a Walker A and Walker B motif for nucleotide binding and hydrolysis, as well as an asparagine and an arginine residue that assist in ATP hydrolysis (Buchberger et al., 2015). Depending on the type of nucleotide bound by the D1 domain, the N-domain is either oriented coplanar to the D1-domain (ADP bound state) or flipped upwards by about 38 Å compared to the D1-domain (ATP bound state) (Xia et al., 2016). A second small linker (459-480) connects the D1 and D2 ATPase domains. After the D2-domain follows an unstructured C-terminal tail (762-806) which is important for the interaction with a few other adapters that do not bind to the N-domain (Buchberger et al., 2015). The D2 domain is responsible for the majority of the ATPase activity of p97 and is thought to be the main driver of substrate unfolding, while the D1 domain is important for hexamer formation (Xia et al., 2016).

Substrate translocation by p97 involves engagement of target proteins by adapter proteins bound close to the N-domain, which guide the substrate into the central pore, were it is translocated and exits at the D2 domain (Twomey et al., 2019a). Contrary to related AAA+ ATPases like VAT, p97 lacks aromatic pore loop residues in the D1 domain. These pore loop residues are thought to be responsible for pushing the substrate downward through the pore of an AAA+ ATPase (Puchades et al., 2019). Concomitant removal of the N-domains and mutation of the D1 to include aromatic pore loops lead to a mutant of p97 (ΔND1YY) that was capable to unfold YFP-ssrA, a model substrate for VAT (Rothballer et al., 2007). This might be the result of the “activated” D1 domain nonspecifically engaging the substrate. In the native p97, the lack of pore loops in the D1 domain necessitates the function of an adapter protein or cofactor to facilitate substrate engagement.

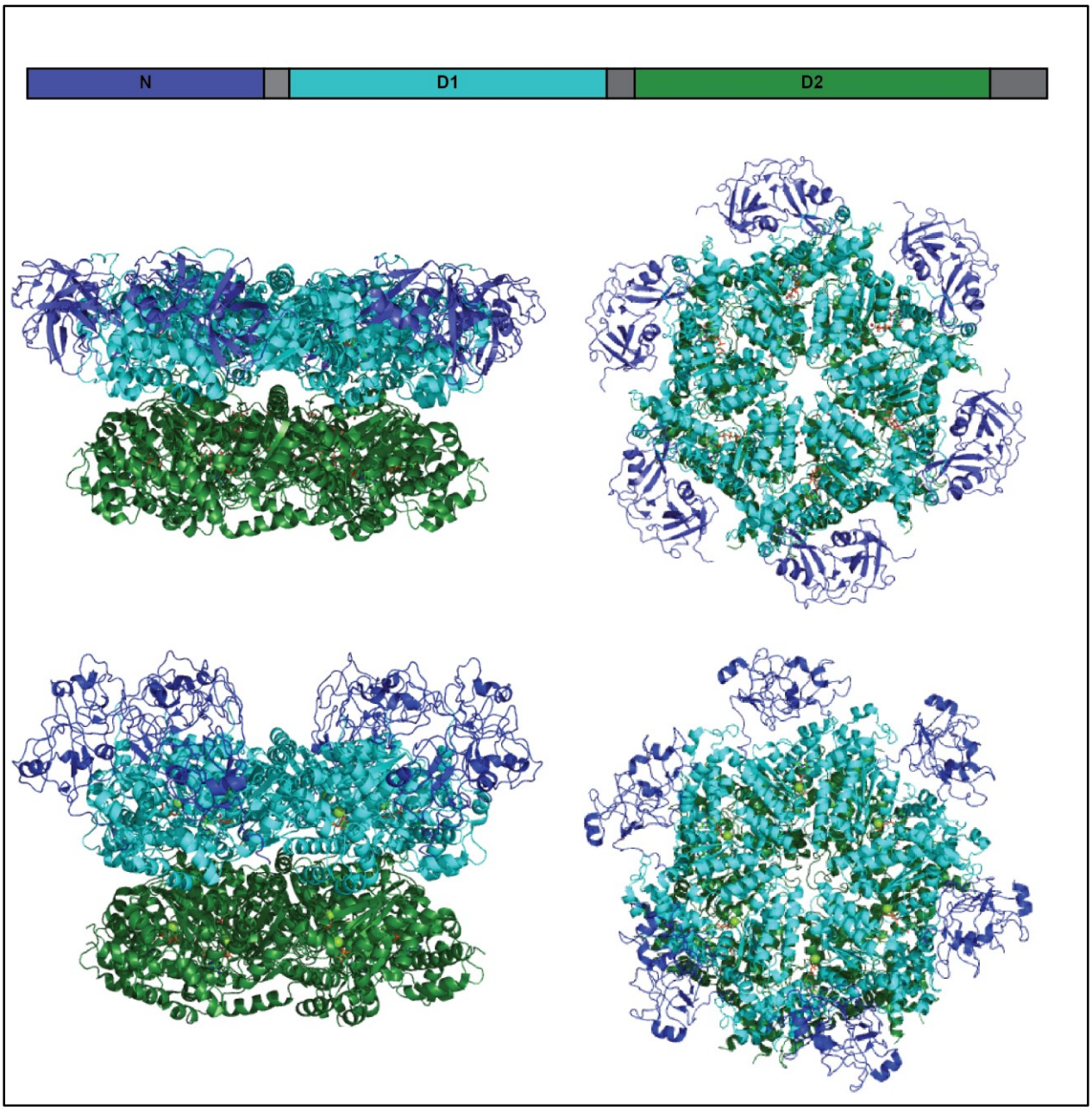

Figure 7: Domain structure of p97. The p97 protomer consist of an N-terminal N-domain (blue), and two ATPase domains D1 (cyan) and D2 (green). These are connected by two linkers (N-D1 and D1-D2) and followed by an unstructured C-terminus. Six p97 protomers assemble into a helix, where the ATPase domains form a pore, while the N-domain position is either coplanar to the D1 domain (ADP) or flipped upwards (ATP) depending on the nucleotide bound in the D1 domain. Structures based on pdb 5ftk (ADP bound, visible residues: 21-763) and 5ftn (ATPγS bound, visible residues: 12-768) *(Banerjee et al., 2016)*.

1.9 Interaction of p97 with adapters and cofactors

The diversity of processes in which p97 is involved is a result of the large number of p97 adapter proteins and cofactors which mediate the interaction with specific substrates. In total there are about 30 different proteins with known p97 interaction sites. Most of these proteins interact with the N-domain of p97, while a few also bind to the C-terminus. The main interaction motifs with the N-domain are the UBX-domain (ubiquitin regulatory x), the SHP box, the VIM and VBM, while interactions with the C-terminus are mediated through a PUB or PUL domain. The UBX-domain has a high structural similarity to ubiquitin and interacts with the N-domain of p97, by inserting into the hydrophobic cleft formed by the two parts of the N-domain. The VIM (vcp interacting motif) also interacts with p97 at this position. The second major interaction site for adapters of p97 on the N-domain is with adapters that carry a SHP box. The SHP box is a short 14-15 amino acid long sequence which binds to a site of the Nc-domain of p97. Since both the UBX-domain and the VIM bind to the same region on the p97 N-domain, competing adapters cannot bind on the protomer. A smaller subset of adapters including PNGase and PLAA bind to the C-terminal tail of p97 (Buchberger et al., 2015), (Xia et al., 2016).

The p97 interacting proteins can be divided into adapter proteins that directly facilitate substrate binding by p97 and regulatory cofactors that assist indirectly substrate processing, for example by recruiting p97 to a specific cellular location (e.g. UBXD8 recruits p97 to the ER membrane), functioning as a deubiquitinating enzyme (YOD1, VCIP135) or substrate processing factors such as PNGase (Zhao et al., 2007) or the yeast E4 enzyme Ufd2 (Rumpf and Jentsch, 2006), which adds further ubiquitin chains to the substrates. Only Ufd1-Npl4 and the SEP domain proteins p47 and p37 have been so far identified as genuine adapter proteins.

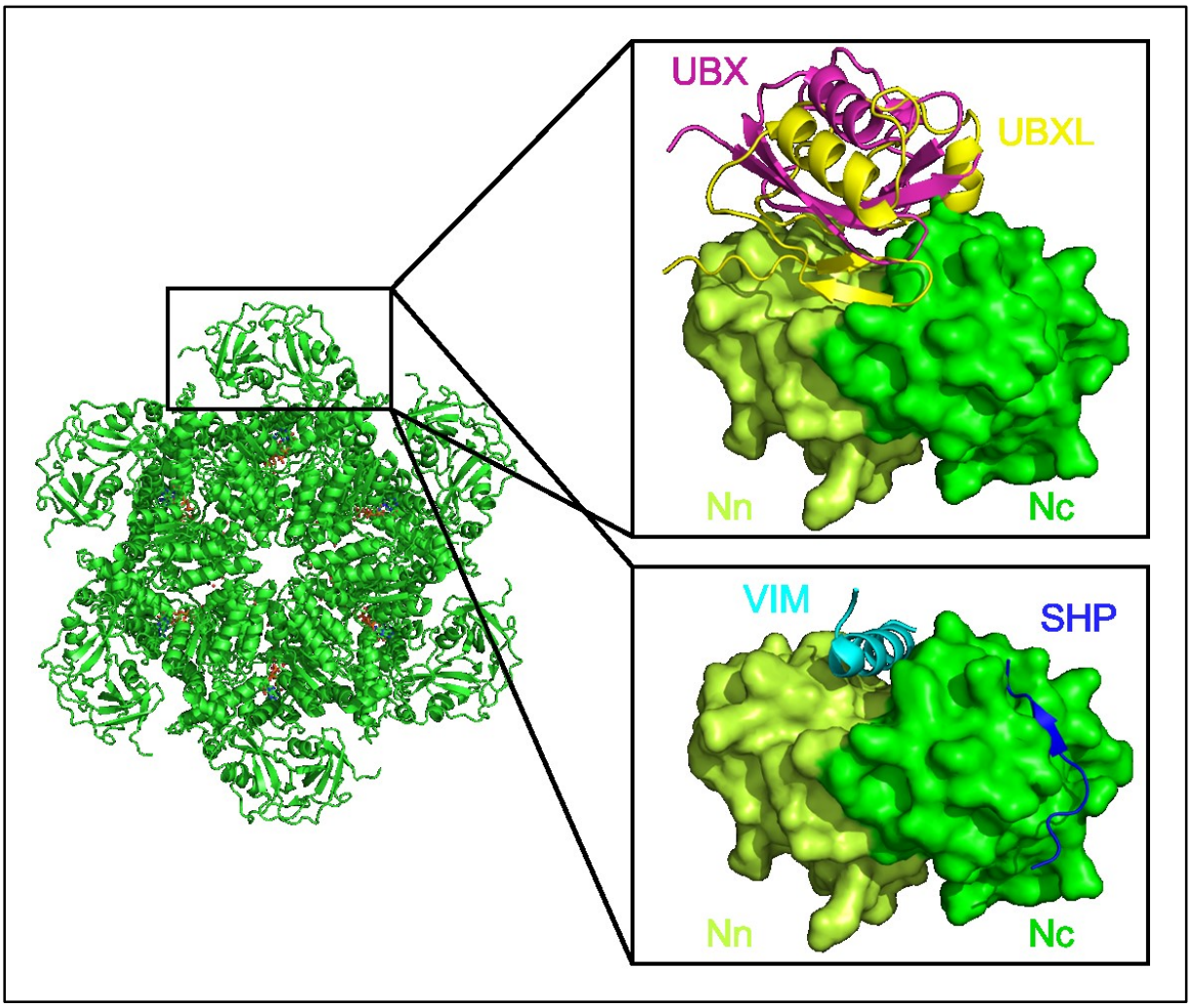

Figure 8: Binding sited of p97 adapter proteins on the p97 N domain. Left: orientation of the N-domain of p97 in the down conformation (PDB: 5FTK) with one N-domain marked with a black box. Right: Binding sites of the UBX of FAF1 (PDB: 3QQ8, purple), UBXL of NPL4 (PDB: 2PJH, yellow), VIM of gp78 (PDB 3TIW, cyan), and SHP of Ufd1 (PDB: 5C1B, blue) bound to the N-domain of p97 (PDB: 5C1B, Nn in limegreen, Nc in green).

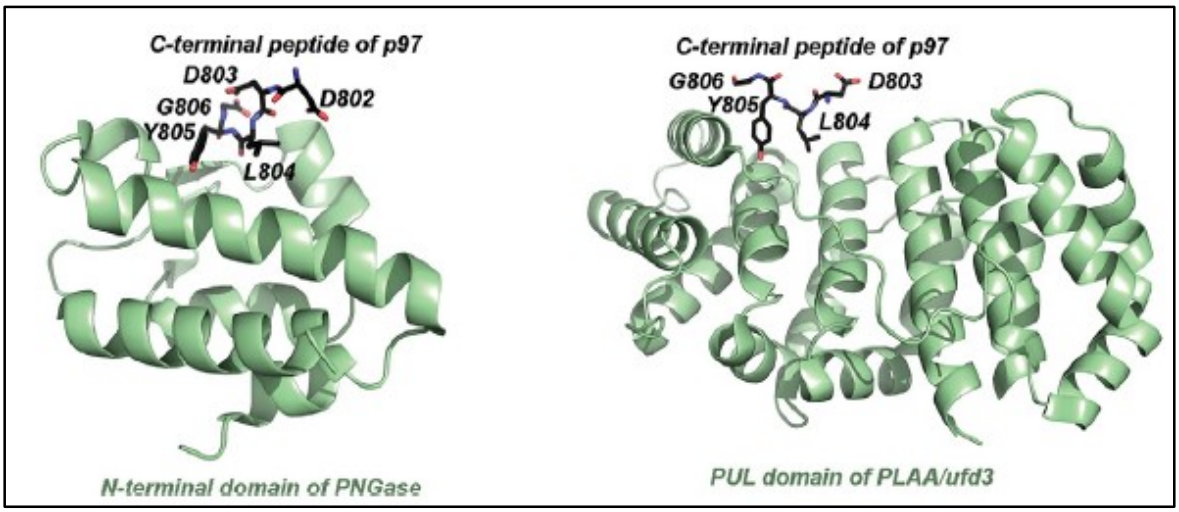

Figure 9: Binding sites of p97 adapters at the C-terminal tail of p97 (*Xia et al., 2016*). Left: interaction of the cofactor PNGase with the C-terminal peptide of p97. Right: interaction of the PUL domain of PLAA with the C-terminal peptide of p97.

1.10 Specific adapter proteins of p97

1.10.1 The Ufd1-Npl4 adapter and mechanism of ubiquitin substrate translocation

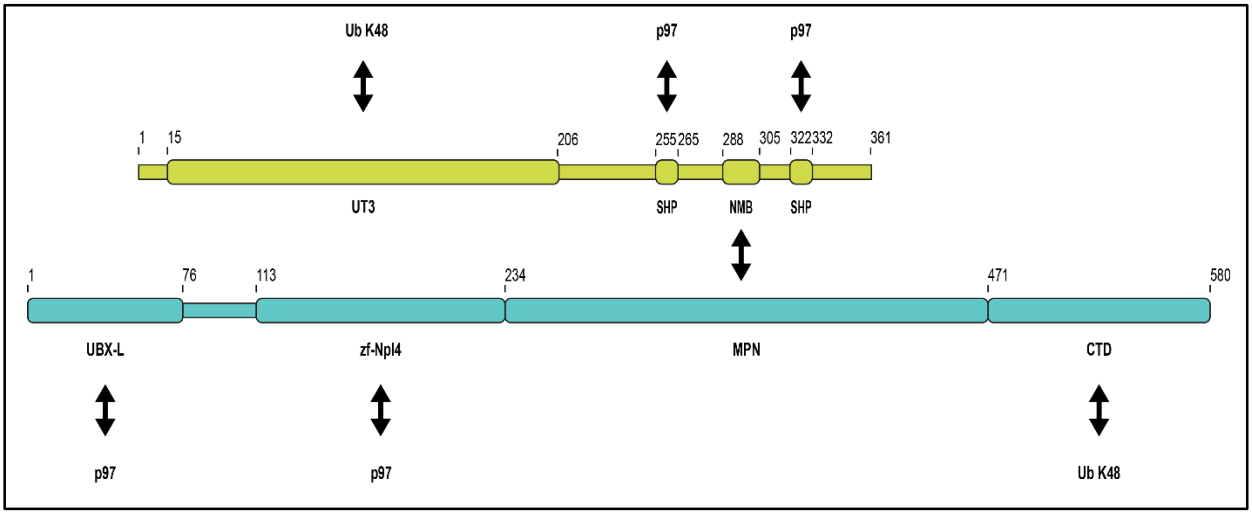

Figure 10: Structure and interactions of the yeast Ufd1-Npl4 heterodimer. Ufd1-Npl4 bind to each other via the interaction of the NMB domain in Ufd1 with the MPN domain in Npl4. The adapter pair binds to p97 via the UBX-L domain and the zinc-finger domain in the N-terminus of Npl4 and two SHP boxes in the C-terminus of Ufd1. K48 linked ubiquitin chains are recognized via the UT3 domain of Ufd1 and the C-terminal domain of Npl4.

The best understood adapter of p97 is the heterodimer of Ufd1 and Npl4. This adapter pair is the major adapter for processes involving ubiquitinated substrates. Its main function is the recruitment of ubiquitinated substrates to p97. Npl4 contains an N-terminal UBXL

domain which binds to N-domain of p97. This is followed by a zinc-finger domain (zf-Npl4), a MNP-domain (Mpr1/Pad1 N-terminal) and a C-terminal domain (CTD). The metazoan Npl4 also includes a NZF domain at the C-terminus, which binds ubiquitin indiscriminate of the chain type. The yeast variant lacks this C-terminal NZF domain and specifically binds to K48 linked ubiquitin via its MPN-domain and CTD. Ufd1 consists of a UT3 domain in its N-terminal part responsible for binding of K48 linked Ub chains and a UT6 segment in its C-terminal part that includes two SHP boxes for binding two p97 (SHP1 and SHP2) and an NMB sequence which binds the MPN-domain of Npl4.

As the major adapter protein for processing of ubiquitinated substrates by p97, several studies have investigated the role of Ufd1-Npl4 in the unfolding mechanisms of p97 (Bodnar and Rapoport, 2017), (Blythe et al., 2017). These studies were successful in reconstituting p97-Ufd1-Npl4 mediated unfolding of a ubiquitin substrate *in vitro* by fusing a fluorescent reporter protein to an N-terminal ubiquitinated degron. This provided the loss of fluorescence upon unfolding by p97-Ufd1-Npl4 as a readout for unfolding activity. By combining this experimental strategy with a FtsH protease that was fused to the C-terminus of Cdc48, the Rapoport group could show that unfolding of the ubiquitin substrate involved translocation through the central pore (Bodnar and Rapoport, 2017). In addition, they observed that a minimum of five ubiquitin modifications on the substrate were required to be recruited and unfolded by p97-Ufd1-Npl4. Furthermore, complete translocation and subsequent release required the trimming of the substrate ubiquitin chain by a DUB.

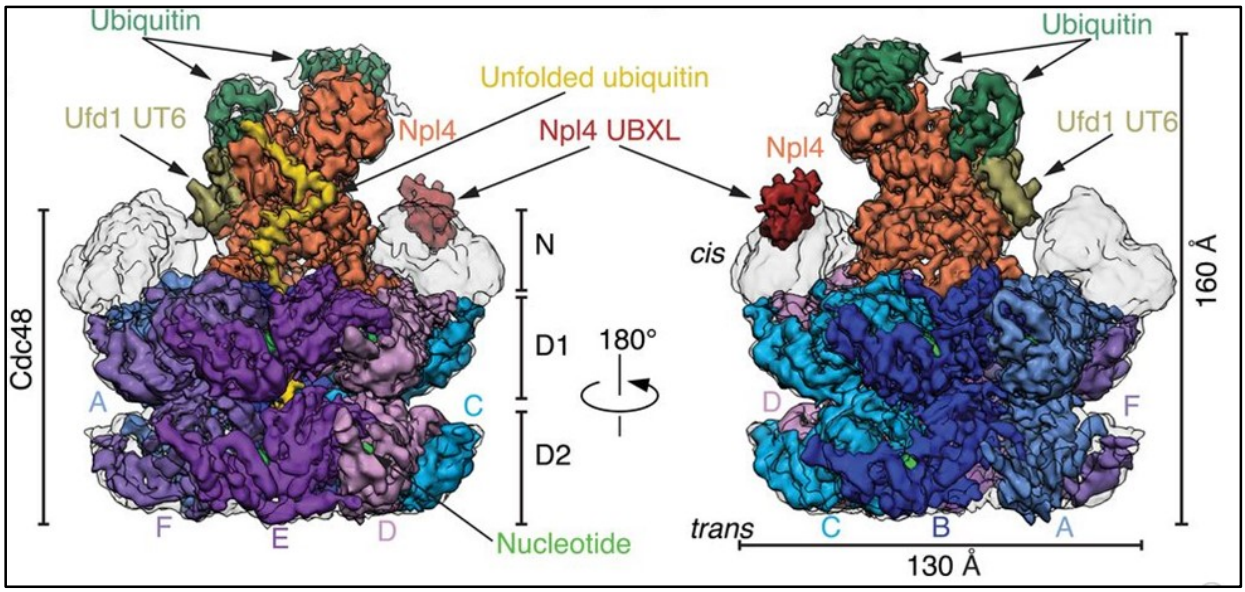

Figure 11: Cryo-electron microscopy-based structure of the slowly translocating Cdc48 mutant E588Q (Walker B in D2) together with Ufd1-Np4l in the process of unfolding a ubiquitin chain (yellow) (Twomey et al., 2019). Npl4 (orange) sits on top of the Cdc48 hexamer and guides an unfolded ubiquitin chain (yellow) into the central pore. The two proximate ubiquitins in the chain that are still folded (green) are bound to the backside of Npl4. The N-domains (white) of Cdc48 are positioned in the up conformation and with one of them bound by the UBXL domain of Npl4 (red). Only a small part of the UT6 region of Ufd1 (brown) was resolved in this structure, bound to Npl4 and in close proximity to the N-domain of one Cdc48 protomer. The D1 and D2 domains of the six Cdc48 protomers (A-F) are shown in different shades of blue/purple, with bound nucleotides in green.

The first structure of Cdc48, the yeast homologue of p97, in the process of unfolding a ubiquitin substrate was published by Twomey at al. in 2019. They analyzed the structure of Cdc48 in complex with the yeast Ufd1-Npl4 adapter pair, unfolding a polyubiquitinated model substrate by cryo-EM (Twomey et al., 2019a). The resulting structure showed Npl4 sitting on top of Cdc48 bound to the ubiquitin chain that was fed into the pore of p97. The structure included a two folded ubiquitins (Ub1 and Ub2) bound to backside of Npl4. In addition, the proximal ubiquitin (Ub1) was connected to an unfolded polypeptide chain, that stretched along Npl4 into the central pore of Cdc48, which was identified as unfolded ubiquitin. This unfolded chain consisted of two linear elements which were connected by a kink in the center of the Npl4 groove. Twomey et al. further investigated the importance of the interaction between Npl4 and the unfolded ubiquitin stretch, by systematically mutating residues in the Npl4 groove. The effect of these mutations ranged from a mild reduction in unfolding activity compared to wild type Npl4, to an almost complete

abrogation of unfolding, underscoring the importance of the Npl4 groove for substrate unfolding.

The threading of the substrate through the pore of p97, is proposed to be function in a hand over mechanism, where the p97 protomers are oriented in a staircase conformation, where ATP hydrolysis in the D2-domain of the lowest protomer in the staircase causes the protomer to shift upwards and reassociate with the substrate at the top position after binding of ATP. This movement causes the aromatic pore loops to push the substrate in the central pore downwards, which results in substrate translocation.

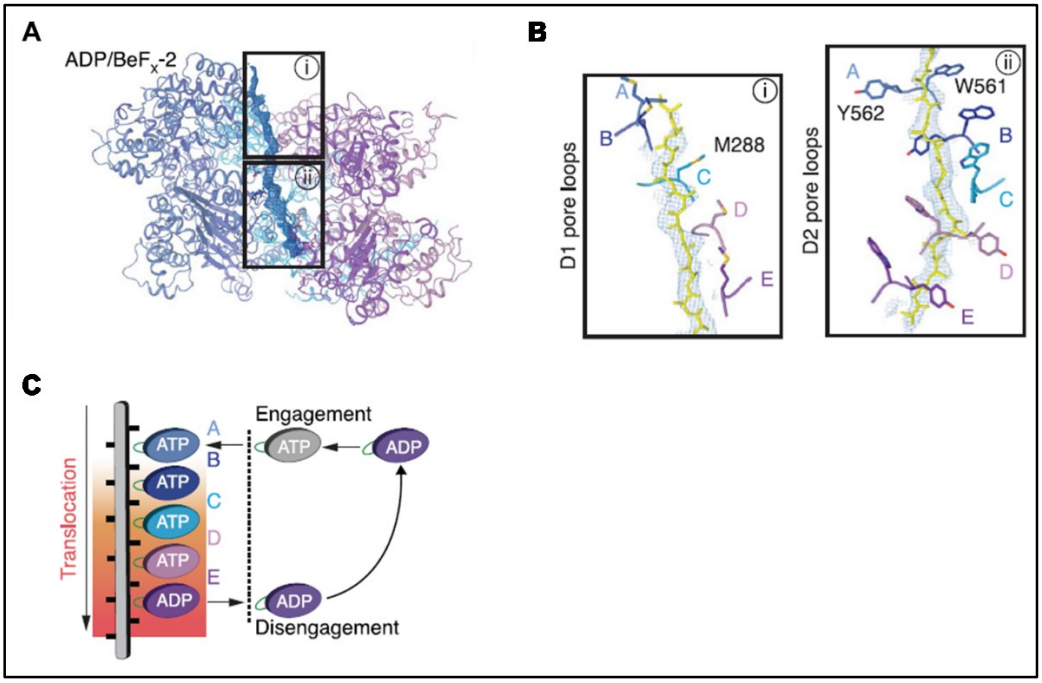

Figure 12: Translocation of ubiquitin-Eos model substrate by Cdc48 (Twomey et al., 2019). **A** Structure based on a ADP/BeF structure of Cdc48 in complex with (yeast) Ufd1-Npl4 and the Ub-Eos3.2 substrate. **B** Positioning of the pore loops of the six Cdc48 protomers in D1 and D2 domain. **C** ATP hydrolysis causes the respective protomer to disengage from the substrate. The protomer then reattaches to the substrate at the top of the stair case after ADP is replaced by ATP, which results in a downward movement of the substrate relative to the p97 hexamer.

1.10.2 The SEP domain adapter family

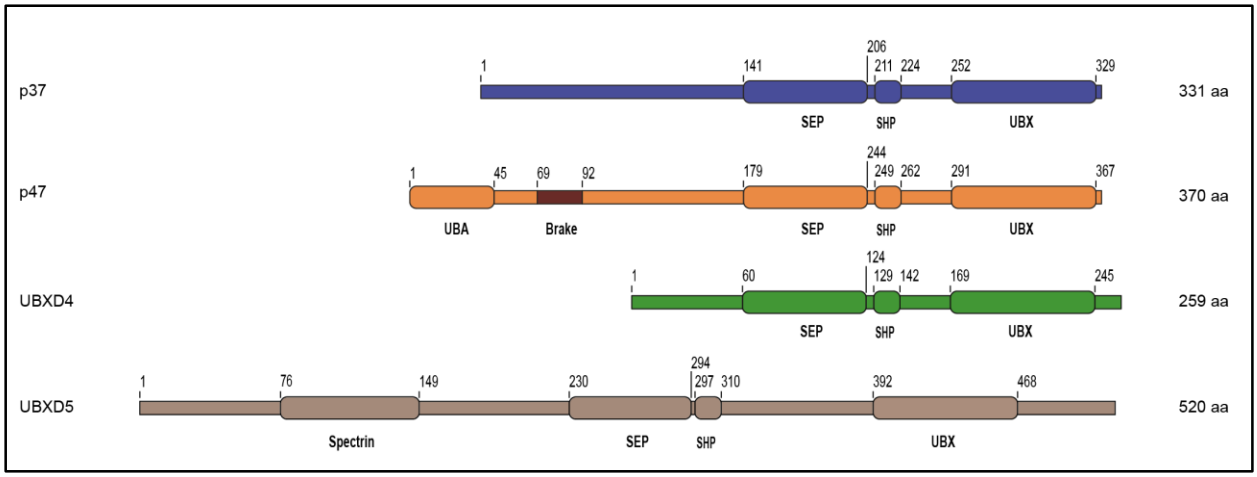

Figure 13: Domain architecture and function of the SEP domain adapter proteins. UBA = "ubiquitin-associated domain" (ubiquitin binding), Brake = inhibits the ATPase activity of p97 when bound by p47, SEP = "Shp1, eyc and p47" (potential substrate binding site), SHP = binding of p97, UBX = "ubiquitin regulatory X" (binding of p97), Spectrin = interaction with the cytoskeleton.

The SEP domain adapter protein family share a similar arrangement of protein domains in the C-terminal half of the proteins. The characteristic SEP domain (the name is derived from the proteins **S**hp1 (homologue of p47 in yeast), **e**yc (homologue of p47 in flies) and **p**47, where this domain was first identified), is situated at the center of the protein, followed by a SHP-box and a UBX-domain for p97 binding, interspaced by short linker sequences (Dreveny et al., 2004). In humans there are four different SEP domain proteins p47, p37, UBXN2A and UBXN11. Other species harbor only one SEP domain protein, for example the yeast Shp1 (homologue of p47) or UBXN-2 in worms (homologue of p37). While all four human SEP domain proteins share similar domain arrangement in the C-terminal part, the N-terminal sequences show significant differences.

The oligomeric state of the SEP domain adapters has been under debate, because both p37 and p47 run at higher apparent molecular sizes in gel filtration (Kondo et al., 1997), (Zhang et al., 2015). Crosslinking experiments with p47 pointed towards a the formation of trimers, which was dependent on the SEP domain (Yuan et al., 2004). Further studies by the group of Tsui-Fen Chou suggested a connection between the oligomerization state of p47 and the inhibitory effect of p47 on the p97 ATPase activity, where trimerization at higher concentrations of p47 reduces the inhibitory effect (Zhang et al., 2015). However, it is unclear if trimerization is also relevant for substrate processing by p97 since these

observations were based on the “idle” activity of p97 and not while p97 was actively unfolding a substate.

The p47 (also called NSFL1C) adapter was the first identified adapter protein of p97 (Kondo et al., 1997). In addition to the SEP-SHP-UBX domains it includes a ubiquitin binding UBA domain at the N-terminus that is connected to the SEP domain via a long unstructured linker. In contrast to Ufd1-Npl4, which mediates binding of polyubiquitinated substrates, the UBA domain of p47 preferably binds monoubiquitinated substrates (Meyer et al., 2002). The protein cooperates with p97 in membrane fusion and post mitotic ER and golgi stack reassembly (Kondo et al., 1997), by mediating the interaction between p97 and the SNARE complex protein syntaxin 5 (Rabouille et al., 1998). Surprisingly, p47 was found to inhibit the ATPase activity of p97 by around 75% (Meyer et al., 1998). This inhibitory effect is caused by a “brake” motif in the linker between the UBA domain and the SEP domain of p47, between residues 69-92 (Zhang et al., 2015). Disassembly of the p97/p47/syntaxin 5 complex depends on the additional activity of the DUB VCIP135 (Uchiyama et al., 2002). Other studies have implicated a role for p47 in dendritic arborization in neurons (Wang et al., 2018). The next most similar member of the SEP domain protein family in humans is the protein p37, which is slightly shorter than p47 (331 vs 370 amino acids). In contrast to p47, the N-terminus of p37 does not contain an UBA domain for ubiquitin binding or a brake motif that inhibits ATPase activity. Instead, binding of p37 to p97 increases the ATPase activity of p97 (Zhang et al., 2015). Like p47, p37 has been found to function in the reassembly of the ER and golgi apparatus after mitosis. Of note, while the function of p47 in this process was dependent on the activity of the DUB VCIP135 (Wang et al., 2004), the function of p37, which lacks an UBA domain, was dependent on the presence, but not the activity of VCIP135, suggesting a potentially ubiquitin-independent role. Instead of syntaxin 5, the p97-p37 complex interacts with the SNARE GS15 (Uchiyama et al., 2006). In addition, both p47 and p37 have been connected to mitotic regulation, by limiting the recruitment of Aurora A kinase to centromers (Kress et al., 2013). Furthermore, p37 also contributes to correct spindle orientation, by limiting the association of the nuclear and mitotic apparatus (NuMA) with the cell cortex during metaphase. Cortical localization of NuMA depends on dephosphorylation by the PP1α-Repo-Man complex, whose activity is negatively regulated by p37 (Lee et al., 2018). The third and shortest of the human SEP domain

proteins is UBXN2A, with 259 amino acids and a very small N-terminus without any defined structure. UBXN2A was shown to prevent ERAD of nicotinic acetylcholine receptors (nAChRs) that include an α3 subunit, by blocking ubiquitination by the E3 ligas CHIP (Teng et al., 2015). This effect depends on binding of the α3 subunit by the SEP domain. Another function of UBXN2A is the binding of the anti-apoptotic chaperone Mortalin (mot-2), which prevents mot-2 association with p53 and induces apoptosis through nuclear translocation of p53 (Sane et al., 2014). The fourth of the human SEP domain proteins is UBXN11. The protein is significantly larger than the other three, with a total length of 520 amino acids. The defining feature is a spectrin domain in the N-terminus, which is associated with cytoskeleton interactions (Djinovic-Carugo et al., 2002). UBXN11 in particular is involved in the disassembly of actin stress fibers (Katoh et al., 2002).

Despite these numerous functions of the SEP domain adapters, no exact molecular mechanism for the processing of a substrate by a p97-SEP domain adapter complex has been identified so far. Recently, our group identified the disassembly of the ternary SDS22-PP1-I3 (SPI) complex as a p97-SEP domain adapter dependent process (Weith et al., 2018). This has enabled us to investigate the role of these adapters more closely.

1.11 Protein Phosphatase 1

Protein phosphatase 1 (PP1) is a serine/threonine phosphatase enzyme that together with Protein Phosphatase 2A (PP2A) is responsible for a more than 90% of the total phosphatase activity in eucaryotes (Bollen et al., 2010). The protein is highly conserved from yeast (Glc7 in *S. cerevisiae*) to higher eukaryotes. In humans, there are three different isoforms of PP1, PP1α (*PP1CA*), PP1β (*PP1CB*, also known as PP1δ), PP1γ (*PP1CC*) that mostly differ in the length of their C-termini (da Cruz e Silva et al., 1995) (Virshup and Shenolikar, 2009). Due to alternative splicing two variants of PP1γ, PP1γ1 and PP1γ2 exist, although PP1γ2 is only expressed in the testis, while the other three can be found in all cell types (Chun et al., 1994). The three isoforms differ in their subcellular location, with all isoforms being present in the cytosol and the nucleus during interphase (Andreassen et al., 1998). Inside the nucleus, PP1α is found at the nuclear matrix, PP1β associates with both non-nucleolar chromatin and the nucleoli and PP1γ1 associates at the nucleoli (Lesage et al., 2005). At the center of the PP1 protein sits the active site, which consist of a β-α-β-α-β scaffold with two metal ions M1 and M2 (Goldberg et al., 1995). In mammals, the M1 site is occupied by Fe^{+2} and the M2 site by Zn^{+2}, while mammalian PP1 that has been expressed in bacteria contains Mn^{+2} at both sites (Bollen et al., 2010). The active site is surrounded by acidic residues, with the C-terminus of PP1 in close proximity (Goldberg et al., 1995). PP1 forms holoenzyme complexes with at least 200 interaction partners (PIPs, for PP1 interacting protein), which function as substrate specifiers for the multitude of different substrates (Heroes et al., 2013). While most PIPs bind to all isoforms of PP1, some are specific for a certain isoform (Heroes et al., 2013). The majority of these proteins interact with PP1 via a common RVxF motif on PIP side, which binds to a hydrophobic site on PP1 distant from the active site (Bollen et al., 2010). While the RVxF motif is found in most PIPs, it is also degenerate and allows the general sequence $[K_{55}R_{34}][K_{28}R_{26}][V_{94}I_6]\{FIMYDP\}[F_{83}W_{17}]$ with the numbers in the subscript representing the percentage occurrence of that residue and the residues in curly brackets are excluded (Wakula et al., 2003), (Heroes et al., 2013). Additionally, there are around eight other protein interaction sites like the SILK, SpiDoC (spinophilin docking site for the C-terminal groove), BiSTriP (bipartite docking site of SDS22 that interacts with the α4–6 triangular region of PP1), MyPhoNE (myosin phosphatase N-terminal element) and IDoHA (inhibitor-2 docking site for the hydrophobic and acidic grooves) motif. These

motifs are responsible for the binding of PIPs that specify and mediate subcellular location and substrate specification of the PP1 complex, but can also bind regulating factors, such as inhibitor-2 that binds to the IDoHA motif that overlaps the active site and inhibits phosphatase activity (Heroes et al., 2013). of While most PP1 holoenzyme complexes are dimeric and consist of PP1 and one PIP, there are also several trimeric complexes that include an inhibitor protein as the third member. The PIPs in trimeric PP1 complexes mostly bind to different interaction sites on PP1, although there are exception such as the PP1-spinophilin-inhibitor-2 complex, where both PIPs compete for the RVxF motif binding site (Heroes et al., 2013). Formation of these trimeric complexes can be, but is not necessarily, supported by additional interactions between the two PIPs, such as for the Mypt1/PP1/CPI-17 complex (Eto et al., 2007).

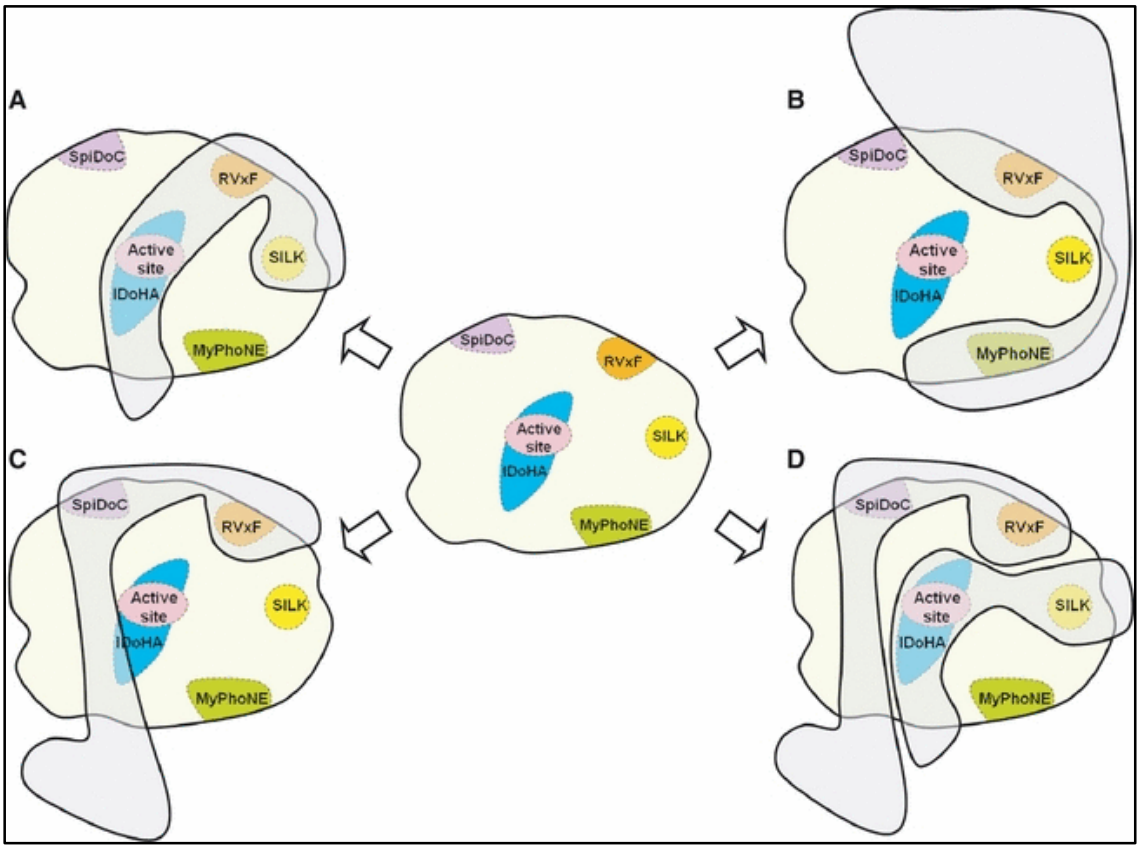

Figure 14: Overview of selected binding sites of PP1 interactors. The active site as well as the binding site for the SpiDoC, RVxF, iDoHA, SILK and MyPhoNE binding motifs are indicated. The Cartoon figures A-D showcase the shape of different PIPs superimposed on the PP1 binding sites. **A** inhibitor-2, **B** Mypt1, **C** spinophilin, **D** spinophilin and inhibitor-2 *(Heroes et al., 2013)*.

PP1 was initially discovered for its involvement in glycogen metabolism by counteracting phosphorylase kinase activity (Brautigan, 2013). In addition, PP1 is also important for cell division, protein synthesis, actin and myosin organization, apoptosis and receptor signaling (Ceulemans and Bollen, 2004). During mitosis, PP1 is recruited to the kinetochore by KLN1 (Kinetochore null 1) where it counteracts the aurora B kinase, contributing to correct spindle orientation (Liu et al., 2010). In similar fashion, the PP1 and Aurora B balance phosphorylation of histone H3 during mitosis (Hsu et al., 2000). PP1 affects various factors involved in protein synthesis, with the transcription factor CREB (cAMP response element-binding protein) and the translation initiation factor eIF2α (eukaryotic initiation factor 2α) among them (Alberts et al., 1994), (Ernst et al., 1982). Regulation of cytoskeletal organization by PP1 is mediated two types of PIPs, Neurabins and Mypts (Ceulemans and Bollen, 2004). Neurabins primarily bind to PP1α and contribute to actin remodeling, while Mypts bind to PP1β and mediate myosin dephosphorylation. Furthermore, PP1 activity affects apoptosis through dephosphorylation of the pro-apoptotic factor Bad (Bcl-2-Antagonist-of-Cell-Death) by PP1, which is activated by Ras (Ayllón et al., 2000). In addition, PP1 is involved in synaptic signaling, for example through interaction with NMDA receptors (Hou et al., 2013).

This study focused on a complex consisting of PP1γ and the interactors SDS22 (suppressor 2 of the dis2-mutant SH3) and I3 (inhibitor-3), called the SPI complex. From here on PP1γ will always be referred to as PP1, unless specified otherwise.

1.11.1 The SDS22-PP1-I3 complex

The PIPs SDS22 (suppressor of Dis2 mutant 2, also known as PPP1R7) and I3 (inhibitor-3 or Inh3, also known as PP1R11) form a trimeric complex with PP1 that is highly conserved, whose homologues in the yeast *S. cerevisiae* are Sds22 (SDS22), Glc7 (PP1) and Ypi1 (I3) (Pedelini et al., 2007). Unlike most other PIPs, SDS22 does not bind to PP1 via the RVxF motif, but instead through 12 leucin rich repeats (LLRs) that form a curved superhelix that binds adjacent to the active site of PP1 (Choy et al., 2018). Binding of SDS22 to PP1 is further influenced by the metal-loading state of PP1, where SDS22 binds only to PP1 that lacks any metal ion, or has only one metal ion bound at the M2 site (Choy et al., 2019). I3 is a 126 amino acids long proteins that binds to PP1α and PP1γ, but not PP1β, through the RVxF motif $_{39}$KKVEW$_{43}$ (Zhang et al., 2008), (Huang and Lee, 2008). In addition, residues 65-77 were found to be important for the inhibitory effect of I3 on PP1 (Zhang et al., 2008). In contrast to SDS22, I3 seems to be highly unstructured when not bound to PP1, as evidenced by the fact that it runs higher than expected in SDS-gel electrophorese (above 20 kDa instead of around 14 kDa) and tends to aggregate when expressed on its own in bacteria or insect cells (results from our lab, data not shown).

While both SDS22 and I3 inhibit the phosphatase activity of PP1 *in vitro* and *in vivo*, they are also crucial for the proper function of PP1 (Pedelini et al., 2007), (Lesage et al., 2007). The main role of the SDS22-PP1-I3 complex seems to be the regulation of cytokinesis during cell division (Eiteneuer et al., 2014; Pedelini et al., 2007). First evidence for this came from experiments with temperature sensitive yeast mutants, which showed that a mutation of Sds22, which weakened binding between Sds22 and Glc7 (PP1 in yeast) *in vitro*, lead to chromosome instability at higher temperatures that was connected to a reduction in the nuclear localization of Glc7 (Peggie et al., 2002). This negative effect on cell viability was rescued in strains that were also mutated in Ipl1 (Aurora B kinase in yeast), suggesting that the Sds22-dependent function of PP1 in the nucleus counteracted Ipl1 (Peggie et al., 2002). Similarly, I3 was shown to be important for centrosomal or nucleolar localization of PP1 in interphase HEK cells, which was dependent on a nuclear localization signal at the N-terminus of I3 and a basic cluster at the C-terminus that was responsible for recruitment to the nucleoli (Huang et al., 2005). Further studies in yeast and human cells showed that depletion of SDS22 and I3 produced similar effects on the localization and function of PP1 suggesting a synergistic role for the regulation of PP1

activity (Pedelini et al., 2007), (Lesage et al., 2007), (Bharucha et al., 2008). The mitotic function of PP1 was traced to interaction with KLN1 at the kinetochore through the RvXF motif, which counteracts Aurora B activity at the centromere and is essential for proper chromosome biorientation (Eiteneuer et al., 2014). Depletion of I3 lead to association of SDS22 to PP1 at the kinetochore, which inhibited the phosphatase activity of PP1(Eiteneuer et al., 2014). The fact that binding of SDS22 and I3 to PP1 was required to reach its destination but did also inhibits PP1 activity suggested that SDS22 and I3 function as chaperones for PP1.

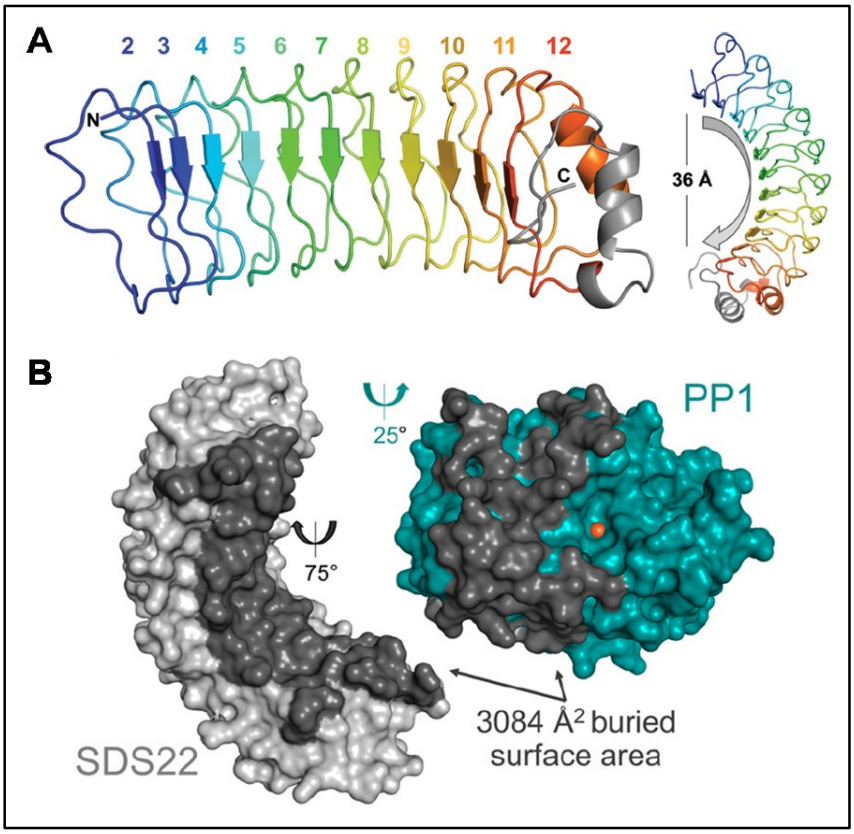

Figure 15: Structure of SDS22 bound to PP1 A The structure of SDS22 (residues 100-300, pdb: 6mky) consist of 12 LRR repeats that form a curved superhelix with a distance of 36 Å between N- and C-terminus *(Choy et al., 2018)*. **B** Structure of the $SDS22_{56–360}$-$PP1_{1–300}$ interaction site (pdb: 6OBN). SDS binds adjacent to the catalytic center of PP1 and coveres surface area of 3084 $Å^2$ *(Choy et al., 2019)*.

1.11.2 The SDS22-PP1-I3 complex is a target of p97

A connection between PP1 and p97 was first established by the fact that mutation of a protein, which was later identified as the SEP domain protein Shp1 (**S**uppressor of **h**igh **c**opy PP**1**), rescued the negative effect of PP1 (GLC7 in yeast) overexpression in *S. cerevisiae* (Zhang et al., 1995). A similar effect was observed with a yeast strain in which Shp1 could not bind Cdc48 due to mutations of the SHP box and UBX domain (Böhm and Buchberger, 2013). In addition, mutation or depletion of Cdc48, Sds22 or Ypi1 lead to aggregation of Glc7 in budding yeast and the Sds22-Glc7-Ypi1 complex was found to be associated with Shp1-p97^{QQ} mutant, which is ATPase inactive (Cheng and Chen, 2015). Furthermore, a mass spectrometry screen for interaction partners of UBX domain-containing adapter proteins of p97 showed association of human SEP domain proteins with the SDS22+PP1+I3 complex (Raman et al., 2015).

Our group proceeded to investigate the role or p97 and the SEP domain adapter for the regulation of PP1 activity (Weith et al., 2018). The fact that SDS22 and I3 are both required for PP1 function, but also inhibit PP1 activity suggested a role of these two PIPs in PP1 biogenesis. Co-immunoprecipitation of PP1, SDS22, I3 and NIPP1 (Nuclear inhibitor of protein phosphatase 1) from rabbit reticulocyte lysate that expressed radioactively labeled PP1 showed that SDS22 and I3 were associating with PP1 immediately after biosynthesis and were dissociating from PP1 over the course of two hours (Weith et al., 2018). In contrast, NIPP1 association was initially weak, but increased over the same time period. Dissociation of SDS22 was suppressed by knockdown of I3, suggesting that dissociation of SDS22 and I3 from PP1 is linked. The dissociation of SDS22 and I3 could be suppressed by the addition of the p97 inhibitor NMS-873, suggesting that p97 is involved in this process. This was supported by the fact that the components of the SPI complex could be co-immunoprecipitated with the substrate trapping p97^{E578Q} mutant. Furthermore, treatment with NMS-873 suppressed phosphatase function of PP1 after isolation from cells and incubation with trypsin, suggesting that PP1 activation is dependent on p97 (Weith et al., 2018).

Additional co-immunoprecipitation experiments from HEK cells revealed that the SEP domain adapters p37, p47 and UBXN2A interacted with the SPI complex, although the interaction with p47 was markedly weaker than with the other two. The fourth member of

the human SEP domain proteins, UBXN11 as well as the Ufd1-Np4 adapter did not interact with the SPI complex. Individual knockdown of p37 or UBXN2A or knockout of p47 did not abrogate the interaction between the SPI complex and p97. Instead, depletion of all three adapters was required to arrest the disassembly of freshly synthesized SPI complex in cells, suggesting that the three adapters work redundantly (Weith et al., 2018).

In order to test if p97 and a SEP domain adapter were sufficient to disassemble the SPI complex without any other interacting factor, Jonas Seiler developed an *in vitro* disassembly assay with purified proteins (Weith et al., 2018). Incubation of p97 and p37 with the SPI complex and NIPP1 showed that SDS22 and I3 dissociation and NIPP1 association with PP1 was dependent on the addition of ATP. SPI complex disassembly worked at substoichiometric concentrations of p97 and preceded faster at higher enzyme concentrations. Strikingly, none of the involved proteins were ubiquitinated, in contrast to established processes that involved p97 and the Ufd1-Npl4 adapter.

Utilizing a genetically encoded crosslinking strategy, Weith et al. identified the SEP domain of p37 as an interaction partner of I3, implicating I3 as the potential primary target of p97. In addition, I3 was shown to be essential for the interaction, as mutant I3 that could not bind to PP1 prevented binding between p97-p37 and SDS22-PP1 *in vitro*. Further evidence for I3 as the substrate came from experiments with genetically encoded crosslinkers at the entrance of the p97 pore and inside the D2 ring, which showed that I3 was the only component of the SPI complex that could be trapped at the entrance of the pore, while additional crosslinks with the D2 domain depended on the presence of ATP. These results hinted at I3 as the primary target of p97 in this process (Weith et al., 2018).

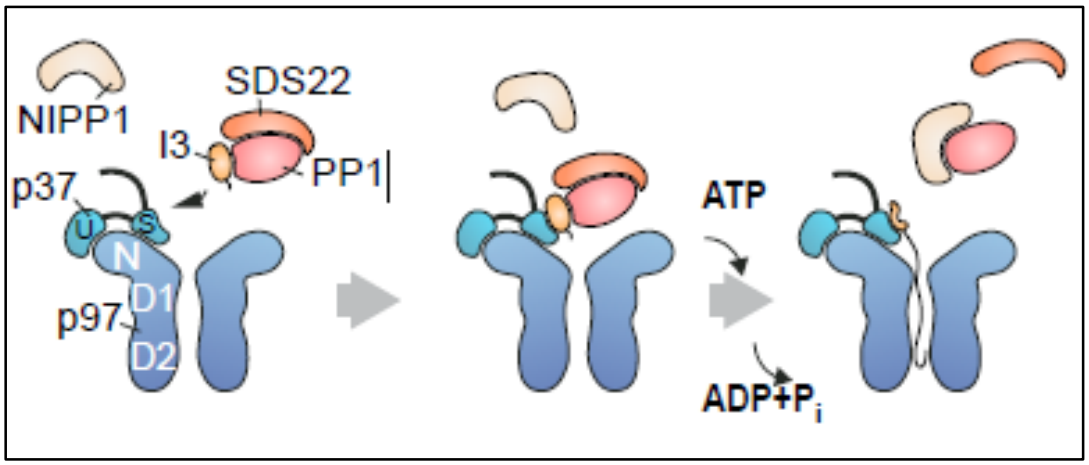

Figure 16: Model for the disassembly of the SDS22-PP1-I3 complex by p97-p37. The adapter binds to the N-domain of p97 through the UBX domain (U) and SHP box and mediates recruitment of the SPI complex. I3 is recognized via the SEP domain and then pulled into the central pore of p97, powered by ATP hydrolysis. This leads to the disassembly of the SPI complex and allows other PIPs like NIPP1 to bind to PP1 *(Weith et al., 2018)*.

1.12 Aims of this thesis

Since most of the substrates of p97 are ubiquitinated, the majority of research on how p97 adapters facilitate substrate processing has been focused on the function of the Ufd1-Npl4 adapter proteins that control unfolding of ubiquitinated substrates. Our group had identified the disassembly of the SDS22+PP1+I3 (SPI) complex as a ubiquitin independent substrate of p97, a process which depended on adapter proteins from the SEP domain family, based on data from experiments with proteins that had been immunoprecipitated from cells. Preliminary data suggested that the I3 protein is the major target of p97 in this process. To verify the hypothesis that I3 was unfolded in this process, we planned to establish a new *in vitro* unfolding assay that allowed us to monitor the unfolding reaction in real time. For this purpose, a model substrate with a fluorescent reporter was to be developed, in order to track the unfolding reaction in real time. Once this assay was set up, we planned on comparing the effect of the different members of the SEP domain adapter family on SPI disassembly and potential unfolding of I3. Furthermore, we planned to investigate the mechanism how the SEP domain adapters are able to facilitate the unfolding of a nonubiquitinated substrate by p97, in particular with a focus to elucidate how the p97-SEP domain adapter complex is capable to specifically unfold the I3 protein, while sparing PP1 and SDS22

2 Results

2.1 Establishment of a p97 unfolding assay for a ubiquitinated model substrate

The activity of p97 has been studied mainly by measuring the rate of ATPase hydrolysis. This has given valuable insights into the effect of different mutations or adapters on p97. However, it is only an indirect measurement of the actual process of substrate unfolding. A more direct read out can be achieved by generating a substrate which is coupled to a fluorescent protein (e.g. GFP), which leads to a loss of fluorescence upon unfolding. This approach has been used by two different groups to investigate p97 or Cdc48 unfolding activity. One group (Blythe et al., 2017) generated a GFP protein with two N-terminal ubiquitin moieties, which were further ubiquitinated with an engineered gp78-ubc7 hybrid (E3-E2 combined) to obtain a polyubiquitinated substrate. This substrate was then bound and unfolded by the p97-Ufd1-Npl4 complex after the addition of ATP. A limited decay of fluorescence was observed, because the GFP protein was unfolded by p97 but rapidly refolded after being processed. This was overcome by the addition of a mutant GroEL D87K chaperone, which trapped the unfolded GFP and prevented refolding. This led to a significant loss of fluorescence over time. An alternative approach was pursued by Bodnar et al. (Bodnar and Rapoport, 2017), who developed an equivalent system for the yeast homologue of p97, Cdc48. Their reporter was based on the photoconvertible fluorescent protein mEos3.2, an engineered monomeric version of the Eos protein from *L. hemprichii*. Irradiation with UV light causes a break in the peptide chain and a shift from a green fluorescent to a red fluorescent form. The peptide backbone break in mEos3.2 prevented refolding after processing by Cdc48. The substrate consisted of one mEos3.2 with an N-terminal peptide sequence that included a degron for the ubiquitin ligase Ubr1. After UV irradiation and ubiquitination, this substrate was unfolded by Cdc48 and Ufd1-Npl4.

In a first approach, we aimed to set up a ubiquitin-dependent unfolding assay for comparison before concentrating on the analysis and further dissection of SPI disassembly as the main focus of the thesis. We decided to combine the advantages of the two published systems. We kindly received the plasmid DNA for their GFP substrate with two N-terminal ubiquitins and the gp78-ubc7 hybrid, as well as a small sample of purified substrate as a reference from the group of Raymond Deshaies. The substrate was adapted by replacing the GFP with an mEos3.2 sequence (Addgene Plasmid #54550,

(Zhang et al., 2012)). The construct was expressed and purified from BL21 and irradiated with a 365 nm UV lamp to induce the break in the peptide backbone. The effectiveness of the treatment was assessed by SDS gel electrophoresis and spectroscopic analysis (**Figure 17**). After 40 min of irradiation, bands appear in the SDS-PAGE at 19 and 27 kDa, representing the N-terminal (27kDa) and C-terminal (19 kDa) fragment. These bands increase in intensity with extended irradiation times (120 min and 160 min). The absorbance spectrum of the substrate showed a major peak at 510 nm before irradiation. After 40 min, a new peak appears around 580 nm, representing the converted species. The size of this peak increases with longer irradiation times. After more than 2 hours, around 40%of the total substrate had been transformed. Further irradiation did not significantly increase this result (data not shown).

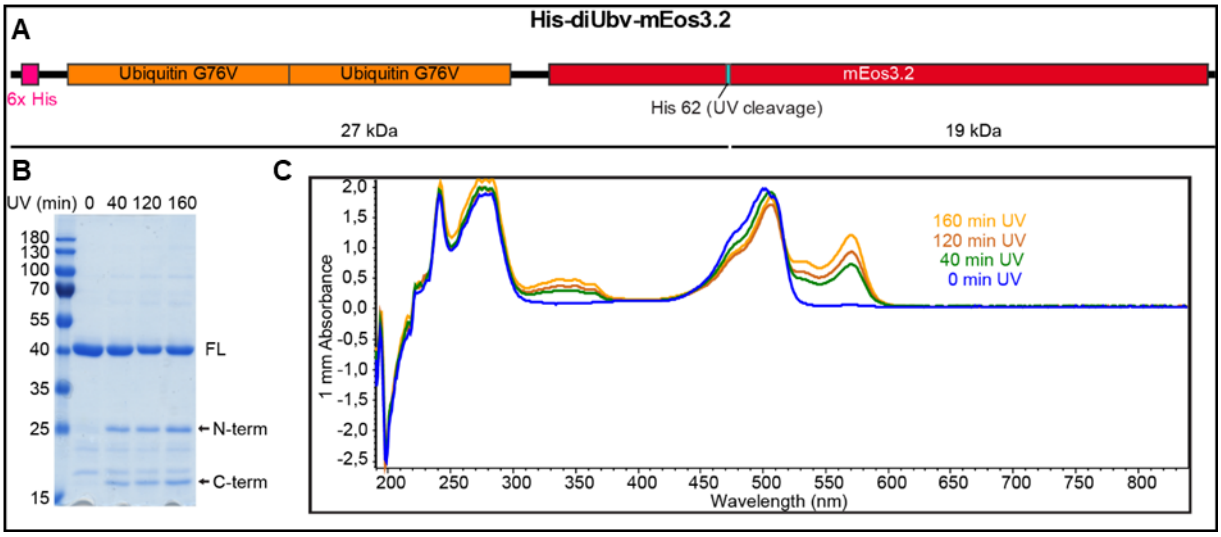

Figure 17: Design and photoconversion of the ubiquitin-Eos model substrate. **A** Cartoon-structure of the Ubiquitin-Eos substrate, based on the Ubiquitin-GFP substrate from Blythe et al. The protein carries a 6xHis-tag at the N-terminus for purification, followed by two ubiquitin moieties whose final glycine has been replace by valine. A break in the peptide backbone of mEos3.2 after His 62 was introduced by UV irradiation (365 nm). **B** Coomassie stained SDS gel of unirradiated substrate (0 min) compared to three different UV-irradiation timepoints (40 min, 120 min, 160 min). Cleavage of the full-length substrate (FL) resulted in two fragments, visible in the SDS-gel at 27 kDa (N-terminal fragment) and 19 kDa (C-terminal fragment). **C** The absorbance spectra of the samples were recorded on a Nanodrop® spectrophotometer and showed the emergence of the photoconverted form at 570 nm.

The substrate was then incubated over night with Ube1, gp78-ubc7 (E2+E3 hybrid), ubiquitin and ATP in order to add K48 linked ubiquitin chains. The resulting polyubiquitinated substrate was further purified by gel filtration (**Figure 18**). Fractions were

analyzed by SDS-PAGE and those containing medium to high levels of ubiquitination were pooled and concentrated.

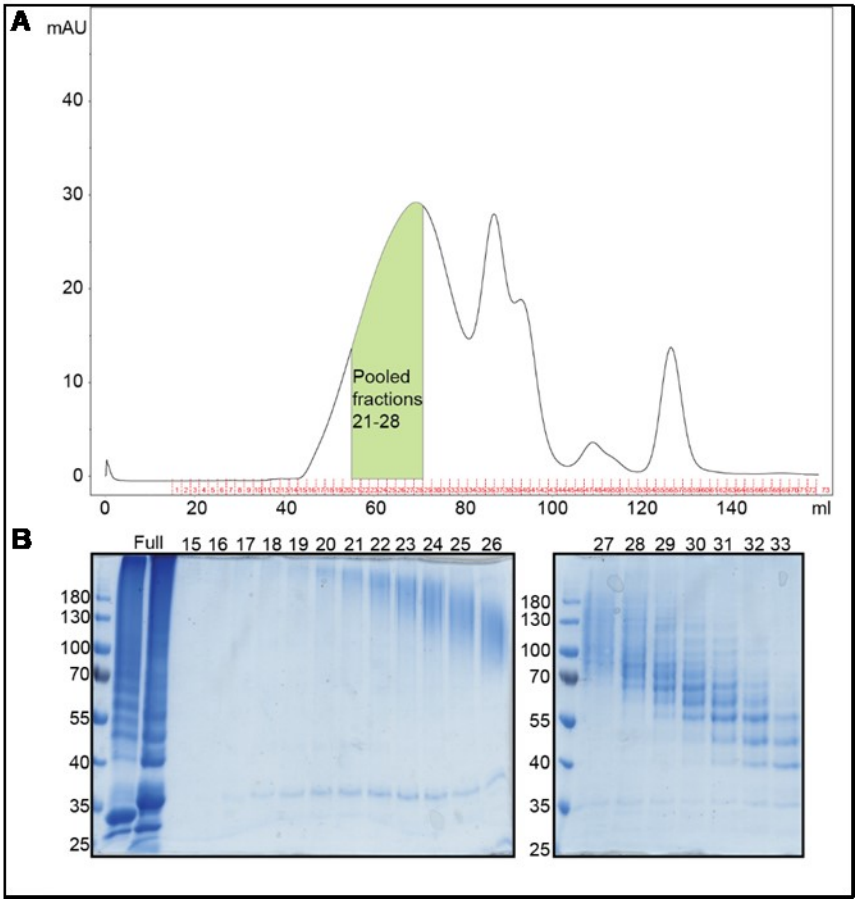

Figure 18: Purification of polyubiquitinated Ub^{n}-Eos substrate via gel filtration. After ubiquitination overnight, the substrate was purified first with a NiNTA column (data not shown) to remove the ubiquitination enzymes and free ubiquitin chains. **A** Afterwards, it was further purified by size exclusion chromatography on a gel filtration column (HiLoad® 16/600 Superdex® 200 pg, GE). **B** The resulting fractions (2 ml) were analyzed by SDS-PAGE and fractions with high degree of ubiquitination (21-28) were pooled and concentrated.

The purified substrate (25 nM), abbreviated as Ub-Eos from now on, was then incubated with p97 (75 nM) and the adapter heterodimer Ufd1-Npl4 (150 nM), and the decay of fluorescence after addition of ATP was monitored. The fluorescence of the unconverted (“green”) fraction of mEos3.2 did decrease slightly by about 10% and then reached a plateau, reflecting a balance between unfolding by p97 and refolding. The converted (“red”) fraction experienced an irreversible loss of fluorescence over time. The unfolding reaction was tested with p97 from two different sources. His-p97 was expressed and

purified from BL21 bacterial cells, while p97-His was expressed and purified from Sf9 insect cells. Both were based on the human p97 sequence. The unfolding reaction proceeded faster with the p97 from insect cells than that from bacteria. This was true for both the green and the red form of the Ub-Eos substrate.

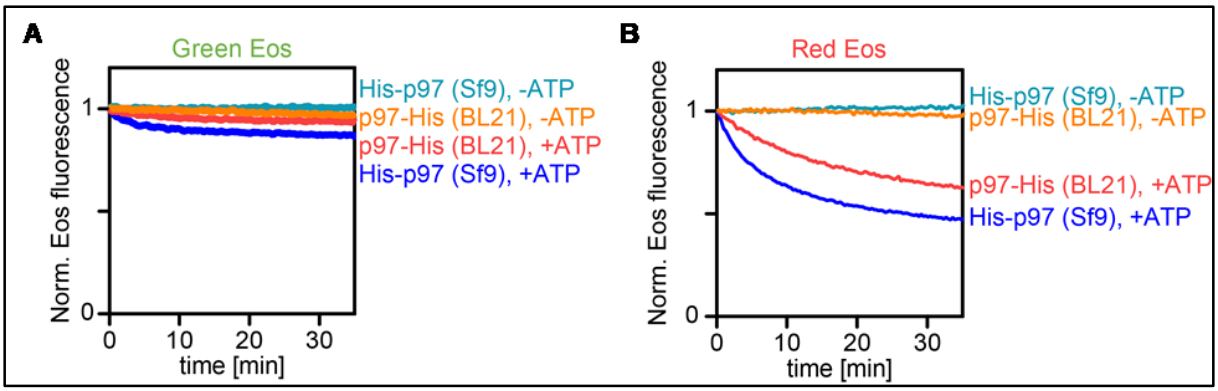

Figure 19: Unfolding of the ubiquitinated model substrate by p97 and Ufd1-Npl4. Comparison of Ub-Eos unfolding by p97 from BL21 and Sf9. The Ub-Eos substrate (25 nM), p97 (75 nM) and Ufd1-Npl4 (250 nM) were mixed in a cuvette and incubated at 37°C. After the addition of ATP (2 mM) or the same volume of water, the decay in fluorescence of the unconverted "green" (ex. 500 nm, em. 520 nm) and converted "red" (ex. 540 nm, em. 580 nm) substrate was monitored over 30 min. **A** The green uncleaved form of Eos can refold quickly after being unfolded by p97, leading to a steady state with only a small decrease in fluorescence. **B** The red photoconverted from of Eos can no longer refold after being processed by p97, leading to an irreversible loss of fluorescence. Unfolding by p97 expressed in insect cells (Sf9) is faster than by p97 expressed in bacteria (BL21).

2.2 Establishment of a p97 unfolding assay for the SDS-PP1-I3 complex

After the successful establishment of an assay for ubiquitin-dependent unfolding based on the decay of Eos fluorescence, we aimed to apply an equivalent approach to dissect the basis for SPI disassembly. Previous data had indicated that I3 may be directly targeted by the p97 complex during SPI disassembly. This was based on the observation that the SEP-domain of the p37 adapter directly interacted with I3 and that I3 could be crosslinked in the central channel of p97 (Weith et al., 2018). We therefore asked whether SPI disassembly could involve the unfolding of I3 during the process. To address this question, the mEos3.2 reporter was fused to the N-terminus of inhibitor-3. This would enable to

detect possible unfolding of I3 by monitoring the decay in mEo3.2 fluorescence, analogous to the ubiquitin substrate (**Figure 20**).

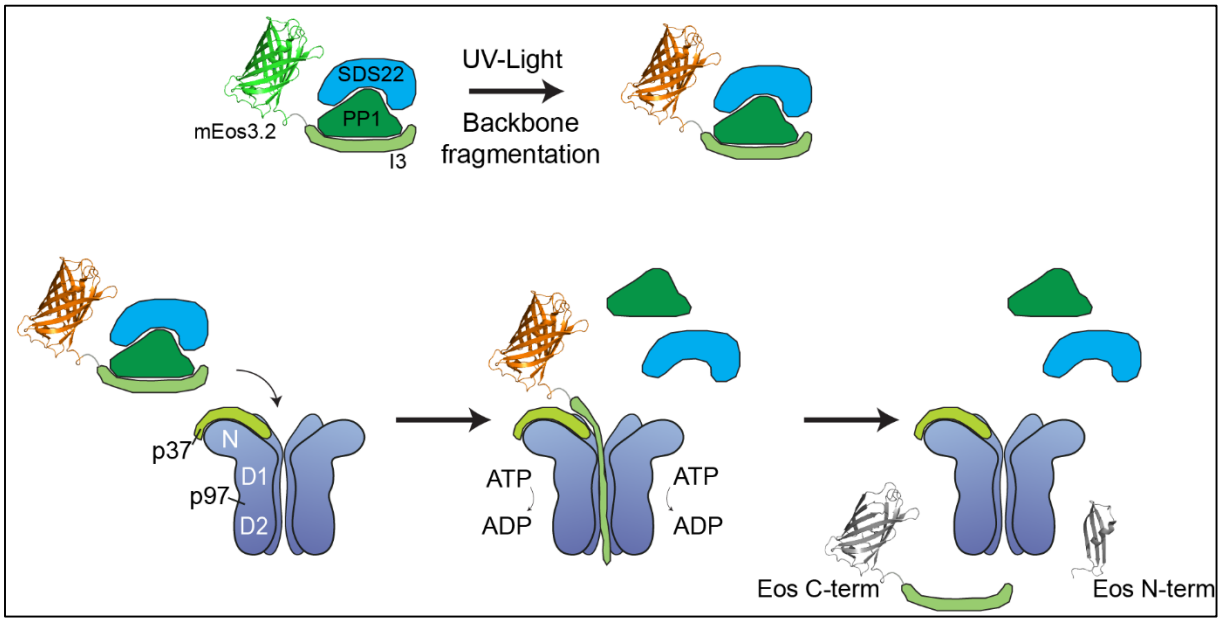

Figure 20: Schematic describing the fluorescence unfolding assay for the SDS22PP1-mEos3.2-I3 substrate (SPEosI). An mEos3.2 was fused to the N-terminus of I3 and the whole SPEosI complex was expressed and purified from Sf9 cells. UV irradiation introduces a backbone break in mEos3.2 which prevents refolding of the fluorescent reporter after unfolding. The substrate is incubated with p97, p37 and ATP, which leads to unfolding of Eos-I3 and irreversible loss of fluorescence. The fluorescence of the red Eos form at 580 nm is measured and normalized to the initial value to plot the progress of the unfolding reaction.

Since the SPI complex could not be co-expressed in bacteria (Weith et al., 2018), the SPEosI-complex (SDS22-PP1-His-mEos3.2-I3) was expressed in Sf9 insect cells using the baculovirus system. Cells were coinfected with a virus carrying His-mEos3.2-I3 and another virus that carried PP1 and SDS22. The complex was purified by His-tag affinity chromatography (NiNTA), followed by ion-exchange chromatography and finally size exclusion chromatography. The purified protein complex was then subjected to UV light (365 nm) to break the peptide backbone of mEos3.2.

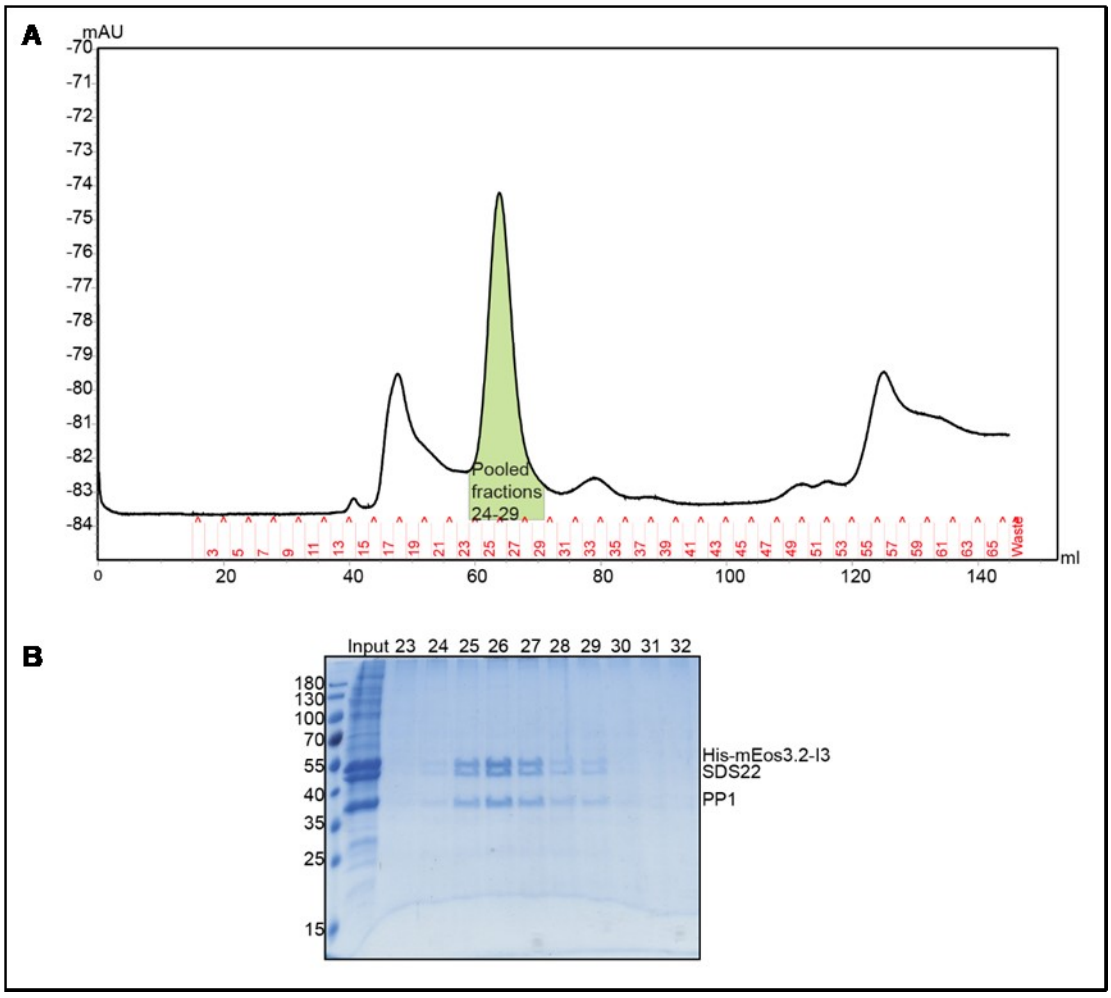

Figure 21: Purification of SDS22-PP1-His-Eos-I3 (SPEosI) complex from Sf9 cells. The three complex components were co-expressed in Sf9 cells with the baculovirus system. The complex was first purified by NiNTA resin, followed by ionexchange chromatography. **A** The last step of purification was gel filtration on a S200 gel filtration column (HiLoad® 16/600 Superdex® 200 pg, GE). **B** Peak fractions were analyzed by SDS-PAGE and fractions with the complex proteins (fractions 24-29) were pooled and concentrated.

The purified SPEosI substrate was tested as a substrate for p97 in an unfolding assay. After mixing the substrate (35 nM) with p97 (175 nM, from Sf9) and p37 (500 nM) and incubating for 5 min at 37°C, ATP was added and the decay in fluorescence of the “red” Eos form at 580 nm was monitored (**Figure 22**). The fluorescence decreased to about 40% of the initial amount after 30 min. Doubling the concentration of p97 (350 nM) increased the loss of fluorescence to about 30%. A decrease by a factor of five to an equimolar ratio between p97 and substrate (35 nM) resulted in a decrease of fluorescence to about 70%. No unfolding was observed if the p37 adapter was replaced by the Ufd1-

Npl4 adapter that promoted ubiquitin dependent unfolding. Similarly, unfolding did not occur when ATP was replaced by the non-hydrolysable ATPγS.

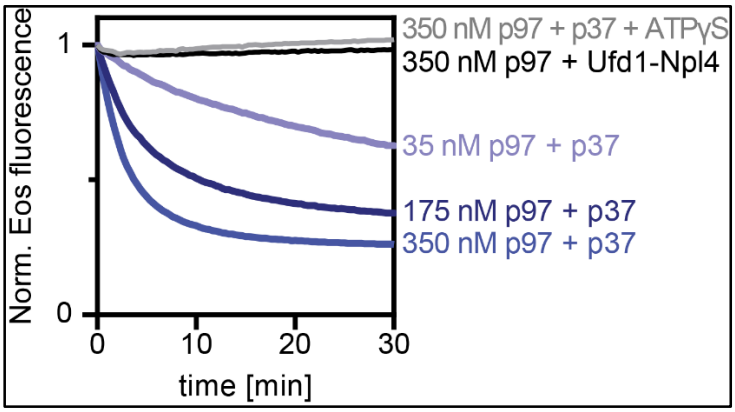

Figure 22: p97 together with unfolds Eos-I3 during SPI disassembly. SPEosI substrate (35 nM), p37 (500 nM) or Ufd1-Npl4 (500 nM) and His-p97 (from Sf9, at indicated concentrations) were mixed in a cuvette at 37°C. ATP or ATPγS (2 mM) when indicated, were added and the fluorescence of the "red" Eos species (ex. 540 nm, em. 580 nm) was monitored over 30 min. SPEosI is unfolded by p97 together with p37, but not with Ufd1-Npl4. The reaction rate increases with higher concentrations of p97 and does not proceed in the presence of the non-hydrolysable ATPγS.

The fact that Eos fused to I3 lost fluorescence in an energy (ATP) and p97 concentration-dependent manner provided strong evidence that Eos-I3 is unfolded during the course of the SPI disassembly reaction. Moreover, given that none of the components were ubiquitinated and no ubiquitin or conjugation machinery was included in the reaction, this finding demonstrates that the unfolding by p97 in this case occurs in a ubiquitin independent manner.

2.2.1 Effect of p97 concentration on the unfolding rate

In order to gauge the effect of p97 concentration on the unfolding rate, multiple unfolding experiments with a constant substrate (35 nM) and p37 (2 µM) concentrations, but with varying concentrations of p97 (10 nm to 1 µM) were measured. The initial rate of each unfolding reaction was determined by plotting the fluorescence intensity every 15 seconds over the first 4 minutes and calculating the slope. The amount of substrate fluorescence lost per minute was calculated from this slope and plotted against the ratio of p97 to substrate (**Figure 23**). Of note, if the concentration of p97 was lower than that of the SPEosI substrate, the decrease in fluorescence was barely noticeable (<5% over 40

minutes, data not shown). The initial unfolding rate increased with higher concentrations of p97 up to a ratio of around 10 p97 hexamers per substrate.

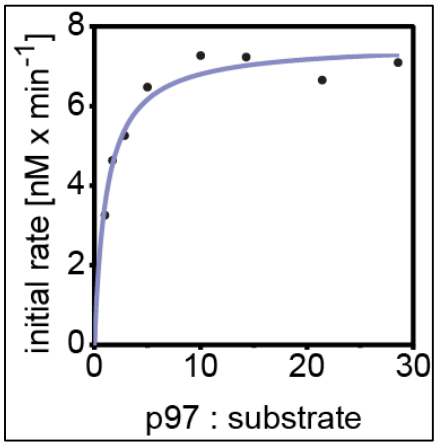

Figure 23: Effect of p97 concentration on the initial unfolding rate. SPEosI substrate (35 nM), p37 (2 µM) and varying concentrations of His-p97 (10 – 1000 nM) were mixed and the fluorescence decay was monitored. The slope of the unfolding decay over the first 4 minutes after addition of ATP was used to calculate the initial unfolding rate. The initial unfolding rates were plotted against the ratio between p97 and substrate. The maximal initial unfolding rate is reached at a ration of 10 p97 hexamers per one substrate molecule.

2.2.2 Differential unfolding rate of p97 expressed in bacteria vs insect cells

We previously noted that unfolding of the ubiquitinated substrate occurs at a higher rate with (human) p97 generated in Sf9 insect cells compared to p97 generated in bacteria (BL21) (**Figure 19**). To clarify whether this generally applies, we compared the two variants also in SPEosI unfolding. The concentration of the proteins was increased to 50 nM SPEosI substrate, 400 nM His-p97 and 800 nM p37, because we reasoned that a potential difference between insect and bacterial p97 would be larger at higher concentrations. The comparison (**Figure 24**) showed a higher rate of unfolding with p97 expressed in insect cells, similar to the effect on the ubiquitin substrate.

A possible explanation for this phenomenon is that endogenous adapter proteins were copurified with the p97 from Sf9 cells and increased the unfolding efficiency. To exclude this possible interference, we tested if unfolding is mediated in the absence of any adapter (only substrate, p97 and ATP). However, no unfolding was observed (**Figure 24**). Instead the increase in unfolding rate could be a result of more efficient hexamer assembly in insect cells compared to bacteria. Another possible explanation could be posttranslational

modifications of His-p97 (human) when expressed in insect cells. Since the effects of different adapters were best visible with a high unfolding rate, all following experiments were conducted with His-p97 purified from insect cells (Sf9 or Hi5).

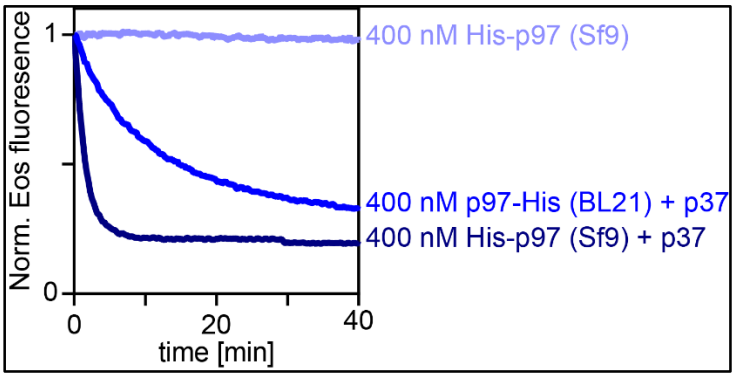

Figure 24: Comparison of SPEosI unfolding by p97 purified from E.coli (BL21) and insect cells (Sf9). SPEosI (50 nM), p97 (400 nM) and p37 (800 nM) or equivalent volume of buffer were mixed in a cuvette at 37°C. After addition of ATP (2 mM) the fluorescence of the "red" Eos (ex. 540 nm, em. 580 nm) was measured over 40 min. Similarly to the ubiquitin substrate, p97 expressed in insect cells (Sf9) is more efficient in unfolding the SPEosI substrate than p97 expressed in bacteria (BL21). The reaction does not proceed in the absence of p37, suggesting that the increase in unfolding rate is caused by copurified adapter proteins.

2.3 Effect of different SEP domain adapters on the unfolding reaction

In addition to p37, the human genome codes for three other p97 adapter proteins, p47 UBXN2A and UBXN11 that contain a similar domain arrangement like p37 with a SEP, SHP and UBX-domain. Previous work by Jonas Seiler and Matthias Weith (Weith et al., 2018) had shown, that p47 and UBXD4 are implicated in the disassembly of the SPI complex. To test the effect of these adapters in the fluorescence unfolding assay, a master mix containing the SPEosI substrate (35 nM) and p97 (175 nM) was prepared and divided into four equal parts. The adapters p37, p47 and UBXD5 were expressed as GST-fusion proteins in bacteria (BL21). In contrast, UBXN2A was not expressed in bacteria and was therefore generated as a GST-fusion protein protein in insect cells (Sf9). The tags where proteolytically removed and each of the four parts of the unfolding master mix was supplemented with one of the adapters. After addition of ATP, the fluorescence level was measured in four cuvettes in parallel. Both p37 and UBXN2A did result in a rapid decrease of substrate fluorescence, while the fluorescence level in the p47 and UBXN11

supplemented samples remained stable. This result mirrored the unpublished observation of an in vitro disassembly experiment by Jonas Seiler, in which p37 and UBXD4 enabled complex disassembly, but p47 did not (personal communication).

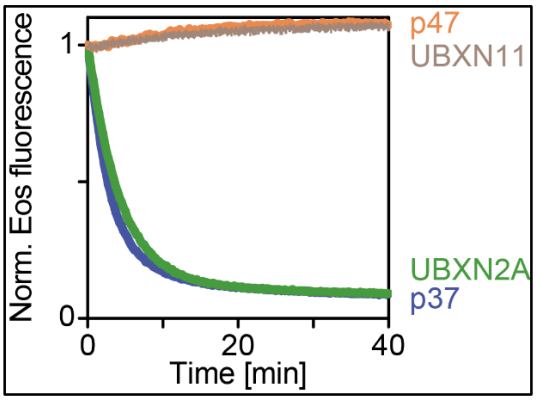

Figure 25: Effect of different SEP domain adapters on p97 mediated unfolding of Eos-I3. While p37 and UBXD4 support unfolding of Eos-I3 by p97, p47 and UBXD5 do not. SPEosI substrate (35 nM), His-p97 (Sf9, 175 nM) and adapter (500 nM) were mixed in a cuvette and incubated at 37°C. After addition of ATP (2 mM) the fluorescence of the "red" Eos (ex. 540 nm, em. 580 nm) was measured over 40 min. While UBXN2A can support unfolding at a comparable rate to p37, this is not the case for p47 and UBXN11.

Since there was no direct connection between the SPI complex and UBXD5 in the literature, a master student in our lab, Alexander Kröning, tested the ability of UBXN11 to bind the SPI complex by pulldown experiments with purified proteins (data not shown, (Kracht et al., 2020)). Pulling on GST-UBXN11 compared to GST-p37 (positive control) or GST (negative control) in the presence of p97 and the SPI complex, showed no significant binding between UBXD5 and any component of the SPI complex.

2.3.1 Effect of the p47 brake motif on the ATPase activity of p97

The p47 adapter contains a sequence (amino acids 69-92, termed "brake motif" from here on) in its N-terminal domain that is unique to p47 and has been shown to inhibit the ATPase activity of p97 in vitro (Zhang et al., 2015). This effect was shown to be reversed at higher concentrations of p47. To assess the effect of a mutant lacking the brake motif on substrate unfolding, the $p47^{\Delta brake}$ mutant was expressed as a GST-fusion protein in bacteria (BL21), and the GST-tag removed after successful purification. The effect of the brake on the ATPase activity of p97 was confirmed by a malachite green ATPase assay (**Figure 26**). Addition of $p47^{wt}$ reduced ATPase activity to about 25%, while addition of $p47^{\Delta brake}$ only lowered activity to around 80%. However, neither the deletion of the brake

motif ($p47^{\Delta brake}$) nor a tenfold increase in the concentration of p47 led to unfolding of SPEosI by p97.

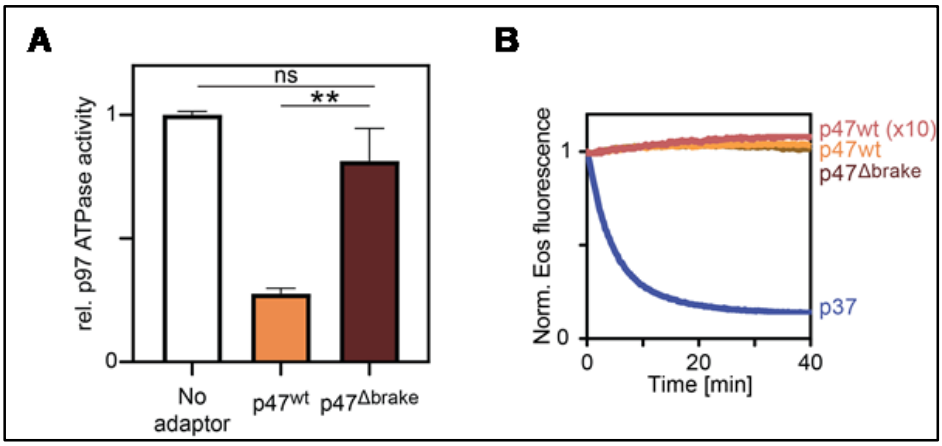

Figure 26: Mutation of the brake motif reduces p97 inhibition but does not support unfolding. A Relative ATPase activity in vitro of p97 without an adapter, with $p47^{wt}$ or with $p47^{\Delta brake}$ measured with the malachite green assay. Removal of the brake motif (69-92) in p47 removes the inhibitory effect of p47 on the ATPase activity of p97. **B** SPEosI substrate (35 nM), His-p97 (Sf9, 175 nM) and adapter (500 nM, 5 µM for p47x10) were mixed in a cuvette and incubated at 37°C. After addition of ATP (2 mM) the fluorescence of the "red" Eos (ex. 540 nm, em. 580 nm) was measured over 40 min. Removal of the brake in p47 does not alter its inability to support unfolding of Eos-I3 by p97. Similarly, a 10-fold increase of p47 does not enable unfolding.

2.3.2 Effect of adapter concentration on the unfolding rate

In the experiments shown so far, p37 was added in excess to avoid a possible limitation. For further detailed analysis, the effect of the adapter concentrations on the unfolding rate was investigated, by varying the concentration of p37 (or UBXN2A) and calculating the initial unfolding rate from the first four minutes. The concentration of p97 was held constant at 400 nM and the substrate at 35 nM. Unfolding reached maximum initial rate at approximately 5 nM of substrate molecules unfolded per minute (**Figure 27**). Interestingly, the maximum unfolding rate was reached at a ratio of roughly 1:1 molecule of p37 per molecule of p97. This is in contrast to previous data reporting p37 (and p47) forming trimers in solution (Zhang et al., 2015), (Yuan et al., 2004). Analogous measurements were done with the UBXN2A adapter, in order to test if the kinetics of the unfolding reaction were similar. Since UBXN2A could not be successfully expressed in bacteria (BL21), it was expressed in insect cells (Sf9). Unfortunately the expression level and yields of UBXN2A was relatively low, which limited the concentration range for this experiment

to up to 275 nM of UBXN2A per 400 nM p97 (**Figure 27**, center panel), below the ratio of 1:1. However, the results closely matched the initial unfolding rates with p37 in the same concentration range (**Figure 27**, right panel).

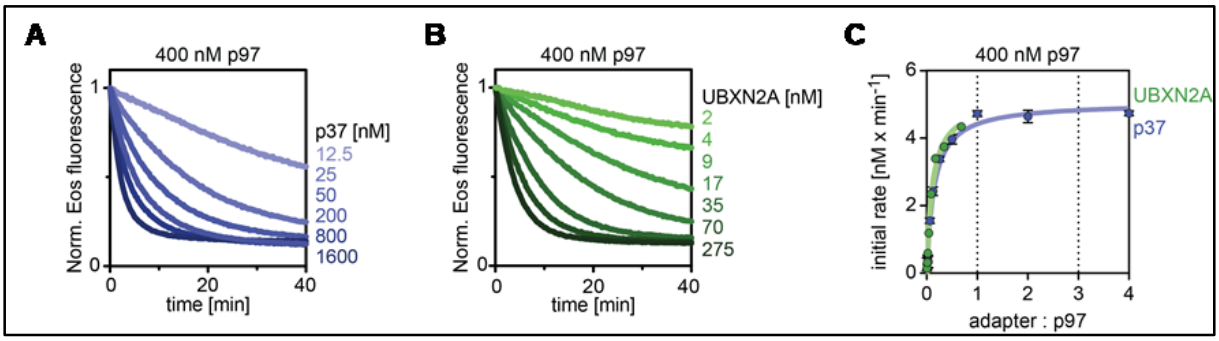

Figure 27: Titration of p37 and UBXN2A adapter concentration. **A** Varying concentrations of p37 (12.5 nm – 1600 nM) were mixed with p97 (400 mM) and SPEosI (35 nM) and incubated in a cuvette at 37°C. After addition of ATP (2 mM) the fluorescence of the "red" Eos (ex. 540 nm, em. 580 nm) was measured over 40 min. **B** Varying concentrations of UBXN2A (2 nM – 275 nM) were mixed with p97 (400 mM) and SPEosI (35 nM) and incubated in a cuvette at 37°C. After addition of ATP (2 mM) the fluorescence of the "red" Eos (ex. 540 nm, em. 580 nm) was measured over 40 min. **C** Initial rates were calculated from the slopes over the first 4 minutes in **A** and **B** and plotted against the ratio of adapter to p97. The maximal initial unfolding rate is achieved at a ration of 1:1 between p37 and p97 hexamer.

2.4 Detailed dissection of differences between p37 and p47 for I3 unfolding associated with SPI disassembly

In order to identify which regions in p37 are critical for substrate unfolding, transplant mutants with the equivalent regions of p47 were generated and tested in the unfolding assay (**Figure 28**). We began by replacing the N-terminal part of p47, upstream of the SEP domain, with that of p37 (**Figure 29 A**). However, the resulting $p47^{p37N}$ mutant did not support unfolding of SPEosI by p97. The converse transplantation $p37^{p47N}$ still supported unfolding, but at a strongly reduced rate. This was likely caused by the inhibition of the p97 ATPase activity by the brake motif which was included in the N-terminal transplantation. Next, we exchanged the SEP domains between p37 and p47, generating $p37^{p47SEP}$ and $p47^{p37SEP}$ (**Figure 29 B**). While $p37^{p47SEP}$ did unfold slightly more slowly than $p37^{wt}$, $p47^{p37SEP}$ like $p47^{wt}$ did not unfold the substrate. Since neither exchange of the N-terminus nor of the SEP domain was successful in enabling the resulting p47 mutant to support unfolding of SPEosI by p97, we tested the effect of exchanging the C-terminus,

including SHP box, UBX domain and the linker inbetween (**Figure 29 C**). The exchange of the p47 C-terminus onto p37, $p37^{p37C}$, did support unfolding, but with a strongly reduced rate. Interestingly, the converse arrangement, $p47^{p37C}$, was able to unfold SPEosI, albeit slowly. While the effect was relatively minor, this was the first p47-based mutant that showed any activity in the unfolding assay. In order to narrow down the critical region, we continued our investigation by dividing the C-terminal region further. Since replacement of the C-terminal region of p37 with the equivalent region of p47 had significantly reduced the unfolding rate, we reasoned that if the UBX domain of p37 was critical for unfolding, then a $p37^{p47UBX}$ mutant would experience the same reduction in unfolding rate. However, the unfolding reaction proceeded even somewhat faster than with the $p37^{wt}$ (**Figure 29 D**). This result suggested, that the linker region between the SHP box and the UBX domain was the critical component. Before we continued with the examination of this linker region, we also tested the effect of transplanting the SEP-SHP region from p47 to p37, because the SHP box had been the last remaining region which had not been exchanged between the two adapters. The generated $p37^{p47SEP-SHP}$ mutant did unfold only slightly slower than the $p37^{wt}$ suggesting that the differences between p37 and p47 in this region were not critical for I3 unfolding (**Figure 29 D**).

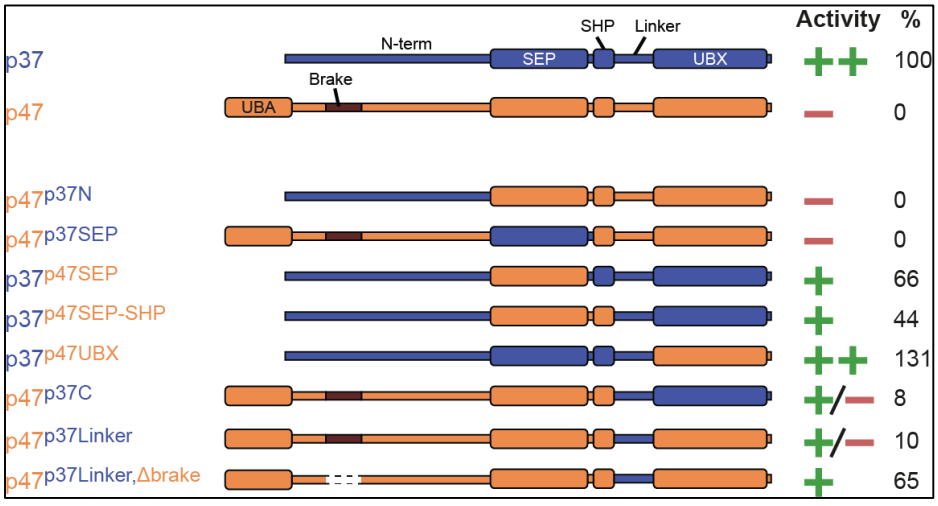

Figure 28: Overview of adapter domain swapping between p37 and p47 and the effect on the relative unfolding rate of p97. Transplanted domains are identifed by color, blue for p37 and orange or p47. The relative unfolding activity was calculated based on the slopes over the first 4 minutes after addition of ATP and classified into four categories: ++ = full activity, + = reduced activity, +/- = strongly reduced activity, - = no unfolding.

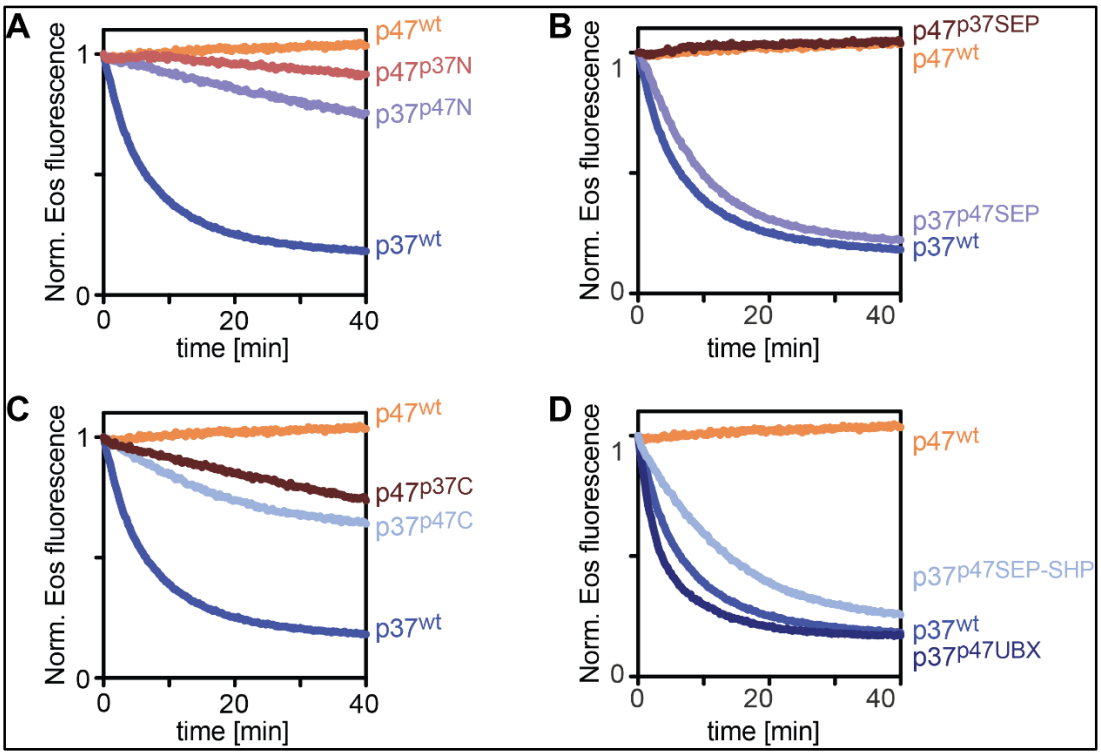

Figure 29: Unfolding of SPEosI by p97 and the different p37/p47 transplantation mutants. SPEosI substrate (35 nM), His-p97 (Sf9, 175 nM) and adapter (500 nM) were mixed in a cuvette and incubated at 37°C. After addition of ATP (2 mM) the fluorescence of the "red" Eos (ex. 540 nm, em. 580 nm) was measured over 40 min. Stepwise exchange of domains show that the C-terminal part of p37 (UBX-domain + Linker) is critical for unfolding.

Next, we generated the $p47^{p37Linker}$ mutant and tested its ability to support SPEosI unfolding (**Figure 30**). The mutant did support a slow but steady unfolding, similar to the $p47^{p37C}$ mutant, establishing the importance of the linker region. As mentioned above, p47 contains an inhibitory "brake" motif in its N-terminal region, which reduces the ATPase rate of p97. We hypothesized that the $p47^{p37Linker}$ mutant was fully capable of mediating the recruitment of the SPI complex and initiated unfolding by p97, but that the N-terminal brake slowed down unfolding. Therefore, an additional p47 mutant was created, which contained the transplanted linker sequence from p37, but lacked the brake motif. This $p47^{p37Linker,\Delta brake}$ variant promoted unfolding at almost the same rate as $p37^{wt}$ (**Figure 30**). Together, these results identified the linker region in p37 as a critical component for SPI unfolding, while the equivalent linker in p47 did not facilitate the process. Transplantation of the p37 Linker and removal of the brake motif in p47 enabled this p47 mutant to support unfolding of SPEosI by p97.

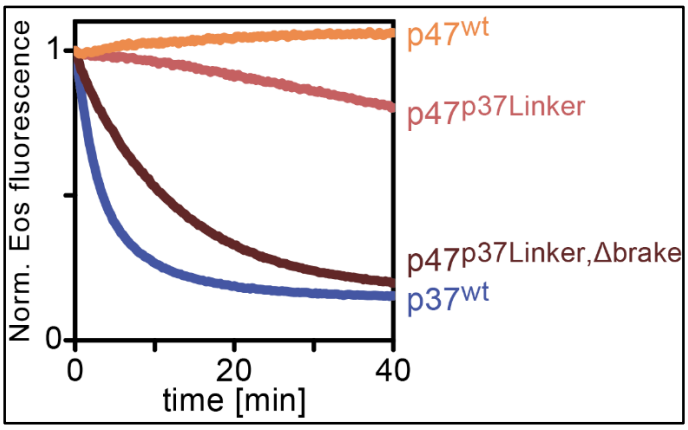

Figure 30: The p37 Linker region between the SHP-box and the UBX-domain is critical for unfolding. Additionally, full activity requires deletion of the brake motif (Δ69-92) in p47. SPEosI substrate (35 nM), His-p97 (Sf9, 175 nM) and adapter (500 nM) were mixed in a cuvette and incubated at 37°C. After addition of ATP (2 mM) the fluorescence of the "red" Eos (ex. 540 nm, em. 580 nm) was measured over 40 min. Transplantation of the Linker between SHP box and UBX domain from p37 to p47 enables p47 to support unfolding of Eos-I3 by p97, albeit at a slow rate. Concomitant removal of the brake motif in p47 leads to an unfolding rate that is comparable to $p37^{wt}$.

2.4.1 Analysis of the SHP-UBX linker

Having identified the importance of the linker region in p37 we continued by investigating if there were specific structural features in said linker, which were responsible for its importance. Since there are no structures of p37 bound to p97 in the pdb, Johannes van den Boom created a model to visualize the position of the linker, using YASARA. This homology model was assembled from three different sources. A homology model of the p37 UBX domain was build based on the UBX domain of Shp1 bound to p97 (pdb: 6OPC). Because this structure did not extend to the SHP box, the p37 SHP sequence was modeled after the SHP box of Ufd1 bound to the p97 N-domain (pdb: 5b6c). The modeled UBX-domain and SHP box were then aligned to structure of p97 in the down-conformation (pdb:5ftk) and connected with energy minimized loops.

This model suggested that the linker consists of two parts (**Figure 31**). The N-terminal part stretches along the N-domain of p97, while the C-terminal part folds into an alpha-helix that interacts with the UBX-domain of p47. Based on this model, two additional p47 mutants were generated, where either the N-terminal part (Link1) or the C-terminal part (Link2) of the linker was transplanted from p37 onto p47. Unfolding was enabled by the Link1, but not the Link2 transplant (**Figure 32**). Conversely, mutating 5 amino acids in the

Link1 region of p37 significantly reduced the unfolding rate, underlining the critical importance of this region.

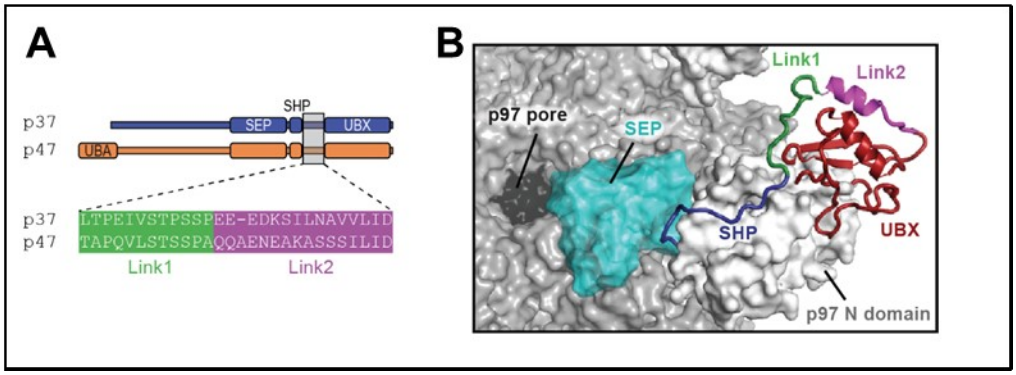

Figure 31: Division of the Linker sequence into Link1 and Link2. A Comparison of the Linker sequence between SHP box and UBX domain in p37 and p47. The partition of the Linker into Link1 (green) and Link2 (purple) is marked. **B** Model of the C-terminal part of p37 bound to p97, based on composite structural data. SHP box (blue), Link1 (green), Link2 (purple) and UBX domain (red) are marked.

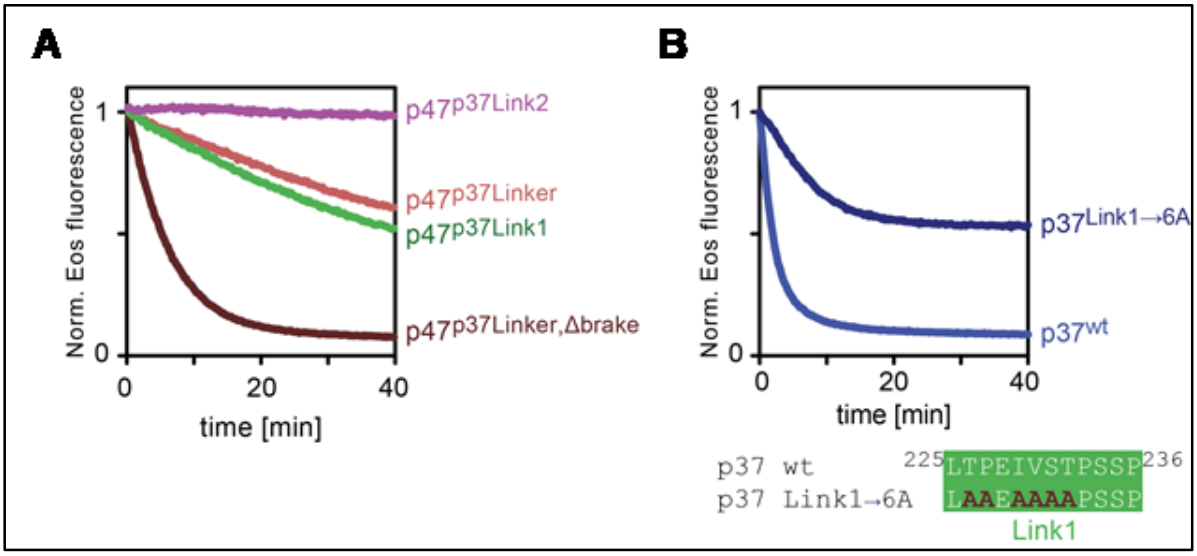

Figure 32: Inserting the Linker1 sequence from p37 into p47 enables unfolding. Conversely, mutation of this region in p37 to alanines significantly reduces unfolding activity. SPEosI substrate (35 nM), His-p97 (Sf9, 175 nM) and indicated adapter variants (500 nM) were mixed in a cuvette and incubated at 37°C. After addition of ATP (2 mM) the fluorescence of the "red" Eos (ex. 540 nm, em. 580 nm) was measured over 40 min. **A** Transplantation of the Link1 sequence from p37 into p47 is sufficient to enable unfolding, while the Link2 sequence has no such effect. **B** Mutation six residues of the Link1 sequence in p37 lead to a reduction of the unfolding rate.

2.4.2 Binding of the SPI complex by p37 is dependent on the SHP-UBX linker

The identification of the Linker as a critical element for successful unfolding raised the question which stage of the process was regulated by the Linker: substrate recruitment, commitment to the pore, or efficient translocation and unfolding. In order to probe for a substrate recruitment, a co-immunoprecipitation experiment was performed with different p47 variants containing p37 transplants. Purified SPI-complex, p97 and adapter (p47 or p37 wt and mutants) were mixed, PP1 immunoprecipitated with a monoclonal antibody and bound proteins detected by Western blot (**Figure 33**). The results showed that $p47^{wt}$ did not bind to the SPI complex. However, transplantation of the Linker from p37 into p47 stimulated binding. Within the Linker region, Link1 was the critical element, while transplantation of the Link2 sequence had no effect. Deletion of the brake motif had had no effect on binding. Conversely, mutation of 6 residues in the Link1 sequence of p37 led to reduced binding to the SPI complex, mirroring the effect in the unfolding assay. Thus, these findings demonstrate that the functional difference between p37 and p47 are caused by distinct linker regions that dictate the ability of the adapter to recruit the substrate SPI complex.

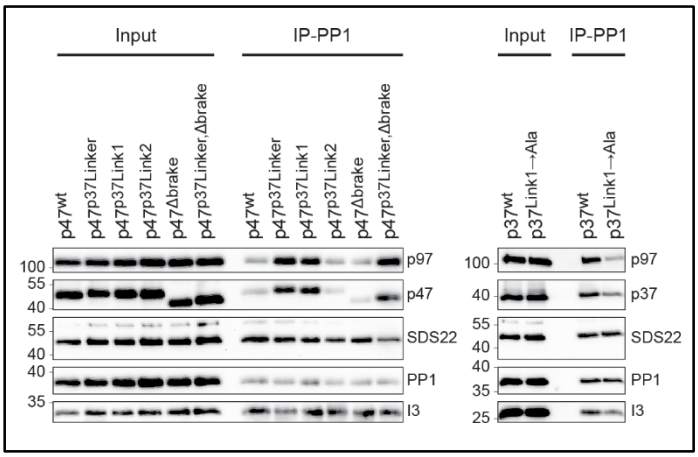

Figure 33: The linker is crucial for binding of the SPI complex by p37. SPI complex (80 nM), p97 (350 nM) and adapter (500 nM) were mixed and PP1 was co-immunoprecipitated with a monoclonal PP1 antibody (sc-515943) and Gammabind G sepharose beads. Input and IP were compared by Western blot. $p47^{wt}$ shows almost no binding towards the SPI complex, compared to $p37^{wt}$. Transplantation of the whole Linker sequence or the Link1 sequence from p37 to p47 enables robust binding of the SPI. The presence or absence of the brake motif has no effect on the interaction between the SPI complex and the adapter. Mutation of the Link1 sequence in p37 reduces the binding to SPI.

2.5 Analysis of the importance of the N-terminal adapter region for SPI unfolding

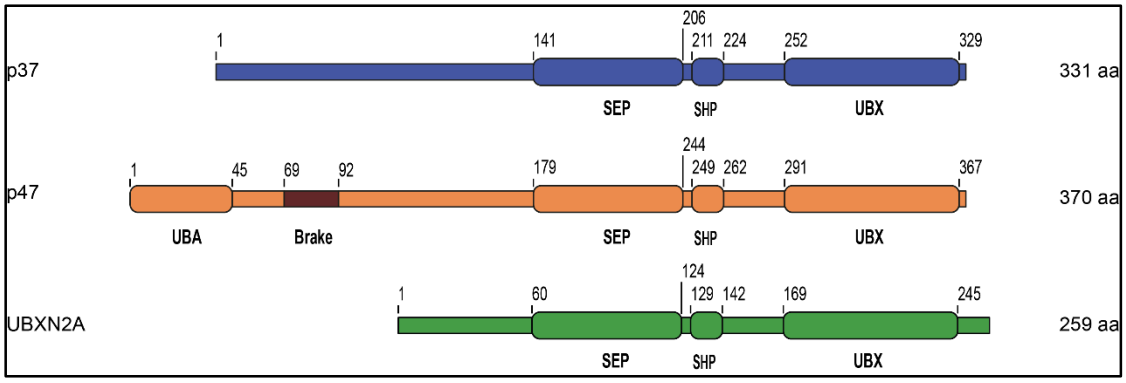

Figure 34: Comparison of the structures of p37, p47 and UBXD4. Schematic representation of the protein sequence with subdomains. The exact boundaries of the proteins domains as well as the position of the N-terminal truncations in p37 are shown.

We continued with our investigation of the structural components of p37 by turning our focus to the N-terminal region. This was of particular interest, because the three adapters p37, p47 and UBXN2A are structurally similar in the C-terminal part of the protein, with a SEP-domain, SHP-box, Linker and UBX-domain, but divergent in the N-terminus (**Figure 34**). Despite this apparent variability, both p37 and UBXN2A supported unfolding of SPEosI by p97 at a comparable rate. Furthermore, p47 also promoted unfolding once the linker was substituted and the brake motif deleted. This suggested that the N-terminus was either dispensable for unfolding or that the relevant elements were conserved in all three adapters.

2.5.1 Effect of N-terminal truncations of p37 on the p97 unfolding rate

We began our investigation of the N-terminus by sequential truncation of the N-terminal region of p37 and testing the variants in the unfolding assay. Three different truncation mutants were generated, $p37^{\Delta 2\text{-}81}$, $p37^{\Delta 2\text{-}107}$ and $p37^{\Delta 2\text{-}129}$. The N-terminus of $p37^{\Delta 2\text{-}81}$ had a similar length to the N-terminus of UBXN2A, which was fully capable to unfold the SPI complex. In the unfolding assay, this mutant did support unfolding of SPEosI, also at a slightly slower rate than $p37^{wt}$ (**Figure 35**). The next truncation mutant, $p37^{\Delta 2\text{-}107}$, showed a significantly stronger abrogation of unfolding efficiency compared to $p37^{wt}$ and $p37^{\Delta 2\text{-}81}$. The removal of the entire N-terminal region up to the SEP domain in the mutant $p37^{\Delta 2\text{-}129}$

led to a complete loss of unfolding activity.

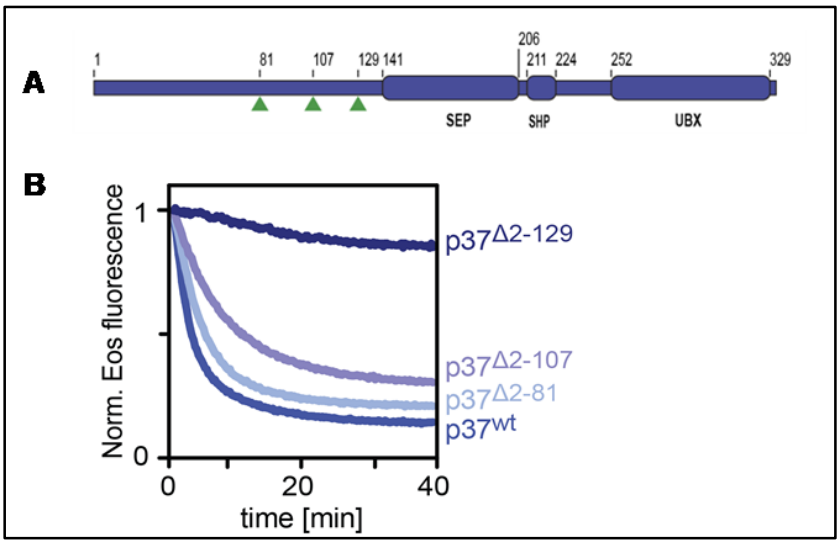

Figure 35: Effect of N-terminal truncations of p37 on unfolding activity. A Schematic representation of the p37 protein sequence with subdomains. The positions of the N-terminal truncations are marked by green arrows. **B** SPEosI substrate (35 nM), His-p97 (Sf9, 175 nM) and p37 or p37 truncation variant (500 nM) were mixed in a cuvette and incubated at 37°C. After addition of ATP (2 mM) the fluorescence of the "red" Eos (ex. 540 nm, em. 580 nm) was measured over 40 min. Removal of the first 81 residues of p37 affects the unfolding rate only marginally. Further removal of the first 107 residues has a stronger effect and removal of the first 129 residues (almost the entire N-terminus) stops unfolding almost completely.

2.5.2 Identification of a conserved N-terminal helix in p37

Next, we aligned the sequences of p37, p47 and UBXN2A with the program ClustalW (https://embnet.vital-it.ch/software/ClustalW.html), to find potentially conserved regions. A short sequence of around 10 amino acids was identified to be conserved in the N-terminal regions, corresponding to residues 84-93 in p37, which was still present in the $p37^{\Delta 2\text{-}81}$ mutant, but was missing in $p37^{\Delta 2\text{-}107}$. This region was then analyzed with the secondary structure prediction program Jpred (https://www.compbio.dundee.ac.uk/jpred/), to detect secondary structure elements. The result predicted that the conserved sequence formed an alpha helix. We reasoned that the helical arrangement of the amino acid side chains in this helix could have a potential significance for the adapter function and used an online tool to project a helical wheel plot of the sequence (**Figure 36**). The projection showed that negatively charged and polar amino acids clustered at one side of the helix, while aliphatic and aromatic amino acids clustered at the opposite side. This spatial division of

amino acids suggested that either the polar or the nonpolar residues could be important for adapter function.

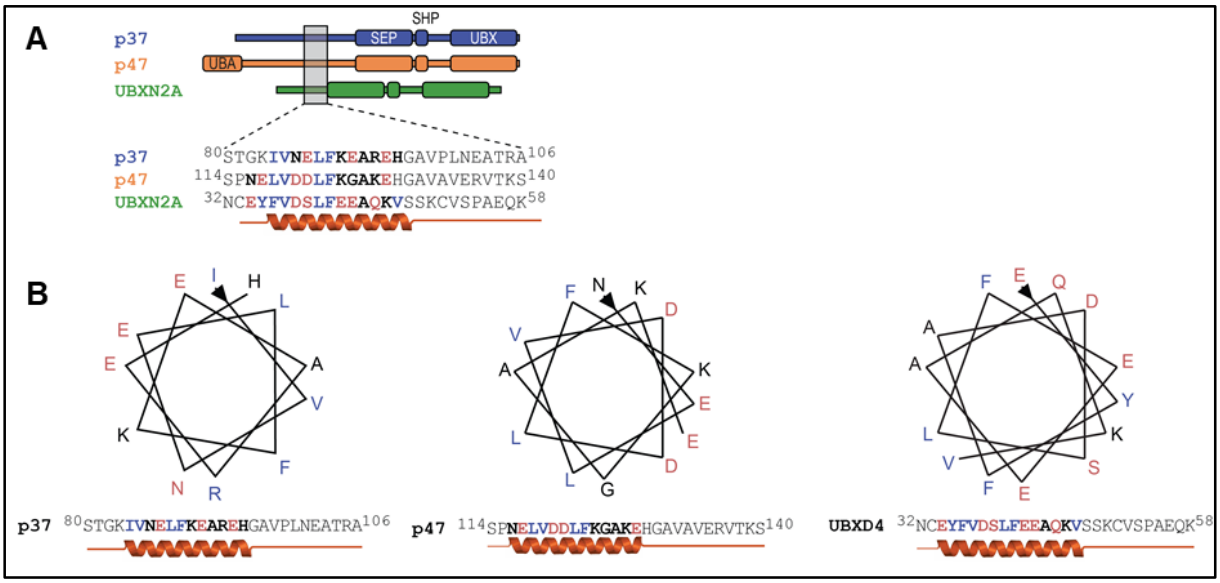

Figure 36: The N-termini of p37, p47 and UBXN2A contain a conserved α-helix. A Schematic representation of p37, p47 and UBXD4 with a detailed display of the putative helix sequence in the N-terminus. **B** Helical wheel plot of the helix sequence in p37, p47 and UBXN2A. Amino acids are colored according to negative charged/polar (red), nonpolar (blue) or else (black).

In order to test the hypothesis that the charge separation in this predicted helix was important for unfolding, three different mutants of p37 were generated. In the first variant ($p37^{helix\ 3E\rightarrow3A}$), all three negatively charged glutamates in the helix were mutated to alanines, which did not carry a charge, but had a high propensity to maintain the helical structure. Conversely, in the second variant four of the nonpolar amino acids of the helix (IVLF) were replaced by alanines ($p37^{helix\ IVLF\rightarrow4A}$). The third variant lacked the residues 84-95 including the entire helix ($p37^{\Delta helix}$). The three mutants were expressed and purified from Bl21 and tested in the unfolding assay (**Figure 37**).

Mutation of the three polar glutamates in the p37 helix to alanines did not affect the unfolding rate in any way compared to $p37^{wt}$ (**Figure 37, A**). However, mutation of the nonpolar residues (IVLF) in the p37 helix to alanines significantly reduced the unfolding rate. This effect was similar to the removal of the helix from p37 ($p37^{\Delta helix}$). Since the helix was conserved between the SEP domain adapters p37, p47 and UBXD4, we reasoned that mutation of the equivalent residues should have a similar effect on the unfolding activity. The “activated” form of p47 with the p37 Linker and without the brake motif

p47$^{\Delta brake+p37Linker}$, was used as a template to mutate hydrophobic residues in the helix region (LVLF→4A). The resulting variant (p47$^{\Delta brake+helix\ LVLF→4A\ +\ p37\ Linker}$) was then tested with the unfolding assay. The mutant showed a significantly reduced unfolding activity, compared to the fully "activated" p47$^{\Delta brake+p37Linker}$, similarly to p37$^{helix\ IVLF→4A}$ (**Figure 37, B**). This showed that the importance of the hydrophobic residues for substrate unfolding was conserved between p37 and p47.

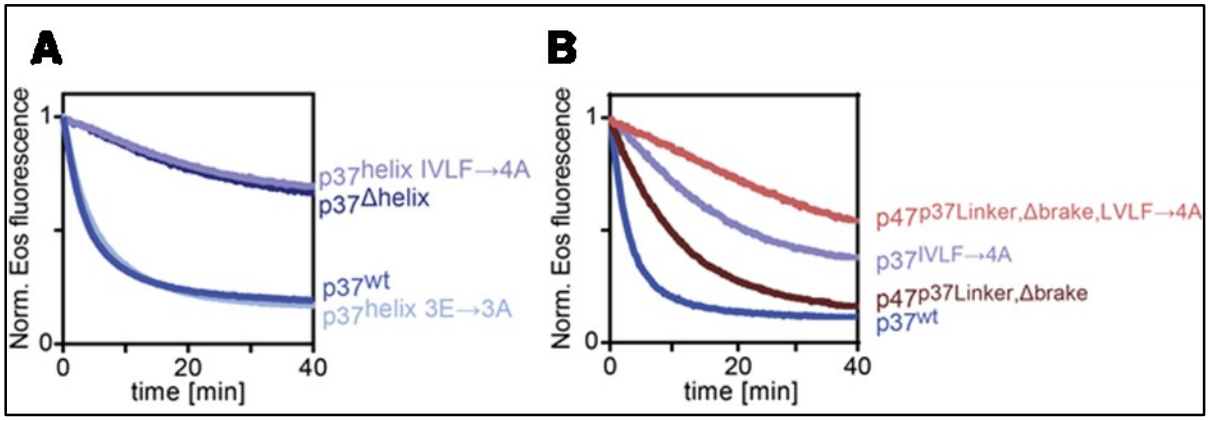

Figure 37: Effect of helix mutation on the unfolding of SPEosI by p97. SPEosI substrate (35 nM), His-p97 (Sf9, 175 nM) and adapter (500 nM) were mixed in a cuvette and incubated at 37°C. After addition of ATP (2 mM) the fluorescence of the "red" Eos (ex. 540 nm, em. 580 nm) was measured over 40 min. **A** Mutation of the polar glutamate residues in the helix of p37 did not affect the unfolding rate. However, mutation of the nonpolar IVLF residues reduced the unfolding rate to the same extent as complete removal of the entire helix. **B** Mutation of the nonpolar LVLF residues in the helix of p47 that was also lacking the brake motif and carried the p37 Linker sequence led to a comparable reduction in the unfolding rate, showing that the function of the helix is conserved between p37 and p47.

2.5.3 The N-terminal helix affects binding of the SPI complex

After the importance of the helix had been established in the unfolding assay, we asked whether its role was in promoting recruitment of substrate or subsequent unfolding. To test a role in binding, a co-immunoprecipitation experiment was done with SPI complex, p97 and different p37 mutants, including N-terminal truncations, helix mutations and p37$^{\Delta SEP}$ as a negative control for binding. SPI complex (80 nM), p97 (350 nM) and p37 variant (500 nM) were mixed, PP1 was pulled down with a monoclonal antibody (Sc-515943) and bound proteins were detected via western blot (**Figure 38**). Comparison of the amount of adapter and p97 pulled down with PP1 with the amount in the input, showed that the removal of the first 81 residues did only slightly affect the binding. A stronger

decrease in binding was observed upon removal of the first 107 residues. Mutation of the negatively charged glutamates in the N-terminal helix of p37 had no effect on binding to the SPI complex. The opposite effect was observed with $p37^{helix\ IVLF\rightarrow 4A}$ which showed a significant decrease in binding of p37 and consequently p97 the SPI complex compared to $p37^{wt}$. The p37ΔSEP was used as a negative control for binding, since Weith et al. had shown that the SEP domain was important for binding of I3 and did only show a very faint binding possibly due to nonspecific interactions.

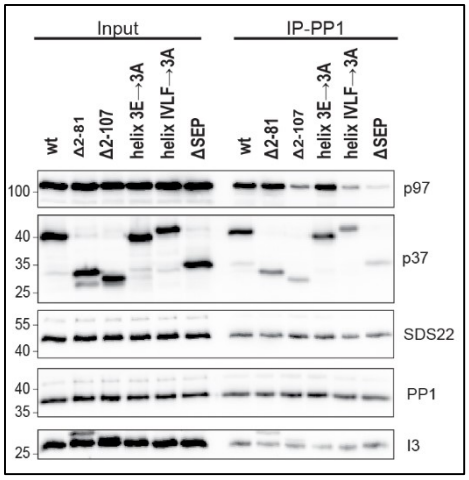

Figure 38: Co-immunoprecipitation analysis of PP1 show that the N-terminal truncations and the helix mutations affect the binding by p37. SPI complex (80 nM), p97 (350 nM) and p37 mutant (500 nM) were mixed and PP1 was co-immunoprecipitated with a monoclonal PP1 antibody (sc-515943) and Gammabind G sepharose beads. Input and IP were compared by Western-blot. Truncation of the N-terminus of p37 had a gradual effect on the ability of p37 to bind the SPI complex. Removal of the first 81 residues retains relative robust binding, while removal of the first 107 resides, which includes the helix, strongly abrogates binding to the SPI complex. Mutation of the nonpolar helix residues had a similar effect, while mutation of the polar glutamates did not reduce binding. The $p37^{\Delta SEP}$ mutant was used as a negative control.

2.5.4 The influence of N-terminal p37 mutations on substrate insertion

The results of the immunoprecipitation binding experiment showed that the effect of mutations on the unfolding rate correlated strongly with the ability to bind the SPI complex. However, we speculated that the mutations might not only affect substrate recruitment, but also affect substrate processing by p97, specifically substrate insertion into the central pore of p97. In order to investigate this hypothesis, we utilized an engineered version of p97, which includes a sensor for insertion close to the entrance of the pore (replacing E314) that could crosslink to a substrate which was inserted into the pore (**Figure 39**, **A**).

This p97 mutant had been generated by Johannes van den Boom by mutating the chosen amino acid to a TAA codon and expressing this p97 mutant in a special strain of BL21, which carried a plasmid coding for a tRNA which leads to translation of TAA to the photocrosslinker amino acid *p*-benzoyl-L-phenylalanine (pBpA). This artificial amino acid crosslinks with other amino acids within a radius of 6 Å after irradiation with low wavelength UV-light (365 nm). The $p97^{E314pBPA}$ mutant thereby traps substrates at the height of the D1 pore, once substrates are successfully positioned at the opening of the pore. The p37 N-terminal truncation and helix mutants were incubated with $p97^{E314pBPA}$ in the presence of the nonhydrolysable ATP analogue ATPγS. After 30 min irradiation with 365 nm, the samples were analyzed by western blot for potential crosslinks of I3 (**Figure 39**, **B**). The results showed that insertion into the pore was unaffected by the removal of the first 81 residues, or by the mutation of the polar residues on the helix but was abrogated by removal of the first 107 amino acids including the helix or mutation of the nonpolar residues on the helix. These results mirrored those obtained in the PP1 co-IP experiment, suggesting that these mutations affected both substrate binding and pore insertion, and that these functions could not be separated by the mutations.

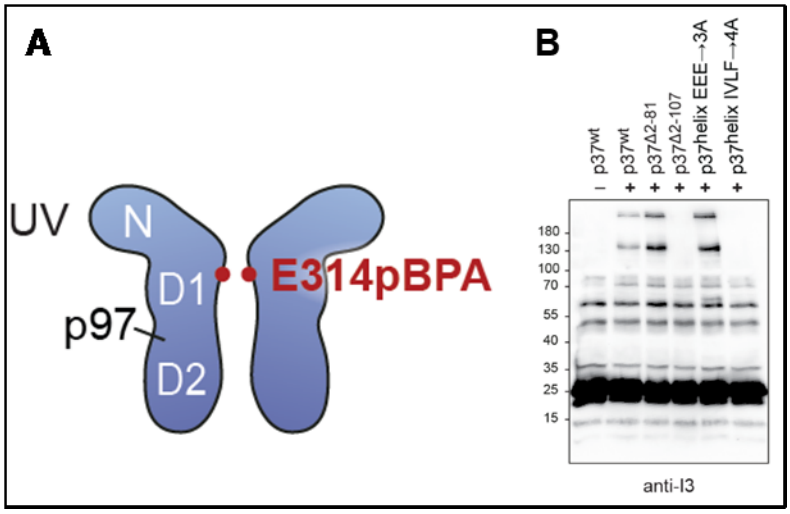

Figure 39: Crosslining of I3 in the D1 pore of p97. A Cartoon structure of $p97^{E314pBpa}$ indicating the position of the sensor for insertion. **B** Crosslinking of I3 in the D1 pore of p97 with the $p97^{E314pBpa}$ mutant shows equivalent result to the co-IP experiments. SPI complex (430 nM), $p97^{E314pBpa}$ (350 nM) and p37 mutant (500 nM) were mixed together with ATPγS (2 mM) and incubated at 30°C for 10 min. Samples were then irradiated with UV-light (365 nm) for 30 min and analyzed by Western-blot. Crosslinks of I3 inside the D1 pore were observed upon UV irradiation in the presence of $p37^{wt}$, $p37^{\Delta 2\text{-}81}$ and $p37^{helixEEE\text{-}3A}$. Loss of the helix ($p37^{\Delta 2\text{-}107}$) or mutation of the nonpolar IVLF helix residues prevented crosslinking in the D1 pore., suggesting a negative effect on substrate insertion.

2.6 Analysis of the spatial orientation of the critical domains of p37 via crosslinks and mass spec

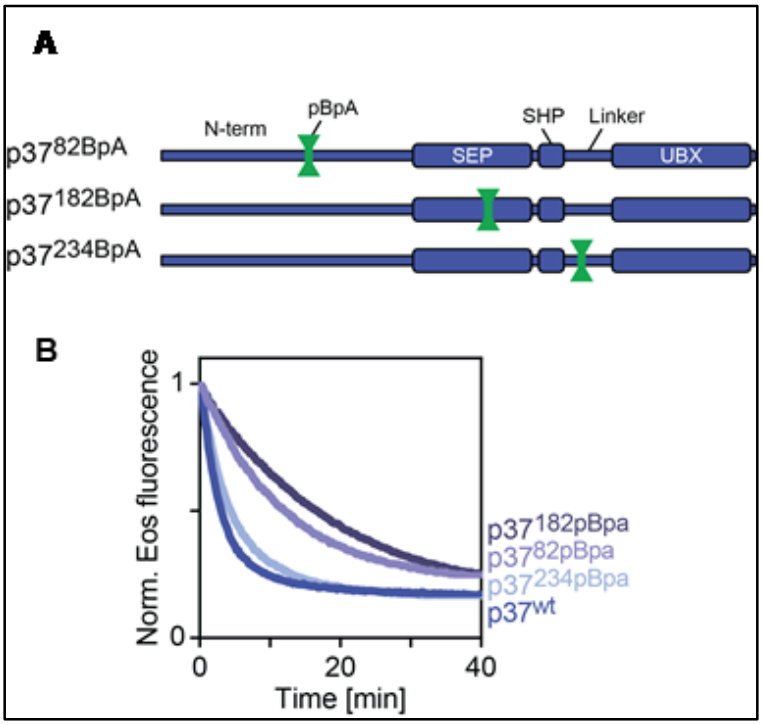

Figure 40: Generation of ^{p37pBpA} crosslinker mutants. A Schematic overview of $p37^{pBPA}$ mutants and the position of the crosslinker amino acid in the protein sequence. **B** SPEosI substrate (35 nM), His-p97 (Sf9, 175 nM) and $p37^{pBpa}$ mutant (500 nM) were mixed in a cuvette and incubated at 37°C. After addition of ATP (2 mM) the fluorescence of the "red" Eos (ex. 540 nm, em. 580 nm) was measured over 40 min. Insertion of BPA crosslinking amino acid in select positions enables identification of binding partners and does affect unfolding rates only slightly.

Unlike ubiquitinated substrates of p97, which have ubiquitin as a recognition signal, it is unclear how the SPI complex is recognized by p37 and p97 and how inhibitor-3 is selected as the target for unfolding. The previous experiments identified several important regions in the p37 adapter necessary for substrate binding and unfolding. We chose to utilize the pBpa-based photocrosslinking strategy, used above, to investigate substrate crosslinking into the p97 pore, to detect which subunits of the SPI complex were in proximity to certain parts of the p37 adapter. Previous work by Weith et al. had used $p37^{F89pBpa}$ and $p37^{L182pBpa}$ to probe for specific subunit interactions with the N-terminus (F89pBpa) respectively the SEP domain (L182pBpa). They had found a crosslink between SEP domain and inhibitor-3, while the N-terminal position did not show any crosslinks to any subunit of the SPI

complex. Incidentally, the phenylalanine replaced by the pBpa photocrosslinker in the F89pBpa mutant was one of the critical residues in the p37 helix (IVL**F**), whose mutation did negatively affect binding and unfolding. This suggested that the lack of detectable crosslinks might by caused by the inability of the $p37^{F89pBpa}$ mutant to mediate binding of the SPI complex. Therefore, a new crosslinking mutant was created to probe for interactions with the N-terminal region of p37, in particular the putative helix. The glycine at position 82 upstream of the helix was chosen and replaced with TAA codon to incorporate the crosslinker. In addition, another p37 mutant was generated, which carried a photocrosslinker in the linker between the SHP box and the UBX domain ($p37^{S234pBpa}$). Before performing crosslinking experiments with these mutants, all three available variants (82, 182, 234) were tested in the unfolding assay to confirm that the introduction of the pBpa did not prevent unfolding of the SPI complex by p97 (**Figure 40**). Both $p37^{G82pBpa}$ and $p37^{L182pBpa}$ caused a reduction of the unfolding rate compared to $p37^{wt}$ but did not abrogate unfolding. The $p37^{S234pBpa}$ variant harboring the crosslinker in the SHP box-UBX domain linker promoted unfolding with the same rate as $p37^{wt}$. We proceeded with the crosslinking experiment, by mixing p97 (175 nM), SPI complex (215 nM) and p37 pBpa mutant (250 nM) together with ATPγS and incubating for 10 min at 30°C before 30 min of crosslinking (365 nm). Afterwards the samples were analyzed by western blot with antibodies against all individual components (**Figure 41**). We confirmed that the L182pBpa positioned in the SEP domain crosslinked with inhibitor-3 (Weith et al., 2018). In addition, the N-terminal position close to the putative helix (G82pBpa) also showed a crosslink with inhibitor-3. Finally, the linker position (S234pBpa) crosslinked with PP1. None of the three probes showed any crosslink with SDS22. Furthermore, both $p37^{G82pBpa}$ and $p37^{S234pBpa}$ showed multiple crosslinks with other p37 molecules, as well as crosslinks with p97.

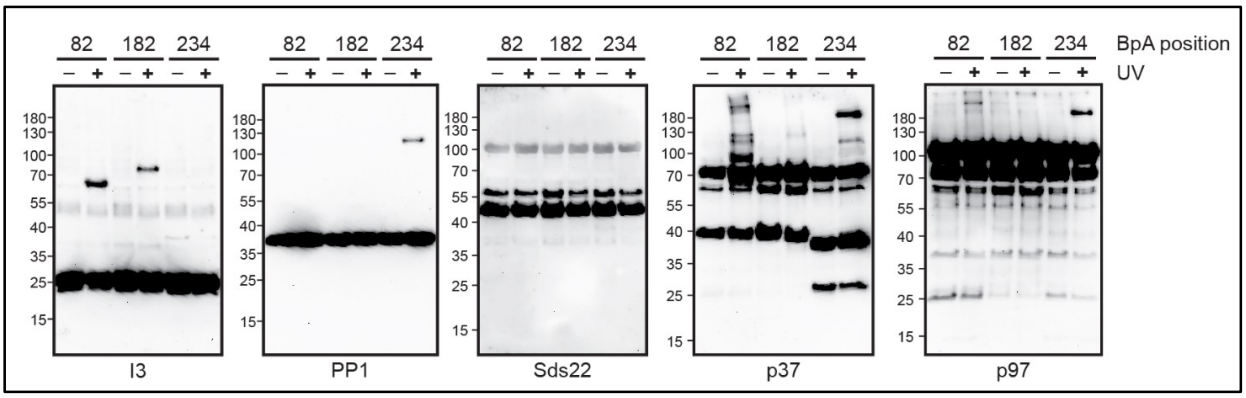

Figure 41: Crosslinking of p37 BPA mutants with parts of the SPI complex and p97. SPI complex (215 nM), p97 (175 nM) and $p37^{pBpa}$ mutant (250 nM) were mixed together with ATPγS (2 mM) and incubated at 30°C for 5 min. Samples were then irradiated with UV-light (365 nm) for 30 min and analyzed by Western-blot. The results showed crosslinks with I3 from the helix (82) and SEP domain (182) crosslinker, as well as a crosslink between PP1 and the Linker (234). No crosslinks could be observed with SDS22. Multiple unidentified crosslinks were observed with between p37 and between p37 and p97.

To further characterize which regions of inhibitor-3 or PP1 interacted with p37, crosslinking samples were analyzed by mass spectrometry in cooperation with the analytics core facility of the University Duisburg-Essen. The crosslinking samples were digested with trypsin and the resulting peptides were subjected to GC/MS analysis. No peptides could be identified for the $p37^{82pBpa}$ crosslinking, possibly due a low signal to noise ratio. Three peptides were identified in the crosslinking sample of $p37^{182pBpa}$ (**Figure 43**). Two were crosslinks with other parts of p37, either internally or with other p37 molecules. The third peptide was based on a crosslink to the N-terminal part of inhibitor-3 (residues 32-39). Analysis of the $p37^{234pBpa}$ peptides revealed two crosslinks to two positions in PP1, one on the N-terminus (residues 7-20) and the other at the C-terminus (residues 315-139) (**Figure 42**). None of the mass spectrometry measurements identified a single crosslink towards SDS22, consistent with the result of the crosslinking western blots (**Figure 41**).

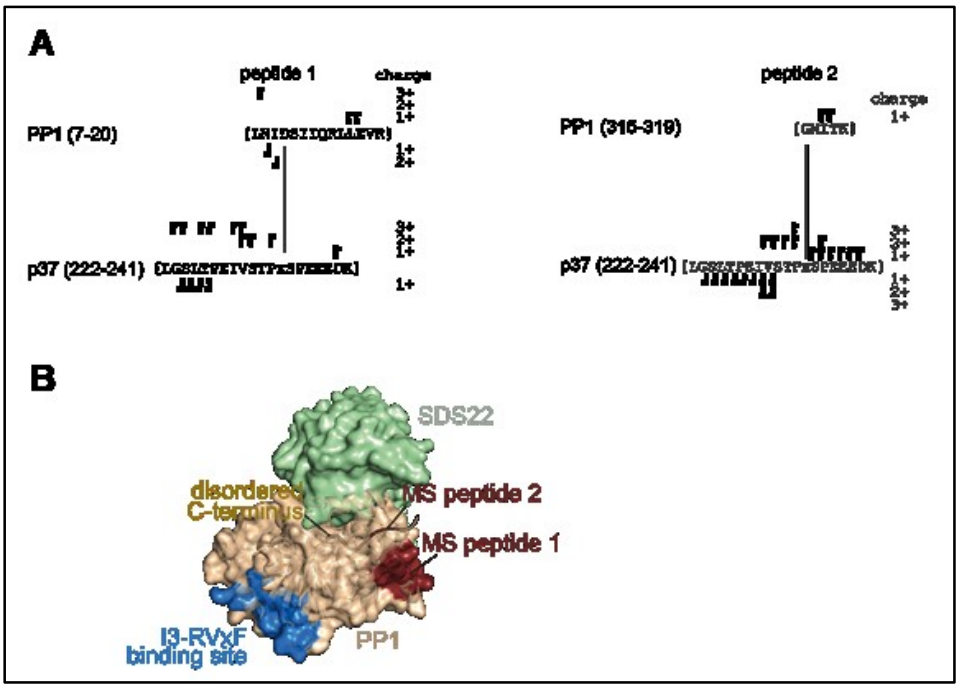

Figure 42: Crosslinking mass spec identified two peptides from PP1 that crosslinked to p37^{234pBpa}. A Peptide 1 was identified to stretch between residues 7-20, while peptide 2 is situated at the C-terminus of PP1 (residues 315-319). The chevrons indicate the length of the identified peptide fragments. The connecting line does not denote the exact position of the crosslink. **B** Model of PP1γ (orange) with bound SDS22 (green) and indication for I3 binding site (RVxF, blue) showing the putative positions of the crosslinked peptides 1 (red) and 2 (orange).

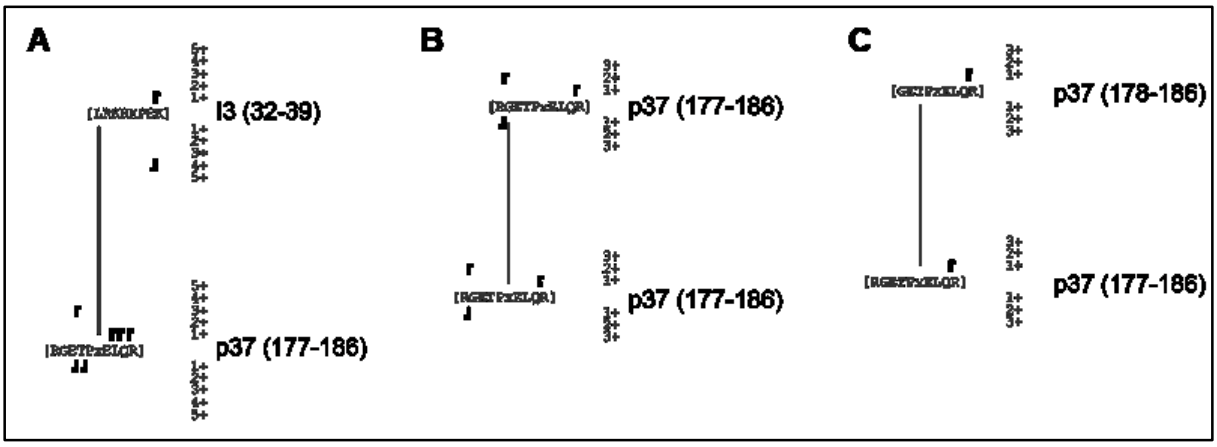

Figure 43: Additionally identified peptides between p37^{182pBpa} and I3, respectively other p37^{182pBpa} molecules in crosslinking mass spec. The chevrons indicate the length of the identified peptide fragments. The connecting line does not denote the exact position of the crosslink. **A** Crosslink between p37^{182pBpa} and I3 close to the N-terminus of I3 (residues 32-39). **B** and **C** crosslinks between p37^{182pBpa} and other p37 molecules.

3 Discussion

3.1 Disassembly of the SPI complex by p97 and p37 involves unfolding of I3

The p97 protein is fundamentally dependent on adapter proteins to recruit and process substrates. Effort have therefore been made to understand how the different types of adapter proteins interact with p97 and its substrates. Recent advances have been focused on the function of the Ufd1-Npl4 adapter, which serves as the main adapter for ubiquitinated substrates (Blythe et al., 2017; Bodnar and Rapoport, 2017; Twomey et al., 2019b). These studies showed that the Ufd1-Npl4 adapter guides an already partially unfolded ubiquitin chain into the central pore of p97 at the D1 domain, where it is translocated and released at the end of the D2 domain. In contrast, the function of the SEP domain adapter proteins, which include the most abundant p97 adapter p47, has been less well understood. While cellular functions for p47 and p37 in p97 dependent membrane fusion have been identified, further investigations were limited by a lack of known substrate. The discovery by our group that the SDS22-PP1-I3 (SPI) complex is a direct target of p97 and that its disassembly by p97 depends on SEP domain adapter proteins (Weith et al., 2018) enabled us to conduct a detailed investigation of SEP domain adapter function. A central question has been if disassembly of the complex occurs on the surface of p97 or if disassembly involves unfolding of one or more subunits.

This study proved the latter model. We established a fluorescence based unfolding assay to study the fate of I3 during SPI complex disassembly, by fusing the Eos reporter protein to the N-terminus of I3. Incubation of the SPEosI substrate with recombinant p97 and p37 resulted in rapid loss of fluorescence after addition of ATP. This demonstrated that SPI-complex disassembly involves unfolding of I3. This result was consistent with the experiments from (Weith et al., 2018) which showed that I3, but not PP1 or SDS22 could be crosslinked in the pore (pBpA crosslinks in the D1 or D2 domain) of p97 upon incubation of SPI complex with $p97^{pBpA\ D1\ or\ D2}$ and p37. Importantly, crosslinks in the D2 domain depended on the addition of ATP, which suggested that unfolding involved translocation of I3 through the central pore in a D1→D2 direction, similar to the ubiquitin substrates. This mode of complex disassembly by substrate unfolding through one directional translocation appears to be a general feature of AAA+ ATPases. VPS4 disassembles ESCRT-III polymers by “walking” along the peptide chain, with the six

subunits forming a spiral staircase (Monroe et al., 2017). Similar mechanisms have been found for the disassembly of SNAREs by NSF (White et al., 2018) and for substrate unfolding by the proteasome (Peña et al., 2018).

An open question that remains is how unfolding of I3 causes the entire SPI complex to disassemble including SDS22. While we identified interaction sites between the p37 adapter and I3 as well as PP1 in this study, no direct interaction with SDS22 could be found. It is possible that pulling of p97 on I3 causes SD22 to disassociate from PP1 through an allosteric mechanism. Another interesting hypothesis which has been proposed is based on the fact that binding between PP1 and SDS22 depends on the metal loading state of PP1 (Choy et al., 2019). In this model, loading of a metal ion into the M1 metal binding site of PP1 causes the dissociation of SDS22 from PP1. Whether this mechanism is involved in SPI complex disassembly by p97 needs to be studied further.

3.2 SPI disassembly and I3 unfolding is ubiquitin-independent

A large fraction of substrates of p97 are ubiquitinated and recognized by p97 adapter proteins through dedicated ubiquitin binding domains (UBA, UIM, NZF) which are present in the majority of p97 adapter proteins. Thereby, ubiquitin functions as a universal recruitment signal which enables processing by p97 without any specific binding sites on the substrate protein (Meyer et al., 2002). This recruitment strategy also enables regulation of p97 unfolding of these substrates by E3 ligases and DUBs. In the case of the Ufd1-Npl4 heterodimer, which is the major adapter protein for the recognition of K48-linked ubiquitin chains, the Rapoport group showed that substrate binding required a chain length of at least five ubiquitins (Bodnar and Rapoport, 2017). In addition, they proposed that substrate release from p97 after unfolding requires trimming of the ubiquitin chains by a DUB. Further work from the same group on the structure of the Cdc48-Ufd1-Npl4 complex showed that the Npl4 adapter is crucial in guiding the already partially unfolded ubiquitin chain into the central pore of p97 (Twomey et al., 2019b).

Prior studies on the SEP domain adapters suggested that SEP domain adapter-dependent unfolding reactions are independent of substrate ubiquitination. The yeast *S. cerevisiae* contains only one SEP domain protein, Shp1 with a ubiquitin binding UBA domain at the N-terminus, while humans harbor four SEP domain proteins. Of these, only

p47, which is the closest homologue of Shp1, contains a UBA domain, while p37, UBXN2A and UBXN11 lack any ubiquitin binding domains or activity. Interestingly, the sole SEP domain protein of the nematode *C. elegans*, UBXN-2B, lacks the UBA-domain, suggesting that ubiquitination may be dispensable for the function of SEP domain adapter protein in higher organisms. This hypothesis has been supported by observations about the effect of p47 and p37 on p97-dependent postmitotic Golgi cisternae reassembly *in vitro*. While both p47 and p37 were able to support this reaction, p47 was (a) dependent on the presence of its UBA domain, was (b) inhibited by a mutant form of ubiquitin that prevented binding and was (c) further dependent on the activity of the deubiquitinating enzyme VCIP135 (Wang et al., 2004). In contrast, p37 showed no dependency on ubiquitination (Uchiyama et al., 2006). However, the lack of a clearly identified substrate precluded a conclusion about the exact role of ubiquitin (or lack thereof) in SEP domain adapter dependent function of p97.

The discovery of the SPI-complex as a substrate whose processing by p97 was dependent on SEP domain adapters allowed us to further investigate this important question. Of note, SPI disassembly could be observed in cells lacking the only ubiquitin-binding SEP domain adapter p47 (Weith et al., 2018). Of note, SPI disassembly could be observed in cells lacking the only ubiquitin-binding SEP domain adapter p47 (Weith et al., 2018). Crucially, the fact that I3 unfolding associated with SPI disassembly is completely independent of ubiquitination could be conclusively demonstrated by the full reconstitution of the reaction from purified proteins that was achieved in this study (Weith et al., 2018), (Kracht et al., 2020). Of note, the proteins used in the reaction were purified to homogeneity. Moreover, the reaction lacked any ubiquitin or ubiquitination machinery. Lastly, there is no evidence that SPI components were ubiquitinated when purified from insect cells. Even possible traces of ubiquitination below the detection limit would not explain the quantitative unfolding of I3 in the reaction. Moreover, the reactions were efficient with the adapters p37 or UBXN2A that lacked ubiquitin-binding domains. Thus, a protein substrate can be targeted for p97-mediated unfolding in the absence of ubiquitination. While our data is conclusive with regard to the basic targeting and commitment activity within the reaction, they do not exclude that ubiquitination may be involved in regulating the process in the cell. The fact that all SEP domain adapters contain a ubiquitin-related UBX domain indicate the evolutionary decent from the ubiquitin

system. Another indication is that p47 in fact contains a UBA domain, even though it is not essential for the unfolding of SPI. Moreover, in analogy to the p97-Ufd1-Npl4 complex, p97-p37 or p97-UBXN2A complexes may associate with additional accessory factors such as FAF1 or FAF2/UBXD8 that contain ubiquitin-binding domains and may enhance recruitment of ubiquitinated substates. Of note, the following substrate commitment step would remain independent of ubiquitin and may even require the removal of ubiquitin by deubiquitinating enzymes as shown for p47 and VCP135 (Wang et al., 2004). Further work is required to explore the possible role of ubiquitination in unfolding reactions governed by SEP domain adapters.

3.3 Substrate recognition by p37 is multivalent

The lack of ubiquitin as a substrate recognition signal necessitates (a) that the adapter protein can recognize the substrate via specific binding site(s) and (b) that, since SPI-complex disassembly does involve unfolding of I3 but not PP1 or SDS22, the adapter has to control the orientation and processing of the complex to only unfold the intended substrate. This study demonstrates that the p37 adapter interacts with the SPI complex through a multivalent binding interface, where both the direct unfolding target I3 and its binding partner PP1 are recognized by different elements of the adapter. Previous work implicated the SEP domain in recognition of I3 (Weith et al., 2018). Deletion of the SEP domain abrogated the interaction with the SPI complex. Moreover, genetically encoded pBpA a position 182 in the SEP domain crosslinked with I3 suggesting that the SEP domain interacted directly with the I3 substrate prior to unfolding.

This study extended the previous analysis. Firstly, we identified a region N-terminal of the SEP-domain in p37, whose deletion abrogated I3 unfolding. Bioinformatic analysis showed that this region was conserved in p47 and UBXN2A and predicted to adopt a helix with a conspicuous separation of polar and nonpolar amino acids to either side of the helix. Mutation of the nonpolar helix residues abrogated the unfolding rate to the same extend as complete removal of the entire helix. A comparable effect on unfolding was observed with the activated p47 mutant $p47^{\Delta brake + helix\ LVLF \rightarrow 4A + p37Linker}$.The reduction in unfolding rate was also reflected in a reduction in binding of the SPI complex in co-immunoprecipitation experiments, as well as a reduction substrate insertion in the D1 pore

monitored by pBpA crosslinks. Closer inspection of the binding site of the helix on the SPI complex with a pBpA mutant at position 82 revealed an interaction with I3. Of note, a recent study (Conicella et al., 2020) independently identified the same helical region as an intramolecular interaction partner of the SEP domain in p47, using NMR in the absence of substrate. This suggests that both regions bind I3 cooperatively. Second, we identified the linker between SHP box and UBX to be critical for SPI interaction by directly binding to the PP1 catalytic subunit. We first noted this fact by comparing the structural elements of p37 and p47 required for I3 unfolding: it was sufficient to transplant this Linker from p37 to p47 to render p47 active in promoting I3 unfolding. This correlated with the ability of p47 to bind the SPI. Conversely, mutation of the Linker in p37 abrogated binding of SPI and unfolding of I3. Further analysis of the role of the linker using the pBpA approach revealed that the Linker bound to the PP1 subunit. Thus, the Linker dictates substate specificity for the SPI complex. It is important to note that mutation of either of the binding sites in p37 largely reduced interaction of the SPI complex suggesting that all sites bind cooperatively. This likely ensures that the individual subunits are only bound in the SPI complex, which prevents futile unfolding of free I3 which is supported also by the fact that I3 is neither bound nor unfolding. The two interaction sites in the p97-p37 complex have important implications for how the whole complex orientated and specifically the substrate is positioned for subsequent engagement in the p97 pore. The position of the C-terminal part of SEP domain adapters on p97 is know from crystal structures of p47 bound to p97 N-domain. The tight association of the C-terminal SHP-box and UBX-domain of the adapter to the N-domain of p97 fixes the SHP-UBX linker which interacts with PP1 in close proximity to the N-domain. This suggest that PP1 is held a distance of the pore. Structures including the SEP domain and the N-terminus are not available. Therefore, the position of the N-terminal part of p37 on p97 is not known. However, data from crosslinking experiments by Johannes van den Boom suggest that the N-terminus of p37 is close to the central pore of the p97 hexamer (Kracht et al., 2020) (**Figure 44**). An pBpA inserted by amber codon suppression at position 278, right at the entrance of the pore of p97, crosslinked with the N-terminus of p37. This suggests that, when SPI is bound, the I3 subunit is positioned close to the pore of p97.

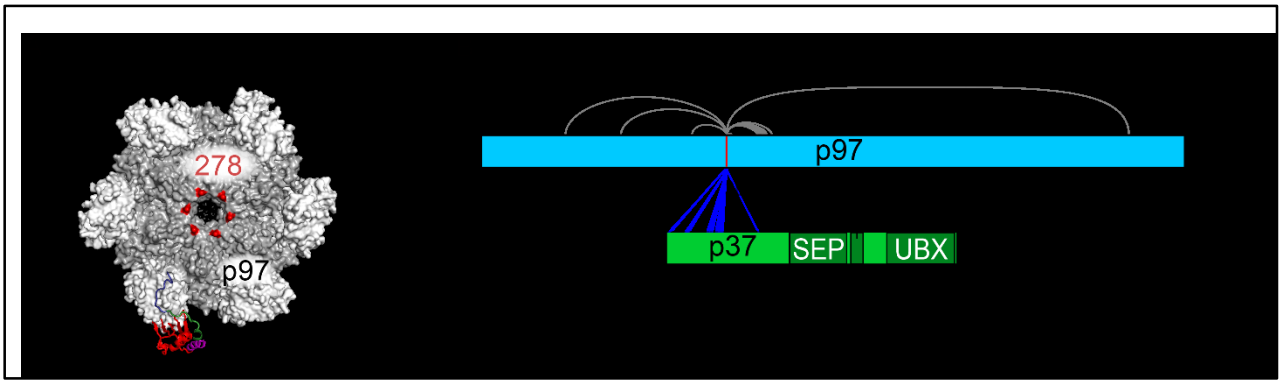

Figure 44 Crosslinks between a pBpA at position 278 of p97, close to the entrance of the central pore and p37, show that the N-terminal part of p37 is close to the pore (data from Johannes van den Boom, (Kracht et al., 2020)).

Based on these findings, we propose a model, in which the SPI complex is recognized via three binding sites on the p37 adapter that control its position relative to the pore of p97 (**Figure 45**). The N-terminal helix together with the SEP domain bind I3 close to the opening of the D1 pore, which primes the I3 subunit to be unfolded. This could be further supported by the lack of additional p97 interaction sites in the N-terminal part of the adapter which might render the exact position of this region more flexible. The linker at the C-terminal end of the adapter between SHP box and UBX domain is comparably fixed in its location and binds PP1 at a safe distance to the pore, thereby preventing its unfolding.

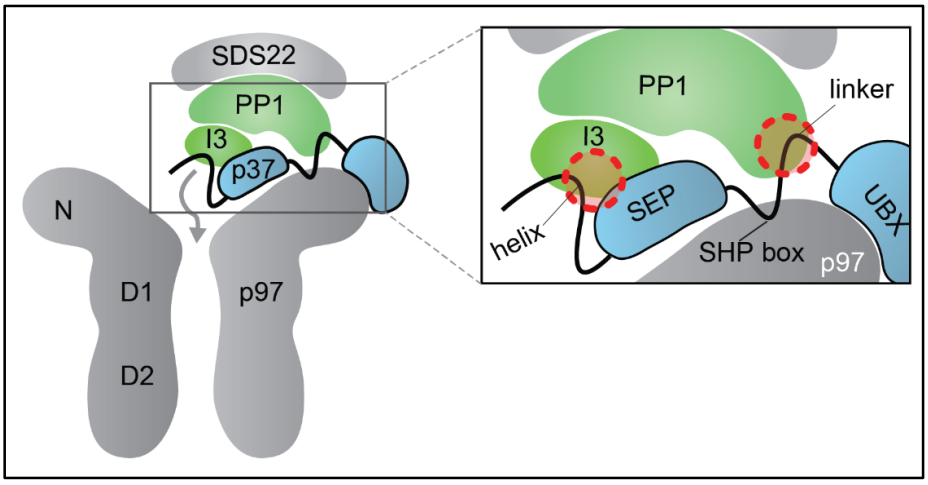

Figure 45 Model for the interaction between the SPI-complex, the p37 adapter and p97. The adapter binds to the N-domain of p97 through the SHP-box and the UBX-domain. The SEP domain and the N-terminal helix bind I3 and position it close to the pore of p97 in order to be unfolded, while PP1 is bound by the linker between the SHP-box and UBX-domain and kept safe from being unfolded (Kracht et al., 2020).

3.4 Stoichiometry of p97 and adapter in the unfolding reaction

Since every protomer of the p97 hexamer contains binding sites for adapter proteins, it could be theoretically possible that up to six adapters bind to one hexamer. However, the number of adapters concurrently binding to p97 is unclear. When the association of p47 with p97 was first discovered (Kondo et al., 1997), it was speculated that p47 forms a trimer when binding to p97, based on the apparent size during size exclusion chromatography. Yuan et al. hypothesized that p47 forms trimers in solution, based on crosslinking experiments (Yuan et al., 2004). Zhang et al. compared the effect of p47 and p37 on the ATPase activity of p97 and hypothesized that activation of p97 by these adapters depends on their trimerization (Zhang et al., 2015). In their model, p37 forms a trimer at low concentrations and thus is able to activate p97, while p47 is in a monomeric state at low concentrations, which instead inhibits the ATPase activity of p97 via its brake motif. At higher concentrations p47 supposedly forms a trimer, which alleviates the inhibition. Conicella et al. (Conicella et al., 2020) investigated the oligomerization state of p47 as well as its association with p97 ND1 in detail, using a multitude of biochemical methods including NMR, size exclusion chromatography and dynamic light scattering. Their data showed that p47 was a monomer in solution and that the apparent size in gel filtration chromatography did not correspond to a trimer. Additionally, they identified a second SHP-box in the N-terminus of p47, upstream of the SEP domain. Since only one SHP-box can bind to the respective binding site on a p97 protomer, they hypothesized that the UBX-domain and the C-terminal SHP-box bind to one p97 protomer and the N-terminal SHP-box binds to a neighboring protomer, which limits the possible number of concurrently binding p47 proteins to a maximum of three.

These studies focused on the conformation of p47 in solution and its binding to p97. We used the unfolding assay for a functional evaluation of the adapter to p97 ratio. Systematic variation of the concentration of p37 or UBXN2A in the unfolding assay showed that the initial reaction rate was not improved beyond a ratio of adapter to p97 hexamer of 1:1. This result concurs with the observed ratio of one Ufd1-Npl4 heterodimer binding the p97 hexamer and being sufficient to unfold a ubiquitinated substrate.

3.5 A function of the adapter in substrate insertion?

The function of adapter proteins for the unfolding of p97 substrates is thought to consist of two steps, substrate recruitment and commitment. The former describes the binding of substrate molecules by the adapter proteins through substrate specific interaction sites (e.g. ubiquitin binding domains for ubiquitinated substrates). In contrast, commitment entails insertion of the substrate into the p97 pore which leads to unfolding. While substrate recruitment through adapter proteins is relatively well understood, the function of adapter proteins for commitment has remained elusive. Evidence obtained from cryo-EM structures of the Cdc48-Ufd1-Npl4 complex unfolding a ubiquitin substrate showed that the Npl4 adapter seemed to partially unfold part of the bound ubiquitin chain before insertion into the p97 pore (Twomey et al., 2019b), implicating the adapter as important for commitment. It has been unclear, if similar the SEP domain adapters include a similar functionality. Based on evidence from Weith et al. and from this study we were able to identify the relevant adapter domains for substrate recruitment. Attempts to delineate a possible function of the adapter for substrate commitment from recruitment has so far been unsuccessful. Crosslinking of inhibitor-3 in the p97 pore with $p97^{314pBpA}$ showed that any observed reduction of crosslinks when using a p37 mutant was proportional to the reduction in substrate binding caused by this mutation. Although these experiments were not exhaustive, this finding could indicate that binding and insertion of the substrate are coupled. Recent structural analysis of adapter and substrate-bound p97 complexes (Cooney et al., 2019), (Twomey et al., 2019b) demonstrate that the p97 hexamer adopts a staircase configuration. This conformation arises from the position of the six protomers of the p97 hexamer which are arranged in a staircase. Hydrolysis of ATP in the D2 domain of the lowest protomer in the staircase causes this protomer to disengage from the substrate and reengage at the top of the staircase. This mechanism causes the poreloops in the D2 domain to push the substrate downwards relative to the hexamer. Since this conformation has not been observed in structures containing only p97 by itself, it is possible that this configuration is induced by the adapter and the substrate bound to the adapter. Moreover, it is conceivable that the staircase configuration facilitates the insertion of the substrate because it opens the pore and makes the pore loop more accessible at least of the upper protomer. In this case, it is interesting to know whether the adapter binds first to p97 and prepares p97 for substrate interaction. Alternatively, the adapter

could first form a complex with the substrate that then binds p97. Further structural analysis is required to understand how this binding then induces the staircase configuration.

An interesting additional question in this context is which element of the substrate is inserted into the pore. Twoney and colleagues (2019) suggested that, in the case of the ubiquitinated substrate, the N-terminus of one ubiquitin moiety is inserted first. In analogy, one of the termini of I3 could be inserted first in the case of the SPI disassembly reaction. This could be a stochastic process once I3 is in proximity to the pore, or the terminus could be more actively guided by the amphipathic helix or the SEP domain of p37. Alternatively, I3 could be inserted through an internal loop in I3. In this case, p37 could even help detaching a I3 loop from the SPI complex and handing it over to the p97 pore. Of note, we detected a critical hydrophic stretch in the p37 helix. It is tempting to speculate that this stretch is involved in initial melting of the SPI structure. This is in analogy to the model for ubiquitin-dependent unfolding that suggested an initial melting of the ubiquitin moiety by the Ufd1-Npl4 adapter (Twomey et al., 2019b). Loop insertion requires the parallel translocation of two protein chains through the p97 channel. However, this ability is also required by the model for ubiquitin-dependent unfolding, once translocation of the ubiquitin peptide enconters an isopeptide bond in the ubiquitin chain. Further work is required to unravel the mechanism of substrate insertion.

3.6 Comparison of SEP domain adapters

As previously discussed, Shp1 is the sole SEP domain adapter in yeast. Its closest homologue in humans is p47, with which it shares the ubiquitin binding UBA domain at the N-terminus. Further homologues are p37 and UBXN2A, which have shorter N-termini compared to p47, and UBXN11, which differs significantly from the other three proteins. However, the latter has been connected to the disassembly of actin stress fibers (Katoh et al., 2002) and does not seem to be relevant for the regulation of the SPI complex (Weith et al., 2018). Previous work in our lab by Weith et al. found that concomitant inhibition or knockout of p47, p37 and UBXN2A was required to completely suppress disassembly of newly synthesized SPI complex in HeLa cells (Weith et al., 2018). However, when the three adapter proteins were tested in the *in vitro* unfolding assay, only p37 or UBXN2A

were capable to support the unfolding reaction. In addition, p47 was not able to bind the SPI-complex in *in vitro* immunoprecipitation experiments. We identified the SHP-UBX linker in p37 as an essential element for the binding of the SPI complex. Transplantation of this linker to p47 enabled binding of the SPI complex and unfolding of I3, albeit at a lower rate than with p37. Concomitant removal of the brake motif resulted in an unfolding activity comparable to p37.The disparity between the lack of p47 activity *in vitro* and its apparent effect on SPI disassembly *in vivo* suggest that p47 might require some kind of "activation" by another factor, for example through a post translational modification. Of note, we used p47 generated in bacteria in this study that lack modifications found in eukaryotic cells. Therefore, p47 from eukaryotic sources might be able to support unfolding. Compared to p37 and UBXN2A, p47 is approximately 100x more abundant in human U2OS cells (Beck et al., 2011), but its knockout had the smallest effect on repressing SPI-complex disassembly in HeLa cells, compared to knockdown of p37 and UBXN2A (Weith et al., 2018). A potential explanation for this matter could be that p37 and UBXN2A are responsible for the basal turnover of the SPI complex, while p47 is activated depending on a specific signaling, stress or cell cycle stage, whereupon it can convert the majority of the SPI complexes in the cell. This would quickly generate a large number of functional PP1 holoenzyme complexes with a decisive effect on the global phosphorylation state of the cell.

Alternatively, p47 could mainly target other substrate proteins. The difference in the linker region which is critical for p37 might stabilize the interaction with other targets. Additionally, the presence of the UBA domain at the N-terminus suggest that potential substrates might carry ubiquitination. If such substrates were to be found, it would be interesting to see if their binding mode also includes the same elements as in p37: Helix, SEP domain and the SHP-UBX linker, or if other regions are involved. Another possibility is that p47 does not primarily function as a substrate processing adapter, but instead as regulatory factor that controls the activity of p97. Depending on a specific signaling, the inhibition of the activity of p97 by p47 could be reversed.

Also regarding the UBXN11 adapter, we could not find any connection to SPI disassembly in our study. Of note, while the adapter may have different substrates, it also shares common structural elements like the SEP domain, SHP box and UBX domain. It is conceivable that UBXN11 interact with its substrates in a similar mechanism.

3.7 Regulation of p97 by p47

Our newly established unfolding assay enabled us to examine the effect that the “brake” motif had on the unfolding of the SPI complex by p97. It has been well established that unlike the Ufd1-Npl4 adapter, as well as the closely related p37, which increase the ATPase activity of p97 upon binding, incubation of p47 with p97 reduces the latter’s ATPase activity by 60-80% in *in vitro* experiments (Meyer et al., 1998). Work by the Chou group identified a region in the N-terminus of p47 stretching residues 69-92, which was not conserved in any of the other SEP domain proteins (Zhang et al., 2015). Deletion of this region removed the inhibitory effect on the *in vitro* ATPase activity. The authors speculated that this “brake” on the activity of p97 could be overcome by trimerization of p47 at higher concentrations. Since these observations were made on the effect of p47 on the “idle” p97 ATPase activity, it was uncertain if this inhibition was also relevant when p97 was unfolding a substrate. Comparison between the ATPase rate of “idle” p97 and p97, which was unfolding a ubiquitin-substrate, had shown that the ATPase rate of “active” p97 was approximately four times higher than that of “idle” p97 (Blythe et al., 2017). Removal of the brake motif residues 69-92 in addition to the replacement of the SHP-UBX linker in the $p47^{\Delta brake+p37Linker}$ mutant had a dramatic effect on the unfolding rate, showing that it was indeed affecting substrate unfolding.

How exactly the brake motif causes the inhibition of p97 is so far unknown. Since the N-terminus of the SEP domain adapters is likely positioned in the vicinity of the D1 domain, it could potentially interfere with ATP hydrolysis there. Although ATPase activity in the D2 domain is responsible for the lions share of the ATPase activity of the whole protein, interference with the D1 hydrolysis might allosterically affect the D2 as well. Alternatively, the brake could influence the movement of the N-domain relative to the D1 domain and favor the down- over the up-conformation. This would in turn affect the ATPase rate as mutations which favor the up-conformation over the down-conformation have been shown to increase the ATPase activity (Huang et al., 2019b), whereas the brake would have the opposite effect.

Another unique feature of p47 among the human SEP domain proteins is the presence of the N-terminal UBA domain. While this domain does not seem to be important for SPI disassembly, it could be relevant for alternative ubiquitinated substrates as discussed

above. An interesting hypothesis is the idea that binding of a ubiquitinated substrate to the UBA domain might be able to overcome the inhibition by the brake motif. This would make the brake motif an additional substrate specifying element, which could only be activated by the correct substrate.

3.8 Implications of our findings for the interpretation of p97 function and physiology

Our findings uncover the molecular basis for an important aspect of PP1 regulation. PP1 is a major phosphatase that interacts with hundreds of substrate specifiers to dephosphorylate a myriad of cellular substrates. After biosynthesis, the protein is bound by SDS22 and I3 and kept in an inactive state. Disassembly of the SPI complex by p97 is dependent on SEP domain adapter proteins. Accordingly, knockdown or knockout of SEP domain adapters causes a shift in the composition of PP1 complexes in the cell, as shown by the PP1 holoenzymes which were identified by a mass spec experiment in cells that lacked p37, p47 and UBXN2A (Weith et al., 2018).

Furthermore, we identified a new unfolding mechanism of p97 which is ubiquitin-independent and differs from the established model from Twoney et al., which describes the unfolding of ubiquitinated substrate by p97-Ufd1-Npl4. It is interesting to speculate if other p97 adapter proteins or cofactors that lack ubiquitin binding domains function in a similar way as the SEP domain adapters. An example for this would be UBXN10, which has been found to be important for ciliogenesis by linking p97 to the intraflagellar transport complex (IFT) (Raman et al., 2015). Of note, UBXN11 was also found to interact with parts of the IFT in affinity purification combined with sequential window acquisition of all theoretical spectra (AP-SWATH) mass spectrometry of interactors of the substrate trapping p97 E578Q mutant (Hülsmann et al., 2018). While no direct interaction between UBXN10 and UBXN11 has been observed, it is possible that these two p97 adapters that both lack ubiquitin-binding domains could function together with p97 on a common substrate.

Most pathological mutations in p97 have been associated with an increase in the ATPase rate as well as a modest increase in the unfolding rate (Blythe et al., 2019). How exactly the increase in activity damages the cell is unclear. It has been hypothesized that the

increase in ATPase activity reflects an increased propensity for the N-domain to be in the up conformation (Huang et al., 2019b) which in turn could affect the binding of different adapter proteins and cofactors. In the context of SPI complex disassembly, a higher turnover rate would result in an increase in other PP1 holoenzyme complexes, which could disturb kinase-phosphatase balance in the cell. While we did not find evidence that p47 is involved in SPI complex turnover in this study, our discovery that the brake motif in p47 is inhibiting the unfolding rate of p97 offers an alternative explanation for the deleterious effect of the disease mutants. The increase in unfolding activity in a disease mutant of p97 might be strong enough to partially overcome the inhibition by the brake motif, thereby circumventing the regulatory effect of the brake. Further research on the exact mechanism of the brake is required to test this hypothesis. A connection to MSP1 could make the brake motif a potential target for small molecules to treat p97 disease mutations.

4 Materials and Methods

4.1 Materials

Table 1: Buffers

Buffer	Components	Used for
1xPBS	137 mM NaCl 2.7 mM KCl 12 mM ($H_2PO_4^-$/HPO_4^{2-}) pH 7.4	Washing of insect cells after centrifugation
Lysis buffer	50 mM HEPES pH 8.0 150 mM KCl 2 mM $MgCl_2$ 5% Glycerol	Lysis of bacterial cells
Ion Exchange buffer Low Salt	20 mM HEPES pH 7.4 25 mM KCl 2 mM $MgCl_2$ 5% Glycerol	Ion Exchange
Ion Exchange buffer Mid Salt	20 mM HEPES pH 7.4 150 mM KCl 2 mM $MgCl_2$ 5% Glycerol	Ion Exchange
Ion Exchange buffer High Salt	20 mM HEPES pH 7.4 1 M KCl 2 mM $MgCl_2$ 5% Glycerol	Ion Exchange
Gel filtration buffer	50 mM HEPES pH 7.4 150 mM KCl 2 mM $MgCl_2$ 5% Glycerol 1 mM DTT	Gel filtration of proteins on 16/600 S75 and S200 (GE)
Ubiquitination buffer	50 mM HEPES pH 7.4 150 mM KCl	Ubiquitination of His-diUb-mEos3.2

	10 mM $MgCl_2$	
Unfolding buffer	25 mM HEPES pH 7.4 100 mM KCl 5 mM $MgCl_2$ 1 mM DTT	Unfolding of proteins in the p97 unfolding assay
6x Laemmli sample buffer	0.35 M Tris, pH 6.8 30 % Glycerol (v/v) 10 % SDS (w/v) 9.3 % DTT 0.02 % Bromophenol blue	Preparation of samples for SDS-PAGE
SDS-running buffer	190 mM Glycine 25 mM Tris 0.1 % SDS (w/v) Set pH to 8.8	SDS-PAGE
Western-transfer buffer	192 mM Glycine 25 mM Tris 0.004 % SDS 20 % Methanol	Western-blot transfer
TE-buffer	10 mM Tris 100 mM Na_2EDTA pH 8.0	Insect cell transfection
TAE buffer	40 mM Tris 1 mM Na_2EDTA 20 mM acetic acid pH 8.0	Agarose gel electrophoresis

Table 2: Plasmids

Plasmid	Antibiotic Resistance	Used for	Proteins
pFL	Ampicillin	Expression in Sf9 cells	SPI, SPEosI, UBXN2A
pGEX6P1	Ampicillin	Expression in BL21 (DE3)	p37 and p47
pET15b	Ampicillin	Expression in BL21 (DE3)	p97-His, $p97^{pBpA}$-SBP-His
pET23	Ampicillin	Expression in BL21 (DE3)	Ubiquitin
pET28a	Kanamycin	Expression in BL21 (DE3)	His-diUb-mEos3.2, His-Ube1, His-gp78-ubc7
pET41b+	Kanamycin	Expression in BL21 (DE3)	
pEVOL-pBpf	Chloramphenicol	Expression of pBpA constructs	Coexpressed with p37 and p97 pBpA constructs

Table 3: Cells and Bacterial Strains

Strain	Source	Identifier	Used for
XL1-blue	Agilent	200249	Cloning
Escherichia coli BL21 (DE3)	New England Biolabs	C2527I	Expression of proteins
DH10EMBACy	(Trowitzsch et al., 2010)		Bacmid generation
Sf9	Invitrogen	11496015	Expression of proteins

Table 4: Proteins

Protein	Vector	Expression Strain	Species	Source
His-diUb-mEos3.2	pET28a	BL21 (DE3)	human/ L. hemprichii	This study
Ub^{wt} untagged	pET23	BL21 (DE3)	mouse	Database
His-mUbe1	pET28a	BL21 (DE3)	mouse	Addgene plasmid # 32534, (Carvalho et al., 2012)
His-gp78-ubc7	pET28a	BL21 (DE3)	human	(Blythe et al., 2017)
p97-His	pET15b	BL21 (DE3)	human	Database
Ufd1-His	pET41b+	BL21 (DE3)	human	Database
Npl4	pET41b+	BL21 (DE3)	human	Database
His-p97	pFL	Sf9	human	(Weith et al., 2018)
$p97^{314pBpA}$-SBP-His	pET15b	BL21 (DE3)	human	Johannes van den Boom
$p97^{278pBpA}$-SBP-His	pET15b	BL21 (DE3)	human	Johannes van den Boom
GST-p37	pGEX6P1	BL21 (DE3)	human	This study
GST-p47	pGEX6P1	BL21 (DE3)	human	(Meyer et al., 2000)
GST-UBXN2A	pFL	Sf9	human	Jonas Seiler
His-I3	pFL	Sf9	human	(Weith et al., 2018)
His-mEos3.2-I3	pFL	Sf9	human/ L. hemprichii	This study

SDS22 + PP1 γ	pFL	Sf9	human	(Weith et al., 2018)
GST-p37$^{\Delta 2\text{-}81}$	pGEX6P1	BL21 (DE3)	human	Jonas Seiler
GST-p37$^{\Delta 2\text{-}107}$	pGEX6P1	BL21 (DE3)	mouse	Jonas Seiler
GST-p37$^{\Delta 2\text{-}129}$	pGEX6P1	BL21 (DE3)	mouse	Jonas Seiler
GST-p37$^{\Delta SEP}$	pGEX6P1	BL21 (DE3)	mouse	Jonas Seiler
GST-p37^{p47SEP}	pGEX6P1	BL21 (DE3)	mouse/human	This study
GST-p47^{p37SEP}	pGEX6P1	BL21 (DE3)	human/mouse	This study
GST-p37^{p47N}	pGEX6P1	BL21 (DE3)	human/mouse	This study
GST-p47^{p37N}	pGEX6P1	BL21 (DE3)	human/mouse	This study
GST-p37^{p47C}	pGEX6P1	BL21 (DE3)	human/mouse	This study
GST-p47^{p37C}	pGEX6P1	BL21 (DE3)	human/mouse	This study
GST-p47^{p37Linker}	pGEX6P1	BL21 (DE3)	human/mouse	This study
GST-p47$^{\Delta 69\text{-}92}$	pGEX6P1	BL21 (DE3)	human	Jonas Seiler
GST-p47$^{\Delta brake+p37Linker}$	pGEX6P1	BL21 (DE3)	human/mouse	This study
GST-p47^{p37Link1}	pGEX6P1	BL21 (DE3)	human	This study
GST-p47^{p37Link2}	pGEX6P1	BL21 (DE3)	human	This study
GST-p37$^{p47SEP\text{-}SHP}$	pGEX6P1	BL21 (DE3)	mouse	This study
GST-p37^{p47UBX}	pGEX6P1	BL21 (DE3)	mouse	This study
GST-p37$^{helix\ 3E\rightarrow 3A}$	pGEX6P1	BL21 (DE3)	mouse	This study
GST-p37$^{helix\ IVLF\rightarrow 4A}$	pGEX6P1	BL21 (DE3)	human	This study
GST-p37^{82pBpA}	pGEX6P1	BL21 (DE3)	human	This study
GST-p37^{182pBpA}	pGEX6P1	BL21 (DE3)	mouse	(Weith et al., 2018)
GST-p37^{234pBpA}	pGEX6P1	BL21 (DE3)	human	This study
GST-p37$^{Link1\rightarrow Ala}$	pGEX6P1	BL21 (DE3)	human	This study
GST-p47$^{\Delta brake+LVLF\rightarrow 4A+p37Linker}$	pGEX6P1	BL21 (DE3)	human/mouse	This study

Table 5: Antibodies

Antibody	Source	Identifier	Used for
Rabbit polyclonal anti-p97	(Meyer et al., 2000)	HME8	Western-Blot, primary 1:2000
Goat polyclonal anti-SDS22	Santa Cruz	E-20, Cat. no. sc-162164	Western-Blot, primary 1:1000
Goat polyclonal anti-PP1γ	Santa Cruz	C-19, Cat. no. sc-6108	Western-Blot, primary 1:1000
Mouse monoclonal anti-PP1γ	Santa Cruz	E-4, Cat. Mp. Sc-515943	Immunoprecipitation
Rabbit polyclonal anti-p37	(Kress et al., 2013)	208880	Western-Blot, primary 1:1000
Rabbit polyclonal anti-Inhibitor-3	(Eiteneuer et al., 2014)	SA7263	Western-Blot, primary 1:1000
Rabbit polyclonal anti-p47	(Meyer et al., 2002)	HME22	Western-Blot, primary 1:2000
Goat polyclonal anti-mouse	BioRad	170-6516	Western-Blot, secondary 1:10000
Goat polyclonal anti-rabbit	BioRad	170-6515	Western-Blot, secondary 1:10000
Mouse polyclonal anti-goat	Santa Cruz	sc-2354	Western-Blot, secondary 1:1000

Table 6: Media

Name	Components	Used for	Source
Luria Bertani (LB) medium	For 1 L: 10 g Peptone 10 g NaCl 5 g yeast extract Set pH to 7.0 with NaOH Autoclave	Multiplication of plasmids in XL1Blue	Made in the lab
Terrific Broth (TB) medium	For 1 L: 12 g Tryptone 24 g yeast extract 4 ml glycerol Ad ddH_2O to 900 ml Autoclave Add 100 ml 10x Phosphate buffer	Expression cultures for BL21(DE3)	Made in the lab
10x Phosphate buffer	For 1 L: 23.1 g KH_2PO_4 125.4 g K_2HPO_4 Ad ddH_2O to 1 L Autoclave	Added to TB medium	Made in the lab
Spodopan		Expression cultures for *Sf9*	PAN-Biotech, P04-850500

Table 7: Reagents and chemicals

Reagent	Supplier	Identifier
ATP	Sigma-Aldrich	A7699-5G
ATPγS	Sigma-Aldrich	A1388-25MG
Dithiothreitol (DTT)	Applichem	A1101.0025
β-Mercaptoethanole	Sigma-Aldrich	M6250-100ML

Yeast extract	Diagonal	A1552.1000
Tryptone	Diagonal	A1553.1000
Peptone	Sigma-Aldrich	70178-500G
Na_2EDTA	Diagonal	A2937.0500
DTT	Applichem	A1101.0025
Glycerol (87 %)	Diagonal	A0970.1000
BSA	Applichem	A1391.0500
BSA (fatty acid-free)	Carl-Roth	0052.3
Nonfat dried milk powder	Applichem	A0830.0500
HEPES	Diagonal	A1069.1000
NaCl	Applichem	A2942.5000
KCl	Carl-Roth	6781.1
NaH_2PO_4 x H_2O	Diagonal	A4229.0500
Na_2HPO_4 x 2 H_2O	Diagonal	A3905.1000
KH_2PO_4	Diagonal	141509.1211
K_2HPO_4	Diagonal	141512.1211
$MgCl_2$ x 6 H_2O	Carl-Roth	6781.1
Triton X-100	Applichem	A1388.0500
Tween-20	Diagonal	A4974.1000
Aluminumsulfate-18-hydrate	Fluka	11044.1000
Tris	Applichem	A1086.5000
Glycine	Applichem	A1067.5000
SDS	Applichem	A1112.0500
Ammonium acetate	Applichem	131114.1210
Acetic acid	Fisher Scientific	A/0400/PB17
NaOH	VWR	28244.295
Guanidine hydrochloride	Applichem	A1106.1000
IPTG	Applichem	A1008.0025
L-glutathione reduced	Applichem	A2084.0025
Imidazole	Sigma-Aldrich	56750-1KG
Coomassie Brilliant Blue G-250	Applichem	A3480.0025

Ethanol (99.8 %)	Fisher Scientific	E/0650DF/17
Methanol	Fisher Scientific	M/4056/17
Perchloric acid	Carl-Roth	9216.1
Bromophenol blue	Riedel-de Haën	32788
PMSF	Diagonal	A0999.0005
p-benzoyl-L-phenylalanine (pBpa)	Bachem	F2800
GammaBind G Sepharose beads	GE Healthcare	17-0885-01
FuGene HD Transfection Reagent	Promega	E2311
Biomol® Green Reagent	Enzo Life Science	BML-AK111-0250
PageRuler™ Prestained Protein Ladder, 10 to 180 kDa	Thermo Fisher Scientific	26617
O'GeneRuler 1 kb DNA Ladder, Ready-to-Use- 250-10,000 bp	Thermo Fisher Scientific	11551615

Table 8: Protein purification columns

Column	**Used for**	**Supplier**	**Identifier**
HisTrap FF Crude 5 ml	Purification of His-tagged proteins	VWR	17-5286-01
GSTrap FF 5 ml	Purification of GST-tagged proteins	VWR	17-5131-01
HiTrap™ Q HP	Anion-Exchange chromatography	VWR	17-1154-01
HiTrap™ SP HP	Cation-Exchange chromatography	VWR	17-1151-01
HiLoad® 16/600 Superdex® 75 pg	Gel filtration	GE-Healthcare	28989333
HiLoad® 16/600 Superdex® 200 pg	Gel filtration	GE-Healthcare	28989335

Table 9: Laboratory appliances

Name	Company	Used for
Cary Eclipse Fluorescence Spectrophotometer	Varian	Fluorescence unfolding assay
Spectra Max Plus	Molecular Devices	ATPase assay
Äkta purifier	GE Healthcare	Protein Purification
Äkta pure	GE Healthcare	Protein Purification
INTAS ECL Chemostar	INTAS	Western-blot analysis
E-Box	VILBER	Agarose gel documentation
Nanodrop	Thermo Fisher	Determination of Eos photoconversion efficiency
Thermocycler nexus GSX1	Eppendorf	PCR
Biophotometer D30	Eppendorf	Determination of DNA and protein concentrations
Fresco 17 centrifuge	Heraeus	Benchtop centrifuge for immunoprecipitation
Megafuge 40R	Heraeus	Protein concentration through centrifugation
Sorvall RC 6+ Centrifuge	Thermo Scientific	Cell harvest and ultracentrifugation
SS-34 fixed angle rotor	Thermo Scientific	Ultracentrifugation with Sorvall RC 6+
F9S-4x 1000y fixed angle rotor	Thermo Fisher	Cell harvest with Sorvall RC 6+
Sonoplus	Bandelin	Cell lysis
New Brunswick™ Innova®44	Eppendorf	Shaker for growth of bacterial cultures
MaxQ 4000	Thermo Scientific	Shaker for growth of insect cell cultures
CL-1000 Ultraviolet Crosslinker	UVP/analytic jena	Crosslinking or proteins with pBpA
UVP Blak-Ray™ B-100AP	UVP/analytic jena	Photoconversion of mEos3.2

ECL Chemostar imager	INTAS	Western-blot

Table 10: Cloning Reagents from New England Biolabs (NEB)

Reagent	Identifier
Phusion® High Fidelity DNA Polymerase	M0530 S
Phusion® HF Buffer 5x	B0518S
DpnI	R0176 L
T4 Polynucleotide Kinase	M0201 S
T4 DNA Ligase	M0202 L
T4 DNA Ligase buffer 10x	B0202S
Taq DNA Ligase	M0208 L
Deoxynucleotide (dNTP) Solution Mix	N0447L
BamHI-HF	R3136L
EcoRI-HF	R3101L
XhoI	R0146S
CutSmart® buffer 10x	B7204S

Table 11: Kits

Name	Used for	Company	Identifier
NucleoSpin Plasmid	Preparation of plasmid DNA from bacterial cultures	Macherey-Nagel	740588.50
NucleoSpin Gel and PCR Clean-up	Extraction of DNA from agarose gel	Macherey-Nagel	740609.50
SuperSignal™ West Pico PLUS Chemiluminescent Substrate	Western-blot detection	Thermo Scientific	34579
Amersham ECL Prime Western Blotting Detection Reagent	Western-blot detection	GE Healthcare	RPN2236

Table 12: Proteases

Name	Cleavage Site	Used Ratio	Source	Identifier
Thrombin, Bovine	LVPR*GS	10 u / 1 mg of substrate	Merck-Millipore	605157
Razor(TM) TEV Protease	ENLYFQ*S	1 µg protease / 100 µg substrate	Biomol	BM-13002-1000
GST-PreScission	LEVLFQ*GP	4 µg protease / 1000 µg substrate	Prepared in the lab	Plasmid from AG Bayer

Table 13: Filters, concentrators and cuvettes

Name	Company	Identfier
Sterilfilter Filtropur S 0.2	Sarstedt	83.1826.001
Rotilabo Spritzenfilter, unsteril, Porengröße 0,8 µm	Carl Roth	P820.1
MEMBRA-CEL dialysis tubing, MWCO 3500	Serva	44310.01
Vivaspin Turbo 15, 5 kDa MWCO	Sartorius	VS15T12
Vivaspin Turbo 15, 10 kDa MWCO	Sartorius	VS15T02
Vivaspin Turbo 15, 100 kDa MWCO	Sartorius	VS15T42
Ultra-Micro Cell 105.250-QS LP 10x2 mm, VOL 100µl, CH 15 mm	Hellma Analytics	105-251-15-40

4.2 Methods

4.2.1 Molecular Cloning

Expression constructs for protein purification were generated by using either Gibson Assembly for insertion or replacement of larger DNA sequences, by site directed mutagenesis to mutate single bases or small DNA sequences or by cloning with restriction enzymes. All strategies involved DNA amplification via polymerase chain reaction (PCR).

4.2.1.1 PCR-Protocol

Table 14 Pipetting scheme for PCR

Component	Volume [µl]
ddH_2O	32.5
Phusion® HF buffer (x5)	10
dNTP mix (10 mM)	1
Template DNA (10 ng/µl)	1
Forward primer (10 µM)	2.5
Reverse primer (10 µM)	2.5
Phusion® HF polymerase	0.5

Table 15 Thermocycle steps for PCR

Step	Temperature [°C]	Time
(1) Initial denaturation	98	2 min
(2) Denaturation	98	30sec
(3) Annealing	Depending on construct	30 sec
(4) Elongation	72	5 min
Repeat steps 2-4 for 30 times		
(5) Final Elongation	72	10 min
(6) Hold	10	∞

4.2.1.2 Gibson-assembly

For the insertion of larger DNA sequences into a construct via Gibson-assembly (Gibson et al., 2009), both the vector backbone and the insert were amplified via PCR to generate two linear fragments, “vector” and “insert”. The primers used for the reaction included overhangs that were complementary between vector and insert. These primers were designed with the NEBuilder tool (https://nebuilder.neb.com/#!/). After the PCR was complete, the original templates were degraded by addition of 1 µl DpnI. The PCR products were then separated via agarose gel electrophoresis (1% agarose, 1xTAE buffer, 100 V, 1 h). DNA fragments were visualized by ethidium bromide and UV light and bands of the correct length were cut out with a scalpel. The DNA was extracted with the NucleoSpin Gel and PCR Clean-up kit (Macherey-Nagel). DNA concentration was determined from the absorbance at 260 nm with a spectrophotometer (Eppendorf) and the vector and insert fragments were ligated using a Gibson Assembly mixture:

Table 16 Gibson-assembly pipetting scheme

Component	**Volume [µl]**
Vector fragment	Equal to 50 ng
Insert fragment	Three times the molar ratio of the vector
Gibson Assembly mix	15
ddH_2O	Add to 20

The Gibson-assembly mix contains T5 exonuclease, Phusion® DNA polymerase and Taq ligase in Gibon-assembly buffer (500 mM Tris pH 7.3, 50 mM MgCl2, 1 mM dNTPs, 50 mM DTT, 5 mM NAD, 25% PEG 8000). The T5 exonuclease creates single stranded overhangs that allow the annealing of vector and insert, the polymerase fills in the gaps and the ligase covalently fuses the DNA fragments to create one single plasmid. The reaction was incubated at 50°C for 1 h. Afterwards, 5 µl were transformed into XL1Blue by heat shock.

Table 17 Construct cloned by Gibson-assembly

Construct	Templates	Primer	Primer sequence
pFL His-mEos3.2-I3	pFL	pFL Eos-Inh3_vf	TGCCTGACAATGCCAGACGAGGTGGCG GTGGCAGCATGGCCGAGGCAGGGGCT
		pFL Eos-Inh3_vr	TCTGGCTTAATCGCACTCATGGATCCC ATGGCGCCCTG
	gBlock mEos-I3 (IDT)	pFL Eos-Inh3_if	TTCAGGGCGCCATGGGATCCATGAGT GCGATTAAGCCAG
		pFL Eos-Inh3_ir	GGCCATGCTGCCACCGCCACCTCGTC TGGCATTGTCAGG
pGEX6P1 GST-p37^{p47SEP}	pGEX6P1 p37 mouse	GST-p37+p47 SEP_vf	ATCGGGACGAGGACTTTGTGAAACCCA GGTTGCGATTC
		GST-p37+p47 SEP_vr	AATACTACATGAACATCTTGGAGCTGA TTTTCCCCATAG
	pGEX6P1 p47	GST-p37+p47 SEP_if	TCTATGGGGAAAATCAGCTCCAAGATG TTCATGTAGTATTGAAACTC
		GST-p37+p47 SEP_ir	TTGAATCGCAACCTGGGTTTCACAAAG TCCTCGTCCCG
pGEX6P1 GST-p47^{p37SEP}	pGEX6P1 p47	p47-w/o SEP for	ATCAAGACCAAGAGTACATAAAGCCCA AAGGAGCCTTC
		p47-w/o SEP rev	AGTAAAACCTGAACATCTTGGCTGGAA TGCTGCCTCTTTTC
	pGEX6P1 p37 mouse	p37 SEP for	AAAAGAGGCAGCATTCCAGCCAAGATG TTCAGGTTTTACTG
		p37 SEP rev	TTGAAGGCTCCTTTGGGCTTTATGTACT CTTGGTCTTGATGATC
pGEX6P1 GST-p37^{p47N}	pGEX6P1 p37 mouse	p37_backbone_fwd	AAAAGAGGCAGCATTCCAGCCAAGATG TTCAGGTTTTACTGAAGCTGTG
		p37_backbone_rev	TCCTGTCGCTCCGCCGCCATGGATCCC AGGGGCCCCTG
	pGEX6P1 p47	p47_N_fwd	TCCAGGGGCCCCTGGGATCCATGGCG GCGGAGCGACAG
		p47_N_rev	AGTAAAACCTGAACATCTTGGCTGGAA TGCTGCCTCTTTTCTCC
pGEX6P1 GST-p47^{p37N}	pGEX6P1 p47	p47-w/o N for	TCTATGGGGAAAATCAGCTCCAAGATG TTCATGTAGTATTGAAACTCTGGAAG
		p47-w/o N rev	GCACGGCCACCCTCCGCCATGGATCC CAGGGGCCCCTG
	pGEX6P1 p37 mouse	p37 N for	TCCAGGGGCCCCTGGGATCCATGGCG GAGGGTGGCCGT
		p37 N rev	AATACTACATGAACATCTTGGAGCTGAT TTTCCCCATAGATATACTCTGATCG

pGEX6P1 GST-p37^{p47C}	pGEX6P1 p37 mouse	p37_p47C_vf	TCATCGTGCAGCGGTTAACATAGGGATCCCCGGAATTC
		p37_p47C_vr	CTCAACACCTGGGGGGCAGTGCTTCCAAGTTTTTGCCC
	pGEX6P1 p47	p37_p47C_if	AAGGGCAAAAACTTGGAAGCACTGCCCCCCAGGTGTTG
		p37_p47C_ir	GGGAATTCCGGGGATCCCTATGTTAACCGCTGCACGATG
pGEX6P1 GST-p47^{p37C}	pGEX6P1 p47	p47_p37C_vf	TGATACTCCAACAGCTAAAATAACCGGAATTCCCGGGTC
		p47_p37C_vr	CTGACGATTTCAGGTGTAAGGCTGCCCAGTTTCTGACC
	pGEX6P1 p37 mouse	p47_p37C_if	AGGGTCAGAAACTGGGCAGCCTTACACCTGAAATCGTCAG
		p47_p37C_ir	CGACCCGGGAATTCCGGTTATTTTAGCTGTTGGAGTATCAC
pGEX6P1 GST-p37$^{p47SEP-SHP}$	pGEX6P1 p37 mouse	p37+p47SEP_SHP_vf	AGGGTCAGAAACTGGGCAGCCTTACACCTGAAATCGTCAG
		p37+p47SEP_SHP_vr	TTCAATACTACATGAACATCTTGGAGCTGATTTTCCCC
	pGEX6P1 p47	p37+p47SEP_SHP_if	ATGGGGAAAATCAGCTCCAAGATGTTCATGTAGTATTGAAACTCTGG
		p37+p47SEP_SHP_ir	CTGACGATTTCAGGTGTAAGGCTGCCCAGTTTCTGACC
pGEX6P1 GST-p37^{p47UBX}	pGEX6P1 p37 mouse	p37+p47UBX_vf	TCATCGTGCAGCGGTTAACATAGGGATCCCCGGAATTC
		p37+p47UBX_vr	TTTGTGGTAGGCTCTGATTCATCAATAAGAACAGCTGCATTC
	pGEX6P1 p47	p37+p47UBX_if	ATGCAGCTGTTCTTATTGATGAATCAGAGCCTACCACAAAC
		p37+p47UBX_ir	GGGAATTCCGGGGATCCCTATGTTAACCGCTGCACGATG
pGEX6P1 GST-p47^{p37Linker}	pGEX6P1 p47	p47+p37Linker_vf	ATGCAGCTGTTCTTATTGATGAATCAGAGCCTACCACAAAC
		p47+p37Linker_vr	CTGACGATTTCAGGTGTAAGGCTGCCCAGTTTCTGACC
	pGEX6P1 p37 mouse	p47+p37Linker_if	AGGGTCAGAAACTGGGCAGCCTTACACCTGAAATCGTC
		p47+p37Linker_ir	TTTGTGGTAGGCTCTGATTCATCAATAAGAACAGCTGC

4.2.1.3 Site directed mutagenesis

Mutations and smaller insertions were introduced into constructs by site directed mutagenesis. Primers including the desired mutations were designed with the NEBaseChanger tool (https://nebasechanger.neb.com/). The template DNA was amplified via PCR and the reaction mixture was purified with the NucleoSpin Gel and PCR Clean-up kit (Macherey-Nagel) afterwards, resulting in 15 µl DNA in ddH_2O. The mutated plasmid was then ligated with a KLD reaction:

Table 18: Site directed mutagenesis pipetting scheme

Component	Volume [µl]
ddH_2O	4
Mutated plasmid DNA	2
T4 Ligase buffer (x10)	1
T4 Ligase	1
T4 Polynucleotide kinase	1
DpnI	1

The non-mutated template DNA is degraded by DpnI, the T4 Polynucleotide kinase phosphorylates DNA ends and T4 Ligase fuses these ends together to generate a new plasmid. The reaction was incubated at room temperature for 1 h, before 5 µl were transformed into XL1Blue by heat shock.

Table 19: Constructs cloned by site directed mutagenesis

Construct	Template	Primer	Primer sequence
GST-p47$^{\Delta brake+p37Linker}$	GST-p47	p47 _delta 69-92_for	CCAGAGGCACAGCTCCTAGTAGGTTTTATGCTG
		p47_delta 69-92_rev	GAGCCCCCAGCATAAAACCTACTAGGAGCTGT
GST-p47^{p37Link1}	GST-p47	p47_p37Link1_for	AGCACCCCTAGCAGCCCGCAACAGGCAGAAAATGAAGC
		p47_p37Link1_rev	CACGATTTCAGGCGTCAGGCTGCCCAGTTTCTGACC
GST-p47^{p37Link2}	GST-p47	p47_p37Link2_for	GAATGCGGTAGTCTTGATTGATGAATCAGAGCCTACCACAAAC
		p47_p37Link2_rev	AAAATGGACTTATCTTCCTCTTCGGCTGGAGAGCTGGTACT

GST-p37$^{helix\ 3E\rightarrow3A}$	GST-p37 (mouse)	p37_helix_E-A_for	GAATGCACTTTTCAAAGCGGCAAGGGCACATGGAGCTGTCCC
		p37_helix_E-A_rev	CATGTGCCCTTGCCGCTTTGAAAAGTGCATTCACAATTTTCCC
GST-p37$^{helix\ IVLF\rightarrow4A}$	GST-p37 (human)	p37_helix_IVLF_for	GTCCGTCCGTCTACCGGCAAAGCCGCTAATGAAGCGGCCAAAGAAGCTCGCGAACACGG
		p37_helix_IVLF_rev	CCGTGTTCGCGAGCTTCTTTGGCCGCTTCATTAGCGGCTTTGCCGGTAGACGGACGGAC
GST-p47$^{\Delta brake+LVLF\rightarrow4A+p37Linker}$	GST-p47$^{\Delta brake+p37Linker}$	p47 LVLF->4A_for	CCAACGAGGCGGCGGATGATGCCGCGAAAGGTGCCAAAGAGCATGG
		p47 LVLF->4A_rev	GCACCTTTCGCGGCATCATCCGCCGCCTCGTTGGGACTTTTCTTCC
GST-p37^{82pBpA}	GST-p37 (human)	p37h_G82TAG_for	GTCTACCTAGAAAATCGTTAATGAACTGTTCAAAGAAGCTCGCG
		p37h_G82TAG_rev	GATTTTCTAGGTAGACGGACGGACGATGTTAAG
GST-p37^{234pBpA}	GST-p37 (human)	p37_S234TAG_for	CCCCTTAGAGCCCGGAAGAGGAAGATAAGTCC
		p37_S234TAG_rev	GGGCTCTAAGGGGTGCTCACGATTTCAGGCG

4.2.1.4 Cloning with restriction enzymes

Inserts were amplified from template DNA with PCR primers that included restriction sites. The PCR product was purified with the PCR clean-up kit (Macherey-Nagel) (elution in 15 µl ddH_2O) and digested with restriction enzymes. The vector was also digested with the same enzymes.

Table 20: Restriction digest pipetting scheme

Component	**Volume [µl]**
ddH_2O	ad to 50 µl
DNA	1 µg vector, or 15 µl PCR product
CutSmart® buffer 10x	1
Restriciton enzyme 1	1
Restriction enzyme 2	1

After 1 hour at 37°C, the samples were purified again with the PCR clean-up kit (Macherey-Nagel) (elution in 15 µl ddH_2O). The vector and the insert fragment were then

ligated together using T4 ligase over night at 4°C. The ligated plasmid was transformed into XL1-blue on the next day.

Table 21: Ligation pipetting scheme

Component	Volume [µl]
ddH_2O	ad to 20 µl
Vector	50 ng
Insert	3x molar excess of vector DNA
T4 DNA Ligase	1
T4 DNA Ligase buffer 10x	2

The pET28a His-diUb-mEos3.2 construct was generated via cloning with restriction enzymes. The vector pET28a His-diUB-GFP was received as a gift from Emily Blythe and Raymond Deshaies (Blythe et al., 2017). The GFP was removed by digestion with BamHI-HF and XhoI and replaced with mEos3.2 that had been PCR amplified from mEos3.2-C1 (addgene plasmid #54550, (Zhang et al., 2012).

The pGEX6P1 GST-p37 (human) construct was generated from a gBlock (IDT) with the DNA sequence for human p37 (Gene ID: 137886) that was codon optimized for expression in *E. coli*. The insert was amplified via PCR with primers carrying BamHI and EcoRI restriction sites and ligated into pGEX6P1.

Table 22: Constructs cloned by restriction digestion

Construct	Templates	Primer/Restriction enzymes	Primer sequence
pET28a His-diUb-mEos3.2	pET28a His-diUb-GFP	BamHI-HF	Vector was not amplified
		XhoI	Vector was not amplified
	mEos3.2-C1	BamHI-mEos for	CACACAGGATCCACCGGTCGC CACCATGAGTGCGATTAAGC
		XhoI-mEos rev	CCAACCCTCGAGTGCGGCCGC TTTATCGTCTGGCATTGTC
pGEX6P1 GST-p37 human	pGEX6P1	BamHI-HF	Vector was not amplified
		EcoRI-HF	Vector was not amplified
	gBlock p37 human (IDT)	p37_ BamHI_f	CTATTGCTGGATCCATGGCGGA GGGCGG
		p37 _EcoRI_r	TGCAGAACGAATTCTTATTTCAG TTGTTGCAGCAGCAC

4.2.1.5 Transformation

Plasmids were transformed into XL1Blue or Bl21(DE3) by heat shock. An aliquot of chemically competent *E*. *coli* (50 – 100 µl) was thawed on ice for 20 min. Roughly 50 ng of plasmid DNA were added, and the mixture was incubated on ice for further 20 min. Then, the bacteria were incubated in a 42°C hot water bath for 30 seconds and then incubated on ice gain for 2 minutes. The bacteria were supplemented with 500 µl of LB medium and incubated at 37°C with constant shaking (600 – 800 rpm) for 1 hour. Afterwards, the mixture was centrifuged for 2 minutes with 4000xg and 500 µl of the supernatant were removed. The bacterial pellet was resuspended in the remaining liquid and spread on a LB agar plate with a drigalski spatula. The plates were supplemented with the antibiotic corresponding to the resistance cassette of the plasmid.

4.2.1.6 Sequencing

The DNA sequences of cloning products were verified vie Sanger sequencing by the companies GATC (now Eurofins) or Microsynth.

4.2.2 Protein expression

4.2.2.1 Protein expression in *E. coli* (BL21 DE3)

Protein constructs in bacterial expression vectors (pGEX6P1, pET 15b, pET 23, pET 28a, pET 41b) were recombinantly expressed in BL21 (DE3). A starter culture in 100 ml LB medium with antibiotic was grown over night at 37°C and 130 rpm shaking. The next morning, this starter culture was used to inoculate 2 – 4 x 1 L TB-media with antibiotics. The cultures were grown to an OD_{600} of 0.6 at 37°C and 130 rpm and expression was induced by addition of IPTG to 0.5 M. After growth over night at 18°C and 130 rpm, bacteria were harvested by centrifugation at 4000xg for 15 min. The supernatant was removed and the bacteria were resuspended in 20 ml of Lysis buffer per 1 L of bacterial culture, before storage at -80°C.

An exception from this protocol was the expression of Ufd1-His and Npl4, which were not grown over night, but for 5 hours at 37°C and 130 rpm before harvesting.

Protein constructs that included an internal amber (TAG) stop codon designed for incorporation of the pBpA crosslinking amino acid were expressed in BL21 (DE3), which was additionally co-transformed with the pEVOL-pBpf plasmid (Addgene plasmid #31190) (Chin et al., 2002). This plasmid encodes for an aminoacyl-tRNA synthetase/tRNA pair that enables the incorporation of the pBpA (p-benzoyl-l-phenylalanine) crosslinker instead of the TAA Stop-codon. The bacterial cultures were grown at 37°C and 130 rpm until an OD_{600} of 0.6 was reached. Expression of was induced by addition of IPTG to 0.5 mM, arabinose to 0.2 % and p-benzoyl-L-phenylalanine (pBpA) to 1 mM. After growth over night at 18°C and 130 rpm, bacteria were harvested by centrifugation at 4000xg for 15 min. The supernatant was removed and the bacteria were resuspended in 20 ml of lysis buffer per 1 L of bacterial culture, before storage at -80°C.

4.2.2.2 Protein expression in Sf9 insect cells

His-p97, GST-UBXN2A and complexes of His-I3+PP1γ+SDS22 or His-mEos3.2-I3+PP1γ+SDS22 were expressed in insect cells (*Sf9*) using a baculovirus system. (Trowitzsch et al., 2010).

In order to create a bacmid for transfection of the insect cells, the constructs were cloned into the pFL vector, which includes two potential multiple cloning sites. While His-p97,

GST-UBXN2A, His-I3 and His-mEos3.2-I3 were inserted individually, SDS22 and PP1 were inserted on the same bicistronic vector (SDS22+PP1). The pFL constructs were transformed into DH5αEmbacY, which incorporated the constructs into the bacmid via Tn7 transposition. An aliquot of 50 µl DH5αEmbacY was thawed on ice and 2 µg of pFL vector were added. After incubation on ice for 1 h, the bacteria were heat shocked by incubation in a 42°C warm water bath for 40 seconds. LB-medium (800 µl) were added and the mixture was shaked with 110 rpm for 6 h. Afterwards, the mixture was centrifuged for 2 minutes with 4000xg and 500 µl of the supernatant were removed. The bacterial pellet was resuspended in the remaining liquid and spread on a LB agar plate with a drigalski spatula. The plates were supplemented with 50ug/ml kanamycin, 10ug/ml tetracycline, 7ug/ml gentamycin, 40ug/ml IPTG and 100ug/ml X-Gal. The DH5αEmbacY contain a lacZ gene in the bacmid that encodes for the β-galactoisdase enzyme. Expression of this enzyme is controlled by a promoter that can be activated by addition of IPTG. The enzyme transforms the colorless X-Gal (5-bromo-4-chloro-indoxyl) into the blue 5,5'-dibromo-4,4'-dichloro-indigo. Successful integration of the pFL constructs results in the disruption of a lacZ reporter, which enables selection via blue/white screening. Colorless colonies were picked from plates after 2 days at 37°C and transferred onto a second plate. Those that did not turn blue after this second incubation at 37°C were picked to inoculate 5 ml of LB medium with antibiotics (kanamycin, tetracycline, gentamycin) and grown over night at 37°C and 150 rpm. On the next day, the bacteria were lysed with the NucleoSpin Plasmid kit (Macherey-Nagel) and the bacmid DNA was precipitated in isopropanol at -20°C over two days. The bacmid was washed with ethanol and then dried before reconstitution in 40 µl of TE-buffer.

Sf9 cells were grown in Spodopan (PAN-Biotech) at 27°C and 120 rpm. Cells were transfected with bacmid DNA using the FuGene HD transfection reagent. A mixture of 20 µl bacmid, 200 µl Spodopan and 5 µl FuGene HD transfection reagent were incubated at room temperature for 20 minutes and then added to 2 ml of *Sf9* cells with a density of 500,000 cell/ml. Cells were grown for four days and then used to infect a 10 ml culture of *Sf9* with a cell density of $1x10^6$ cells/ml. Successful transfection resulted in expression of a YFP reporter from the bacmid. Transfected cells were grown over four further days and the cell supernatant was used to infect a fresh culture of 50 ml with a cell density of $1x10^6$ cells/ml. This was repeated after four more days, before the final 50 ml supernatant was

used to infect 1 L of culture with a cell density of $1x10^6$ cells/ml. For the expression of the SPI complex, the final culture was co-infected with supernatant from His-I3 (or His-mEos3.2-I3) and SDS22+PP1. After four days of growth, cells were harvested by centrifugation (3500 rpm, 15 min), resuspended in 100 ml of ice cold PBS, centrifuged again (1000xg, 15 min) and stored at -80°C.

4.2.3 Protein purification

4.2.3.1 Purification of p97-His, His-p97, p97314pBpA -SBP-His and p97278pBpA - SBP-His

The bacterial cell pellets that had been resuspended in lysis-buffer (50 mM HEPES pH 8.0, 150 mM KCl, 2 mM $MgCl_2$, 5% glycerol) before storage were thawed and supplemented with imidazole (pH 8.0) to 20 mM. Lysozyme (1 g/L) and PMSF (1 mM) were added and the mixture was slowly stirred at 4°C for 30 min. Cells were lysed by sonication (Bandelin Sonoplus, MS 73 tip, 3 pulses at 60%), followed by centrifugation at 20,000 x g for 1 h at 4°C. The supernatant was filtered through a 0.8 µm membrane and loaded onto a His-Trap column (GE Healthcare) using a peristaltic pump (P-1, GE Healthcare) with a flow of 5 ml/min. The column was subsequently washed with 300 ml of lysis buffer + 20 mM imidazole. Afterwards, the column was transferred to an Äkta purifier or Äkta pure system. The column was connected with a QHP anion-exchange column (GE Healthcare) and washed with 30 ml of Mid-Salt ion exchange buffer (20 mM HEPES pH 7.4, 150 mM KCl, 2 mM MgCl2, 5% Glycerol). Bound protein was then eluted from the His-Trap column into the QHP column with Mid-Salt buffer containing 300 mM imidazole. The His-Trap column was disconnected and the QHP column was washed with 25 ml of Mid-Salt buffer. Bound protein was then eluted from the QHP column by a salt gradient over 30 ml between Mid-Salt buffer (containing 25 Mm KCl) and High-Salt buffer (1 M KCl) in fractions of 2 ml. The elution was monitored by the absorbance at 280 nM with the Äkta UNICORN™ software (GE Healthcare). Peak fractions were analyzed by SDS-PAGE and those containing the protein were pooled and concentrated with a concentrator (Vivaspin Turbo 100 kDa MWCO, Sartorius). The protein was washed in the concentrator with Gel filtration buffer (50 mM HEPES pH 7.4, 150 mM KCl, 2 mM $MgCl_2$, 5% Glycerol, 1 mM DTT), aliquoted (20 – 50 µl and flash frozen in liquid nitrogen before storage at -80°C.

The purification of His-p97 from *Sf9* differed in the initial steps. The cell pellets were thawed and resuspended in 100 ml lysis buffer + 20 mM imidazole. PMSF (1 mM) was added and the cells were lysed by sonication (Bandelin Sonoplus, MS 73 tip, 3 pulses at 60%), followed by centrifugation at 20,000 x g for 1 h at 4°C. The supernatant was filtered successively through a 0.8 µm and a 0.2 membrane before being loaded onto a His-Trap column.

4.2.3.2 Purification of His-I3+PP1γ+SDS22, His-mEos3.2-I3+PP1γ+SDS22

Cell pellets were thawed and resuspended in 100 ml of lysis buffer + 20 mM imidazole. PMSF (1 mM) was added and the cells were lysed by sonication (Bandelin Sonoplus, MS 73 tip, 3 pulses at 60%), followed by centrifugation at 20,000 x g for 1 h at 4°C. The supernatant was filtered successively through a 0.8 µm and a 0.2 membrane before being loaded onto a His-Trap column. The column was subsequently washed with 300 ml of Low-Salt buffer (20 mM HEPES pH 7.4, 25 mM KCl, 2 mM MgCl2, 5% Glycerol) + 20 mM imidazole and transferred to an Äkta purifier or Äkta pure system. Bound protein was then eluted into 2 ml fractions with 25 ml of Low-Salt buffer + 300 mM imidazole. Peak fractions were analyzed by SDS-PAGE and those containing the protein complex were pooled and loaded onto a QHP ion-exchange column. Bound protein was eluted from the QHP column by a salt gradient over 30 ml between Low-Salt buffer (25 mM KCl) and High-Salt buffer (1 M KCl). Peak fractions were analyzed by SDS-PAGE and fractions with the protein complex were pooled and further purified by size exclusion chromatography (16/600 Superdex 200 pg, GE Healthcare) with a flow rate of 1 ml/min in Gel-filtration buffer (50 mM HEPES pH 7.4, 150 mM KCl, 2 mM $MgCl_2$, 5 % glycerol, 1 mM DTT). Fractions containing the protein complex were pooled, concentrated (Vivaspin Turbo 100 kDa MWCO, Sartorius), aliquoted and stored at -80°C.

4.2.3.3 Purification of His-diUb-mEos3.2

Cell pellets (in lysis buffer + 20 mM imidazole) were thawed and supplemented with lysozyme (1g/L) and PMSF (1 mM). After stirring at 4°C for 30 min, the cells were lysed by sonication (Bandelin Sonoplus, MS 73 tip, 3 pulses at 60%), followed by centrifugation at 20,000 x g for 1 h at 4°C. The supernatant was filtered through a 0.8 µm membrane and loaded onto a His-Trap column (GE Healthcare) using a peristaltic pump (P-1, GE Healthcare) with a flow of 5 ml/min. The column was subsequently washed with 300 ml

lysis buffer + 20 mM imidazole and transferred to an Äkta purifier or Äkta pure system. Bound protein was then eluted into 2 ml fractions with 25 ml of lysis buffer + 300 mM imidazole. Peak fractions were pooled and further purified by size exclusion chromatography (16/600 Superdex 200 pg, GE Healthcare) with a flow rate of 1 ml/min in Gel-filtration buffer (50 mM HEPES pH 7.4, 150 mM KCl, 2 mM $MgCl_2$, 5 % glycerol, 1 mM DTT). Fractions containing the protein were pooled, concentrated (Vivaspin Turbo 100 kDa MWCO, Sartorius), aliquoted and stored at -80°C.

4.2.3.4 Purification of Ufd1-His and Npl4

The Ufd1-Npl4 adapter pair was co-purified. The pellets of Ufd1-His and Npl4 (both in lysis buffer + 20 mM imidazole) were thawed and mixed together before the addition of lysozyme (1 g/L) and PMSF (1 mM). After stirring at 4°C for 30 min, the cells were lysed by sonication (Bandelin Sonoplus, MS 73 tip, 3 pulses at 60%), followed by centrifugation at 20,000 x g for 1 h at 4°C. The supernatant was filtered through a 0.8 µm membrane and loaded onto a His-Trap column (GE Healthcare) using a peristaltic pump (P-1, GE Healthcare) with a flow of 5 ml/min. The column was subsequently washed with 300 ml of Low-Salt buffer (20 mM HEPES pH 7.4, 25 mM KCl, 2 mM MgCl2, 5% Glycerol) + 20 mM imidazole and transferred to an Äkta purifier or Äkta pure system. The column was connected with a QHP anion-exchange column (GE Healthcare) and washed with 30 ml of Low-Salt ion exchange buffer (20 mM HEPES pH 7.4, 25 mM KCl, 2 mM MgCl2, 5% Glycerol). Bound protein was then eluted from the His-Trap column into the QHP column with Mid-Salt buffer containing 300 mM imidazole. The His-Trap column was disconnected and the QHP column was washed with 25 ml of Low-Salt buffer. Bound protein was then eluted from the QHP column by a salt gradient over 50 ml between Low-Salt buffer (25 mM KCl) and High-Salt buffer (1 M KCl). Peak fractions were pooled and further purified by size exclusion chromatography (16/600 Superdex 200 pg, GE Healthcare) with a flow rate of 1 ml/min in Gel-filtration buffer (50 mM HEPES pH 7.4, 150 mM KCl, 2 mM $MgCl_2$, 5 % glycerol, 1 mM DTT). Fractions containing the protein complex were pooled, concentrated (Vivaspin Turbo 100 kDa MWCO, Sartorius), aliquoted and stored at -80°C.

4.2.3.5 Purification of His-mUbe1 and His-gp78-ubc7

Cell pellets (in lysis buffer + 20 mM imidazole) were thawed and supplemented with lysozyme (1g/L) and PMSF (1 mM). After stirring at 4°C for 30 min, the cells were lysed

by sonication (Bandelin Sonoplus, MS 73 tip, 3 pulses at 60%), followed by centrifugation at 20,000 x g for 1 h at 4°C. The supernatant was filtered through a 0.8 µm membrane and loaded onto a His-Trap column (GE Healthcare) using a peristaltic pump (P-1, GE Healthcare) with a flow of 5 ml/min. The column was subsequently washed with 300 ml of Low-Salt buffer (20 mM HEPES pH 7.4, 25 mM KCl, 2 mM MgCl2, 5% Glycerol) + 20 mM imidazole and transferred to an Äkta purifier or Äkta pure system. The column was connected with a QHP anion-exchange column (GE Healthcare) and washed with 30 ml of Low-Salt ion exchange buffer (20 mM HEPES pH 7.4, 25 mM KCl, 2 mM MgCl2, 5% Glycerol). Bound protein was then eluted from the His-Trap column into the QHP column with Mid-Salt buffer containing 300 mM imidazole. The His-Trap column was disconnected and the QHP column was washed with 25 ml of Low-Salt buffer. Bound protein was then eluted from the QHP column by a salt gradient over 50 ml between Low-Salt buffer (25 mM KCl) and High-Salt buffer (1 M KCl). Peak fractions were pooled and the His-tag was removed by digestion with thrombin (His-Ube1) or TEV (His-gp78-ubc7) at 4°C over night. The protein was run over a His-trap column to remove the cleaved tag and the flowthrough was collected and further purified by size exclusion chromatography (Superdex 75 for gp78-ubc7 or Superdex 200 for mUbe1) with a flow rate of 1 ml/min in Gel-filtration buffer (50 mM HEPES pH 7.4, 150 mM KCl, 2 mM $MgCl_2$, 5 % glycerol, 1 mM DTT). Fractions containing the protein were pooled, concentrated (Vivaspin Turbo 100 kDa MWCO, Sartorius), aliquoted and stored at -80°C.

4.2.3.6 Purification of untagged ubiquitin

Cell pellets (in lysis buffer) were thawed and supplemented with lysozyme (1g/L) and PMSF (1 mM). After stirring at 4°C for 30 min, the cells were lysed by sonication (Bandelin Sonoplus, MS 73 tip, 3 pulses at 60%), followed by centrifugation at 20,000 x g for 1 h at 4°C. The supernatant was supplemented with 2.5 ml of diluted perchloric acid (70 % Perchloric acid in 40 ml of 5 mM Tris pH 7.5, 100 mM KCl) per of 50 ml supernatant. The mixture was incubated on ice for 10 minutes and centrifuged again with 20,000 x g for 1 h at 4°C. The supernatant then dialyzed with 5 L of 25 mM ammonium acetate pH 4.5 using MEMBRA-CEL® dialysis tubing (MWCO 3500, SERVA) at 4°C over night. On the next day, the dialyzed supernatant was loaded on a SP HP Cation-exchange column. The column was washed with 50 ml of 25 mM ammonium acetate pH 4.5 and transferred to

an Äkta purifier or Äkta pure system. Bound protein was eluted with a gradient between 25 mM ammonium acetate pH 4.5 and 250 mM ammonium acetate 200 mM NaCl pH 7.6 over 30 ml. Fractions containing the protein were pooled, concentrated (Vivaspin Turbo 5 kDa MWCO, Sartorius), buffer exchanged to 5% glycerol in H_2O, aliquoted and stored at -80°C.

4.2.3.7 Purification of GST-tagged proteins (p37, p47, UBXN2A)

Cell pellets (in lysis buffer) were thawed and supplemented with lysozyme (1g/L) and PMSF (1 mM). After stirring at 4°C for 30 min, the cells were lysed by sonication (Bandelin Sonoplus, MS 73 tip, 3 pulses at 60%), followed by centrifugation at 20,000 x g for 1 h at 4°C. The supernatant was filtered through a 0.8 µm membrane and loaded onto a GSTrap column (GE Healthcare) using a peristaltic pump (P-1, GE Healthcare) with a flow of 5 ml/min. The column was subsequently washed with 50 ml of lysis buffer and transferred to an Äkta purifier or Äkta pure system. Bound protein was eluted from the GSTrap column with 25 ml of lysis-buffer + 20 mM glutathione. Peak fractions were pooled and buffer exchanged (Vivaspin Turbo 10 kDa MWCO, Sartorius) to Gel-filtration buffer (50 mM HEPES pH 7.4, 150 mM KCl, 2 mM $MgCl_2$, 1 mM DTT, 5% glycerol). The GST-tag was cleaved by digestion with GST-PreScission protease at 4°C over night. The protein was passed through a GSTrap column connected to a gel filtration column (16/600 Superdex 75 pg, GE Healthcare) to remove the protease and the cleaved tag with a flow rate of 1 ml/min in Gel-filtration buffer (50 mM HEPES pH 7.4, 150 mM KCl, 2 mM $MgCl_2$, 5 % glycerol, 1 mM DTT). Fractions containing the protein were pooled, concentrated (Vivaspin Turbo 10 kDa MWCO, Sartorius), aliquoted and stored at -80°C.

4.2.4 Determination of protein concentration

Protein concentrations were determined based on the absorbance at 280 nm and extinction coefficients that were calculated based on the amino acid sequence (https://web.expasy.org/protparam/). For mEos3.2 containing proteins the concentration

was determined via the absorbance at 506 nm (green, not converted Eos) or 573 nm (red, converted Eos).

4.2.5 Photoconversion of Eos

His-diUb-mEos3.2 and SDS22+PP1+His-mEos3.2-I3 were irradiated with a 365 nm longwave UV lamp (UVP Blak-Ray^{TM} B-100AP) to induce a backbone break in the peptide chain. The protein was pipetted on a plastic cover slip and placed on ice. The UV lamp was positioned above and the sample was irradiated for four 30 minute intervals with 30 minute brakes between each irradiation step, resulting in 2 hours of total irradiation. Afterwards, the absorbance spectrum of the protein sample was measured (NanoDrop 2000c, Thermo Scientific). The efficiency of photoconversion was calculated based on the ratio between the absorbance at 508 nm/extinction coefficient at 506 nm and the absorbance at 573 nm/extinction coefficient at 573 nm.

4.2.6 Ubiquitination

The (irradiated) diUb-Eos substrate was enzymatically modified with ubiquitin chains to serve as a substrate for p97-Ufd1-Npl4 based on established procedure (Blythe et al., 2017). The reaction was prepared for a total volume of 10 ml with 10 µM His-diUb-mEos3.2 substrate, 2 µM mUbe1 (E1 enzyme), 20 µM gp78-ubc7 (E2-E3 fusion), 400 µM ubiquitin and 10 mM ATP in ubiquitination buffer (50 mM HEPES pH 7.4, 150 mM KCl, 10 mM $MgCl_2$). The reaction mixture was incubated at 37°C over night (~14-16 h) and then loaded on a 5 ml His-trap column to separate the His-tagged substrate from the remaining enzymes and free ubiquitin chains. The substrate was subsequently eluted from the His-trap column with a buffer containing 300 mM imidazole and further purified by gel filtration on a 16/600 Superdex200 pg column (GE). Peak fractions were analyzed by SDS-PAGE and fractions containing highly ubiquitinated substrate were pooled.

4.2.7 ATPase assay

The ATPase activity of p97 in the presence or absence of p47 was determined with a malachite green assay. Triplicates of His-p97 (30 nM) and p47 (150 nM) were prepared in 40 µl of unfolding buffer (25 mM HEPES pH 7.4, 100 mM KCL, 5 mM $MgCl_2$, 1 mM DTT) and pipetted in a 96 well plate. The plate was incubated at 37°C for 10 minutes and 10 µl of 1 mM ATP were added per well. After 10 more minutes at 37°C, 50 µl of

Biomol®Green reagent (EnzoLifescience) were added and the plate was incubated at room temperature for 30 minutes before measurement of the absorbance at 600 nm. The amount of hydrolyzed ATP was calculated based on the absorbance in relation to a phosphate standard curve. Significance was calculated by ordinary one-way ANOVA with GraphPad Prism 8.

4.2.8 Fluorescence-based unfolding assay

Unfolding of the SPEosI (SDS22+PP1+His-mEos3.2-I3) substrate by p97 was determined through the decrease in I3 linked mEos3.2 fluorescence. Measurements were done on a Cary Eclipse Fluorescence Spectrophotometer (Varian) using Ultra-micro cell type 105.250-QS cuvettes (Hellma Analytics) with excitation at 540 nm and recorded emission at 580 nm. The standard reaction contained 35 nM SPEosI, 175 nM His-p97 and 500 nM adapter protein in 59.4 µl of unfolding buffer (25 mM HEPES pH7.4, 100 mM KCl, 5 mM $MgCl_2$, 1 mM DTT). The mixture was incubated at 37°C for 5 minutes, before the addition of 0.6 µl of 200 mM ATP (2 mM final concentration). The fluorescence decay was measured every 15 seconds over 40 min.

The effect of adapter and p97 concentration on the initial unfolding rate was determined by titration experiments. In the adapter titration experiments, the concentration of p97 was kept constant at 400 µM, while in p97 titration experiments, the concentration of p37 was increased to 2 µM. The slope of the decay over between the fourth and the 13^{th} measurement point (first three minutes) was used to calculate the Initial rates were plotted against the p97:adapter ratio with GraphPad Prism 8.

4.2.9 Immunoprecipitation

Immunoprecipitation experiments with SPI complex, p37/p47 and p97 were done by mixing His-p97 (350 nM), adapter protein (500 nM) and SDS22-PP1-I3 (80 nM) in 24.5 µl of 50 mM HEPES pH7.4, 150 mM KCl, 2 mM $MgCl_2$, 1 mM DTT, 0.1% BSA and 5% glycerol, together with 0.5 µl of mouse-monoclonal anti-PP1γ antibody (Santa Cruz). After incubation on ice for 10 min, the mixture was diluted to 400 µl with buffer containing 1% Triton X-100. An input control of 25 µl was taken and the remainder was added to 20 µl of GammaBind G Sepharose beads. Samples were slowly rotated for 1 h at 4°C and then

centrifuged for 2 min with 1,000xg. The beads were washed three times with 300 µl buffer with 1% Triton X-100. Bound proteins were eluted by the addition of 30 µl of 6xLaemmli buffer followed by boiling at 95°C for 5 min. Elution and input fractions were loaded on an SDS-gel and subsequently analyzed by Western-blot.

4.2.10 SDS-PAGE and Western-blot

Samples from protein purification and immunoprecipitation experiments were analyzed by SDS-PAGE. Samples were supplemented with 6x SDS-sample buffer and boiled at 95°C for 5 min before being loaded into the bags of the SDS-gel. Gels were cast using the Mini-PROTEAN® Tetra Cell system (Bio-Rad). Proteins were separated by size trough a constant current of 20 mA in SDS-running buffer (190 mM glycine, 25 mM Tris, 0.1 % SDS). Protein purification gels were subsequently stained with colloidal coomassie for 1 hour before destaining with water. Immunoprecipitation samples were further analyzed by Western-blot. Proteins were transferred to a nitrocellulose membrane in a Mini Trans-Blot chamber (BioRad), with a constant current of 300 mA in Western transfer buffer (192 mM Glycine, 25 mM Tris, 0.04 % SDS, 20 % methanol) at 4°C over night (14-16 hours). After the transfer was complete, the membrane was stained with Ponceau-S to verifiy that proteins had been transferred uniformly. Afterwards, the membrane was incubated at room temperature for 1 hour in 5 % milk powder dissolved in PBS-T (1xPBS + 0.1 % Tween-20). The membrane was washed 3 x 5 minutes with PBS-T and incubated with the primary antibody diluted in PBS-T + 3 % BSA. After 2 hours at room temperature or overnight at 4°C the primary antibody was removed and the membrane was washed three times for five minutes with PBS-T. The membrane was incubated with the secondary antibody diluted in PBS-T + 3% BSA for 1 hour. After the secondary antibody had been removed, the membrane was washed again three times for five minutes with PBS-T. The membrane was treated with SuperSignal™ West Pico PLUS Chemiluminescent Substrate (Thermo Scientific) or Amersham™ ECL Prime Western Blotting Detection Reagent (GE Healthcare) and bands were visualized with a ECL Chemostar (INTAS) imager.

4.2.11 Generation of the p97-p37 model

Since there is no existing structure of p37 bound to p97, the model of the C-terminus of p37 (SHP-UBX) bound to p97 was generated from three pdb structures of other proteins with similar domains using the program YASARA (http://www.yasara.org). The UBX

domain was built as a homology model of the UBX domain of Shp1 bound to Cdc48 (pdb: 6opc, (Cooney et al., 2019)). The SHP box was modeled after the SHP of Ufd1 bound to the N-domain of p97 (pdb: 5b6c, (Le et al., 2016). The structure of p97 in the up-conformation was selected as the third component (pdb:5ftn, Banerjee et al., 2016a). The SHP box and the UBX domain were then planted on p97 and three residues that were missing between the model of the SHP box and the UBX domain were inserted. Finally, the entire structure was energy minimized.

4.2.12 Crosslinking

Crosslinking of proteins carrying a pBpA residue with was done by mixing of p97, adapter protein, SDS22+PP1+I3 (SPI) and ATPγS in gel filtration buffer (50 mM HEPES pH 7.4, 150 mM KCl, 2 mM $MgCl_2$, 5 % glycerol, 1 mM DTT). The samples were incubated at 30°C for 10 minutes and then pipetted in drops on a parafilm that was placed on an aluminum block on ice. The block was placed in a CL-1000 UV crosslinker (Analytik Jena, 365 nm) and irradiated for 30 min. Afterwards, the samples were transferred back into eppendorf tubes, supplemented with 6x SDS-sample buffer, boiled for 5 minutes at 95°C and loaded on an SDS-gel. Crosslinks between the pBpA carrying protein and interaction partners were detected by Western-blot.

For the $p37^{pBpA}$ mutants (82, 182, 234) His-p97 (175 nM), $p37^{pBpA}$ (250 nM) and SPI (215 nM) were used. In addition the buffer was supplemented BSA to 0.1 mg/ml.

For crosslinking with the $p97^{314pBpA}$ or $p97^{278pBpA}$ mutants, $p97^{pBpA}$-SBP-His (350 nM), adapter protein (500 nM) and SPI (430 nM) were used.

4.2.13 Mass spectrometry

Crosslinking products between $p37^{pBpA}$ and the SPI complex and p97 were analyzed by LC-MS/MS at the Analytics Core Facility Essen (ACE). Samples were prepared as described for crosslinking experiments, but not supplemented with SDS-sample buffer. Proteins were digested with LysC and trypsin before peptide analysis through LC-MS/MS. Detected peptide fragments were identified with StavroX (v3.6.6.). A detailed description of the experimental procedure can be found in the supplementary material of (Kracht et al., 2020).

References

Alberts, A.S., Montminy, M., Shenolikar, S., and Feramisco, J.R. (1994). Expression of a peptide inhibitor of protein phosphatase 1 increases phosphorylation and activity of CREB in NIH 3T3 fibroblasts. Molecular and Cellular Biology *14*, 4398–4407.

Andreassen, P.R., Lacroix, F.B., Villa-Moruzzi, E., and Margolis, R.L. (1998). Differential Subcellular Localization of Protein Phosphatase-1 α, γ1, and δ Isoforms during Both Interphase and Mitosis in Mammalian Cells. Journal of Cell Biology *141*, 1207–1215.

Arita, M., Wakita, T., and Shimizu, H. (2012). Valosin-Containing Protein (VCP/p97) Is Required for Poliovirus Replication and Is Involved in Cellular Protein Secretion Pathway in Poliovirus Infection. J Virol *86*, 5541–5553.

Ayllón, V., Martínez-A, C., García, A., Cayla, X., and Rebollo, A. (2000). Protein phosphatase 1α is a Ras-activated Bad phosphatase that regulates interleukin-2 deprivation-induced apoptosis. The EMBO Journal *19*, 2237–2246.

Banerjee, S., Bartesaghi, A., Merk, A., Rao, P., Bulfer, S.L., Yan, Y., Green, N., Mroczkowski, B., Neitz, R.J., Wipf, P., et al. (2016). 2.3 Å resolution cryo-EM structure of human p97 and mechanism of allosteric inhibition. Science aad7974.

Beck, M., Schmidt, A., Malmstroem, J., Claassen, M., Ori, A., Szymborska, A., Herzog, F., Rinner, O., Ellenberg, J., and Aebersold, R. (2011). The quantitative proteome of a human cell line. Molecular Systems Biology *7*, 549.

Bengtson, M.H., and Joazeiro, C.A.P. (2010). Role of a ribosome-associated E3 ubiquitin ligase in protein quality control. Nature *467*, 470–473.

Beskow, A., Grimberg, K.B., Bott, L.C., Salomons, F.A., Dantuma, N.P., and Young, P. (2009). A Conserved Unfoldase Activity for the p97 AAA-ATPase in Proteasomal Degradation. Journal of Molecular Biology *394*, 732–746.

Bharucha, J.P., Larson, J.R., Gao, L., Daves, L.K., and Tatchell, K. (2008). Ypi1, a Positive Regulator of Nuclear Protein Phosphatase Type 1 Activity in Saccharomyces cerevisiae. MBoC *19*, 1032–1045.

Blythe, E.E., Olson, K.C., Chau, V., and Deshaies, R.J. (2017). Ubiquitin- and ATP-dependent unfoldase activity of P97/VCP•NPLOC4•UFD1L is enhanced by a mutation that causes multisystem proteinopathy. PNAS *114*, E4380–E4388.

Blythe, E.E., Gates, S.N., Deshaies, R.J., and Martin, A. (2019). Multisystem Proteinopathy Mutations in VCP/p97 Increase NPLOC4·UFD1L Binding and Substrate Processing. Structure S096921261930317X.

Bodnar, N.O., and Rapoport, T.A. (2017). Molecular Mechanism of Substrate Processing by the Cdc48 ATPase Complex. Cell *169*, 722-735.e9.

Böhm, S., and Buchberger, A. (2013). The Budding Yeast Cdc48Shp1 Complex Promotes Cell Cycle Progression by Positive Regulation of Protein Phosphatase 1 (Glc7). PLOS ONE *8*, e56486.

Bojkova, D., Klann, K., Koch, B., Widera, M., Krause, D., Ciesek, S., Cinatl, J., and Münch, C. (2020). Proteomics of SARS-CoV-2-infected host cells reveals therapy targets. Nature *583*, 469–472.

Bollen, M., Peti, W., Ragusa, M.J., and Beullens, M. (2010). The extended PP1 toolkit: designed to create specificity. Trends Biochem Sci *35*, 450–458.

van den Boom, J., and Meyer, H. (2017). VCP/p97-Mediated Unfolding as a Principle in Protein Homeostasis and Signaling. Molecular Cell.

van den Boom, J., Wolf, M., Weimann, L., Schulze, N., Li, F., Kaschani, F., Riemer, A., Zierhut, C., Kaiser, M., Iliakis, G., et al. (2016). VCP/p97 extracts sterically trapped Ku70/80 rings from DNA in double strand break repair. Mol Cell *64*, 189–198.

Brandman, O., and Hegde, R.S. (2016). Ribosome-associated protein quality control. Nature Structural & Molecular Biology *23*, 7–15.

Brautigan, D.L. (2013). Protein Ser/ Thr phosphatases – the ugly ducklings of cell signalling. The FEBS Journal *280*, 324–325.

Buchberger, A., Schindelin, H., and Hänzelmann, P. (2015). Control of p97 function by cofactor binding. FEBS Letters *589*, 2578–2589.

Budenholzer, L., Cheng, C.L., Li, Y., and Hochstrasser, M. (2017). Proteasome Structure and Assembly. J Mol Biol *429*, 3500–3524.

Carissimo, G., Chan, Y.-H., Utt, A., Chua, T.-K., Bakar, F.A., Merits, A., and Ng, L.F.P. (2019). VCP/p97 Is a Proviral Host Factor for Replication of Chikungunya Virus and Other Alphaviruses. Front. Microbiol. *10*.

Carvalho, A.F., Pinto, M.P., Grou, C.P., Vitorino, R., Domingues, P., Yamao, F., Sá-Miranda, C., and Azevedo, J.E. (2012). High-Yield Expression in Escherichia coli and Purification of Mouse Ubiquitin-Activating Enzyme E1. Mol Biotechnol *51*, 254–261.

Ceulemans, H., and Bollen, M. (2004). Functional Diversity of Protein Phosphatase-1, a Cellular Economizer and Reset Button. Physiological Reviews *84*, 1–39.

Chen, J., and Chen, Z.J. (2013). Regulation of NF-κB by Ubiquitination. Curr Opin Immunol *25*, 4–12.

Cheng, Y.-L., and Chen, R.-H. (2015). Assembly and quality control of the protein phosphatase 1 holoenzyme involves the Cdc48–Shp1 chaperone. J Cell Sci *128*, 1180–1192.

Chin, J.W., Martin, A.B., King, D.S., Wang, L., and Schultz, P.G. (2002). Addition of a photocrosslinking amino acid to the genetic code of Escherichia coli. PNAS *99*, 11020–11024.

Choy, M.S., Bolik-Coulon, N., Archuleta, T.L., Peti, W., and Page, R. (2018). The structure of SDS22 provides insights into the mechanism of heterodimer formation with PP1. Acta Cryst F *74*, 817–824.

Choy, M.S., Moon, T.M., Ravindran, R., Bray, J.A., Robinson, L.C., Archuleta, T.L., Shi, W., Peti, W., Tatchell, K., and Page, R. (2019). SDS22 selectively recognizes and traps metal-deficient inactive PP1. PNAS *116*, 20472–20481.

Christianson, J.C., and Ye, Y. (2014). Cleaning up in the endoplasmic reticulum: ubiquitin in charge. Nature Structural & Molecular Biology *21*, 325–335.

Chun, Y.S., Shima, H., Nagasaki, K., Sugimura, T., and Nagao, M. (1994). PP1 gamma 2, a testis-specific protein-serine/threonine-phosphatase type 1 catalytic subunit, is associated with a protein having high sequence homology with the 78-kDa glucose-regulated protein, a member of the 70-kDa heat shock protein family. PNAS *91*, 3319–3323.

Conicella, A.E., Huang, R., Ripstein, Z.A., Nguyen, A., Wang, E., Löhr, T., Schuck, P., Vendruscolo, M., Rubinstein, J.L., and Kay, L.E. (2020). An intrinsically disordered motif regulates the interaction between the p47 adaptor and the p97 AAA+ ATPase. PNAS.

Cooney, I., Han, H., Stewart, M.G., Carson, R.H., Hansen, D.T., Iwasa, J.H., Price, J.C., Hill, C.P., and Shen, P.S. (2019). Structure of the Cdc48 segregase in the act of unfolding an authentic substrate. Science eaax0486.

da Cruz e Silva, E., Fox, C., Ouimet, C., Gustafson, E., Watson, S., and Greengard, P. (1995). Differential expression of protein phosphatase 1 isoforms in mammalian brain. J. Neurosci. *15*, 3375–3389.

DeSantis, M.E., and Shorter, J. (2012). The elusive middle domain of Hsp104 and ClpB: Location and function. Biochimica et Biophysica Acta (BBA) - Molecular Cell Research *1823*, 29–39.

Dewar, J.M., Low, E., Mann, M., Räschle, M., and Walter, J.C. (2017). CRL2Lrr1 promotes unloading of the vertebrate replisome from chromatin during replication termination. Genes Dev. *31*, 275–290.

Djinovic-Carugo, K., Gautel, M., Ylänne, J., and Young, P. (2002). The spectrin repeat: a structural platform for cytoskeletal protein assemblies. FEBS Letters *513*, 119–123.

Dobrynin, G., Popp, O., Romer, T., Bremer, S., Schmitz, M.H.A., Gerlich, D.W., and Meyer, H. (2011). Cdc48/p97–Ufd1–Npl4 antagonizes Aurora B during chromosome segregation in HeLa cells. J Cell Sci *124*, 1571–1580.

Dreveny, I., Kondo, H., Uchiyama, K., Shaw, A., Zhang, X., and Freemont, P.S. (2004). Structural basis of the interaction between the AAA ATPase p97/VCP and its adaptor protein p47. The EMBO Journal *23*, 1030–1039.

Eiteneuer, A., Seiler, J., Weith, M., Beullens, M., Lesage, B., Krenn, V., Musacchio, A., Bollen, M., and Meyer, H. (2014). Inhibitor-3 ensures bipolar mitotic spindle attachment

by limiting association of SDS22 with kinetochore-bound protein phosphatase-1. The EMBO Journal *33*, 2704–2720.

Ernst, V., Levin, D.H., Foulkes, J.G., and London, I.M. (1982). Effects of skeletal muscle protein phosphatase inhibitor-2 on protein synthesis and protein phosphorylation in rabbit reticulocyte lysates. PNAS *79*, 7092–7096.

Escobar-Henriques, M., and Anton, V. (2020). Mitochondrial Surveillance by Cdc48/p97: MAD vs. Membrane Fusion. Int J Mol Sci *21*.

Eto, M., Kitazawa, T., Matsuzawa, F., Aikawa, S., Kirkbride, J.A., Isozumi, N., Nishimura, Y., Brautigan, D.L., and Ohki, S. (2007). Phosphorylation-induced conformational switching of CPI-17 produces a potent myosin phosphatase inhibitor. Structure *15*, 1591–1602.

Fullbright, G., Rycenga, H.B., Gruber, J.D., and Long, D.T. (2016). p97 Promotes a Conserved Mechanism of Helicase Unloading during DNA Cross-Link Repair. Molecular and Cellular Biology *36*, 2983–2994.

Gardner, B.M., Castanzo, D.T., Chowdhury, S., Stjepanovic, G., Stefely, M.S., Hurley, J.H., Lander, G.C., and Martin, A. (2018). The peroxisomal AAA-ATPase Pex1/Pex6 unfolds substrates by processive threading. Nature Communications *9*, 135.

Gibson, D.G., Young, L., Chuang, R.-Y., Venter, J.C., Hutchison, C.A., and Smith, H.O. (2009). Enzymatic assembly of DNA molecules up to several hundred kilobases. Nature Methods *6*, 343–345.

Golbik, R., Lupas, A.N., Koretke, K.K., Baumeister, W., and Peters, J. (1999). The Janus Face of the Archaeal Cdc48/p97 Homologue VAT: Protein Folding versus Unfolding. Biological Chemistry *380*, 1049–1062.

Goldberg, J., Huang, H., Kwon, Y., Greengard, P., Nairn, A.C., and Kuriyan, J. (1995). Three-dimensional structure of the catalytic subunit of protein serine/threonine phosphatase-1. Nature *376*, 745–753.

Groll, M., Bajorek, M., Köhler, A., Moroder, L., Rubin, D., Huber, R., Glickman, M., and Finley, D. (2000). A gated channel into the proteasome core particle. Nature Structural Biology *7*, 1062–1067.

Heo, J.-M., Livnat-Levanon, N., Taylor, E.B., Jones, K.T., Dephoure, N., Ring, J., Xie, J., Brodsky, J.L., Madeo, F., Gygi, S.P., et al. (2010). A Stress-Responsive System for Mitochondrial Protein Degradation. Molecular Cell *40*, 465–480.

Heroes, E., Lesage, B., Görnemann, J., Beullens, M., Meervelt, L.V., and Bollen, M. (2013). The PP1 binding code: a molecular-lego strategy that governs specificity. The FEBS Journal *280*, 584–595.

Hou, H., Sun, L., Siddoway, B.A., Petralia, R.S., Yang, H., Gu, H., Nairn, A.C., and Xia, H. (2013). Synaptic NMDA receptor stimulation activates PP1 by inhibiting its phosphorylation by Cdk5. Journal of Cell Biology *203*, 521–535.

Hsu, J.-Y., Sun, Z.-W., Li, X., Reuben, M., Tatchell, K., Bishop, D.K., Grushcow, J.M., Brame, C.J., Caldwell, J.A., Hunt, D.F., et al. (2000). Mitotic Phosphorylation of Histone H3 Is Governed by Ipl1/aurora Kinase and Glc7/PP1 Phosphatase in Budding Yeast and Nematodes. Cell *102*, 279–291.

Hu, X., Wang, L., Wang, Y., Ji, J., Li, J., Wang, Z., Li, C., Zhang, Y., and Zhang, Z.-R. (2020). RNF126-Mediated Reubiquitination Is Required for Proteasomal Degradation of p97-Extracted Membrane Proteins. Molecular Cell *79*, 320-331.e9.

Huang, H.-S., and Lee, E.Y.C. (2008). Protein Phosphatase-1 Inhibitor-3 Is an in Vivo Target of Caspase-3 and Participates in the Apoptotic Response. J Biol Chem *283*, 18135–18146.

Huang, H.-S., Pozarowski, P., Gao, Y., Darzynkiewicz, Z., and Lee, E.Y.C. (2005). Protein phosphatase-1 inhibitor-3 is co-localized to the nucleoli and centrosomes with PP1γ1 and PP1α, respectively. Archives of Biochemistry and Biophysics *443*, 33–44.

Huang, R., Ripstein, Z.A., Rubinstein, J.L., and Kay, L.E. (2019a). Cooperative subunit dynamics modulate p97 function. Proceedings of the National Academy of Sciences *116*, 158–167.

Huang, R., Ripstein, Z.A., Rubinstein, J.L., and Kay, L.E. (2019b). Cooperative subunit dynamics modulate p97 function. Proceedings of the National Academy of Sciences *116*, 158–167.

Hülsmann, J., Kravic, B., Weith, M., Gstaiger, M., Aebersold, R., Collins, B.C., and Meyer, H. (2018). AP-SWATH Reveals Direct Involvement of VCP/p97 in Integrated Stress Response Signaling Through Facilitating CReP/PPP1R15B Degradation. Mol Cell Proteomics *17*, 1295–1307.

Ju, J.-S., Miller, S.E., Hanson, P.I., and Weihl, C.C. (2008). Impaired Protein Aggregate Handling and Clearance Underlie the Pathogenesis of p97/VCP-associated Disease*. Journal of Biological Chemistry *283*, 30289–30299.

Katoh, H., Harada, A., Mori, K., and Negishi, M. (2002). Socius Is a Novel Rnd GTPase-Interacting Protein Involved in Disassembly of Actin Stress Fibers. Molecular and Cellular Biology *22*, 2952–2964.

Kirchner, P., Bug, M., and Meyer, H. (2013). Ubiquitination of the N-terminal Region of Caveolin-1 Regulates Endosomal Sorting by the VCP/p97 AAA-ATPase. J Biol Chem *288*, 7363–7372.

Komander, D., and Rape, M. (2012). The Ubiquitin Code. Annual Review of Biochemistry *81*, 203–229.

Kondo, H., Rabouille, C., Newman, R., Levine, T.P., Pappin, D., Freemont, P., and Warren, G. (1997). p47 is a cofactor for p97-mediated membrane fusion. Nature *388*, 75–78.

Kracht, M., van den Boom, J., Seiler, J., Kröning, A., Kaschani, F., Kaiser, M., and Meyer, H. (2020). Protein Phosphatase-1 Complex Disassembly by p97 is Initiated through Multivalent Recognition of Catalytic and Regulatory Subunits by the p97 SEP-domain Adapters. Journal of Molecular Biology *432*, 6061–6074.

Kress, E., Schwager, F., Holtackers, R., Seiler, J., Prodon, F., Zanin, E., Eiteneuer, A., Toya, M., Sugimoto, A., Meyer, H., et al. (2013). The UBXN-2/p37/p47 adaptors of CDC-48/p97 regulate mitosis by limiting the centrosomal recruitment of Aurora A. J Cell Biol *201*, 559–575.

Kunjappu, M.J., and Hochstrasser, M. (2014). Assembly of the 20S Proteasome. Biochim Biophys Acta *1843*.

Lasker, K., Förster, F., Bohn, S., Walzthoeni, T., Villa, E., Unverdorben, P., Beck, F., Aebersold, R., Sali, A., and Baumeister, W. (2012). Molecular architecture of the 26S proteasome holocomplex determined by an integrative approach. PNAS *109*, 1380–1387.

Le, L.T.M., Kang, W., Kim, J.-Y., Le, O.T.T., Lee, S.Y., and Yang, J.K. (2016). Structural Details of Ufd1 Binding to p97 and Their Functional Implications in ER-Associated Degradation. PLOS ONE *11*, e0163394.

Lee, B.H., Schwager, F., Meraldi, P., and Gotta, M. (2018). p37/UBXN2B regulates spindle orientation by limiting cortical NuMA recruitment via PP1/Repo-Man. J Cell Biol *217*, 483–493.

Lesage, B., Beullens, M., Ceulemans, H., Himpens, B., and Bollen, M. (2005). Determinants of the nucleolar targeting of protein phosphatase-1. FEBS Letters *579*, 5626–5630.

Lesage, B., Beullens, M., Pedelini, L., Garcia-Gimeno, M.A., Waelkens, E., Sanz, P., and Bollen, M. (2007). A Complex of Catalytically Inactive Protein Phosphatase-1 Sandwiched between Sds22 and Inhibitor-3. Biochemistry *46*, 8909–8919.

Li, J.-M., Wu, H., Zhang, W., Blackburn, M.R., and Jin, J. (2014). The p97-UFD1L-NPL4 Protein Complex Mediates Cytokine-Induced IκBα Proteolysis. Molecular and Cellular Biology *34*, 335–347.

Li, M., Brooks, C.L., Wu-Baer, F., Chen, D., Baer, R., and Gu, W. (2003). Mono- Versus Polyubiquitination: Differential Control of p53 Fate by Mdm2. Science *302*, 1972–1975.

Lin, Y.-T., Prendergast, J., and Grey, F. (2017). The host ubiquitin-dependent segregase VCP/p97 is required for the onset of human cytomegalovirus replication. PLOS Pathogens *13*, e1006329.

Liu, D., Vleugel, M., Backer, C.B., Hori, T., Fukagawa, T., Cheeseman, I.M., and Lampson, M.A. (2010). Regulated targeting of protein phosphatase 1 to the outer kinetochore by KNL1 opposes Aurora B kinase. Journal of Cell Biology *188*, 809–820.

Lu, J., and Deutsch, C. (2008). Electrostatics in the Ribosomal Tunnel Modulate Chain Elongation Rates. Journal of Molecular Biology *384*, 73–86.

Lumb, J.H., Connell, J.W., Allison, R., and Reid, E. (2012). The AAA ATPase spastin links microtubule severing to membrane modelling. Biochimica et Biophysica Acta (BBA) - Molecular Cell Research *1823*, 192–197.

McLelland, G.-L., Goiran, T., Yi, W., Dorval, G., Chen, C.X., Lauinger, N.D., Krahn, A.I., Valimehr, S., Rakovic, A., Rouiller, I., et al. (2018). Mfn2 ubiquitination by PINK1/parkin gates the p97-dependent release of ER from mitochondria to drive mitophagy. ELife *7*, e32866.

Meyer, H.H. (2005). Golgi reassembly after mitosis: The AAA family meets the ubiquitin family. Biochimica et Biophysica Acta (BBA) - Molecular Cell Research *1744*, 108–119.

Meyer, H., and Weihl, C.C. (2014). The VCP/p97 system at a glance: connecting cellular function to disease pathogenesis. J Cell Sci *127*, 3877–3883.

Meyer, H.-J., and Rape, M. (2014). Enhanced protein degradation by branched ubiquitin chains. Cell *157*, 910–921.

Meyer, H.H., Kondo, H., and Warren, G. (1998). The p47 co-factor regulates the ATPase activity of the membrane fusion protein, p97. FEBS Letters *437*, 255–257.

Meyer, H.H., Shorter, J.G., Seemann, J., Pappin, D., and Warren, G. (2000). A complex of mammalian Ufd1 and Npl4 links the AAA-ATPase, p97, to ubiquitin and nuclear transport pathways. The EMBO Journal *19*, 2181–2192.

Meyer, H.H., Wang, Y., and Warren, G. (2002). Direct binding of ubiquitin conjugates by the mammalian p97 adaptor complexes, p47 and Ufd1–Npl4. The EMBO Journal *21*, 5645–5652.

Monroe, N., Han, H., Shen, P.S., Sundquist, W.I., and Hill, C.P. (2017). Structural basis of protein translocation by the Vps4-Vta1 AAA ATPase. ELife *6*, e24487.

Moreno, S.P., Bailey, R., Campion, N., Herron, S., and Gambus, A. (2014). Polyubiquitylation drives replisome disassembly at the termination of DNA replication. Science *346*, 477–481.

Nguyen, T.V., Li, J., Lu, C.-C. (Jean), Mamrosh, J.L., Lu, G., Cathers, B.E., and Deshaies, R.J. (2017). p97/VCP promotes degradation of CRBN substrate glutamine synthetase and neosubstrates. PNAS *114*, 3565–3571.

Olszewski, M.M., Williams, C., Dong, K.C., and Martin, A. (2019). The Cdc48 unfoldase prepares well-folded protein substrates for degradation by the 26S proteasome. Commun Biol *2*, 1–8.

Olzmann, J.A., Kopito, R.R., and Christianson, J.C. (2013). The Mammalian Endoplasmic Reticulum-Associated Degradation System. Cold Spring Harb Perspect Biol *5*.

Pan, M., Zheng, Q., Yu, Y., Ai, H., Xie, Y., Zeng, X., Wang, C., Liu, L., and Zhao, M. (2021). Seesaw conformations of Npl4 in the human p97 complex and the inhibitory mechanism of a disulfiram derivative. Nature Communications *12*, 121.

Papadopoulos, C., Kirchner, P., Bug, M., Grum, D., Koerver, L., Schulze, N., Poehler, R., Dressler, A., Fengler, S., Arhzaouy, K., et al. (2017). VCP/p97 cooperates with YOD1, UBXD1 and PLAA to drive clearance of ruptured lysosomes by autophagy. The EMBO Journal *36*, 135–150.

Pedelini, L., Marquina, M., Ariño, J., Casamayor, A., Sanz, L., Bollen, M., Sanz, P., and Garcia-Gimeno, M.A. (2007). YPI1 and SDS22 Proteins Regulate the Nuclear Localization and Function of Yeast Type 1 Phosphatase Glc7*. Journal of Biological Chemistry *282*, 3282–3292.

Peggie, M., MacKelvie, S., Bloecher, A., Knatko, E., Tatchell, K., and Stark, M. (2002). Essential functions of Sds22p in chromosome stability and nuclear localization of PP1. Journal of Cell Science *115*, 195–206.

Pelkmans, L., Bürli, T., Zerial, M., and Helenius, A. (2004). Caveolin-Stabilized Membrane Domains as Multifunctional Transport and Sorting Devices in Endocytic Membrane Traffic. Cell *118*, 767–780.

Peña, A.H. de la, Goodall, E.A., Gates, S.N., Lander, G.C., and Martin, A. (2018). Substrate-engaged 26S proteasome structures reveal mechanisms for ATP-hydrolysis–driven translocation. Science eaav0725.

Puchades, C., Rampello, A.J., Shin, M., Giuliano, C.J., Wiseman, R.L., Glynn, S.E., and Lander, G.C. (2017). Structure of the mitochondrial inner membrane AAA+ protease YME1 gives insight into substrate processing. Science *358*.

Puchades, C., Sandate, C.R., and Lander, G.C. (2019). The molecular principles governing the activity and functional diversity of AAA+ proteins. Nat Rev Mol Cell Biol.

Rabouille, C., Kondo, H., Newman, R., Hui, N., Freemont, P., and Warren, G. (1998). Syntaxin 5 Is a Common Component of the NSF- and p97-Mediated Reassembly Pathways of Golgi Cisternae from Mitotic Golgi Fragments In Vitro. Cell *92*, 603–610.

Radulovic, M., Schink, K.O., Wenzel, E.M., Nähse, V., Bongiovanni, A., Lafont, F., and Stenmark, H. (2018). ESCRT-mediated lysosome repair precedes lysophagy and promotes cell survival. The EMBO Journal *37*, e99753.

Ramadan, K., Bruderer, R., Spiga, F.M., Popp, O., Baur, T., Gotta, M., and Meyer, H.H. (2007). Cdc48/p97 promotes reformation of the nucleus by extracting the kinase Aurora B from chromatin. Nature *450*, 1258–1262.

Raman, M., Sergeev, M., Garnaas, M., Lydeard, J.R., Huttlin, E.L., Goessling, W., Shah, J.V., and Harper, J.W. (2015). Systematic proteomics of the VCP–UBXD adaptor network identifies a role for UBXN10 in regulating ciliogenesis. Nature Cell Biology *17*, 1356–1369.

Repnik, U., Česen, M.H., and Turk, B. (2013). The Endolysosomal System in Cell Death and Survival. Cold Spring Harb Perspect Biol *5*, a008755.

Riemer, A., Dobrynin, G., Dressler, A., Bremer, S., Soni, A., Iliakis, G., and Meyer, H. (2014). The p97-Ufd1-Npl4 ATPase complex ensures robustness of the G2/M checkpoint by facilitating CDC25A degradation. Cell Cycle *13*, 919–927.

Ritz, D., Vuk, M., Kirchner, P., Bug, M., Schütz, S., Hayer, A., Bremer, S., Lusk, C., Baloh, R.H., Lee, H., et al. (2011). Endolysosomal sorting of ubiquitylated caveolin-1 is regulated by VCP and UBXD1 and impaired by VCP disease mutations. Nature Cell Biology *13*, 1116–1123.

Rothballer, A., Tzvetkov, N., and Zwickl, P. (2007). Mutations in p97/VCP induce unfolding activity. FEBS Letters *581*, 1197–1201.

Rumpf, S., and Jentsch, S. (2006). Functional Division of Substrate Processing Cofactors of the Ubiquitin-Selective Cdc48 Chaperone. Molecular Cell *21*, 261–269.

Sane, S., Abdullah, A., Boudreau, D.A., Autenried, R.K., Gupta, B.K., Wang, X., Wang, H., Schlenker, E.H., Zhang, D., Telleria, C., et al. (2014). Ubiquitin-like (UBX)-domain-containing protein, UBXN2A, promotes cell death by interfering with the p53-Mortalin interactions in colon cancer cells. Cell Death Dis *5*, e1118.

Schmidt, C.C., Vasic, V., and Stein, A. (2020). Doa10 is a membrane protein retrotranslocase in ER-associated protein degradation. ELife *9*, e56945.

Semlow, D.R., Zhang, J., Budzowska, M., Drohat, A.C., and Walter, J.C. (2016). Replication-Dependent Unhooking of DNA Interstrand Cross-Links by the NEIL3 Glycosylase. Cell *167*, 498-511.e14.

Simões, T., Schuster, R., den Brave, F., and Escobar-Henriques, M. (2018). Cdc48 regulates a deubiquitylase cascade critical for mitochondrial fusion. ELife *7*, e30015.

Skowyra, M.L., Schlesinger, P.H., Naismith, T.V., and Hanson, P.I. (2018). Triggered recruitment of ESCRT machinery promotes endolysosomal repair. Science *360*.

Skrott, Z., Mistrik, M., Andersen, K.K., Friis, S., Majera, D., Gursky, J., Ozdian, T., Bartkova, J., Turi, Z., Moudry, P., et al. (2017). Alcohol-abuse drug disulfiram targets cancer via p97 segregase adaptor NPL4. Nature *552*, 194.

Snider, J., Thibault, G., and Houry, W.A. (2008). The AAA+ superfamily of functionally diverse proteins. Genome Biol *9*, 216.

Stringer, D.K., and Piper, R.C. (2011). A single ubiquitin is sufficient for cargo protein entry into MVBs in the absence of ESCRT ubiquitination. Journal of Cell Biology *192*, 229–242.

Suzuki, M., Otsuka, T., Ohsaki, Y., Cheng, J., Taniguchi, T., Hashimoto, H., Taniguchi, H., and Fujimoto, T. (2012). Derlin-1 and UBXD8 are engaged in dislocation and degradation of lipidated ApoB-100 at lipid droplets. Mol Biol Cell *23*, 800–810.

Tang, W.K., Odzorig, T., Jin, W., and Xia, D. (2019). Structural Basis of p97 Inhibition by the Site-Selective Anticancer Compound CB-5083. Mol Pharmacol *95*, 286–293.

Teng, Y., Rezvani, K., and De Biasi, M. (2015). UBXN2A regulates nicotinic receptor degradation by modulating the E3 ligase activity of CHIP. Biochem Pharmacol *97*, 518–530.

Trowitzsch, S., Bieniossek, C., Nie, Y., Garzoni, F., and Berger, I. (2010). New baculovirus expression tools for recombinant protein complex production. Journal of Structural Biology *172*, 45–54.

Twomey, E.C., Ji, Z., Wales, T.E., Bodnar, N.O., Ficarro, S.B., Marto, J.A., Engen, J.R., and Rapoport, T.A. (2019a). Substrate processing by the Cdc48 ATPase complex is initiated by ubiquitin unfolding. Science eaax1033.

Uchiyama, K., Jokitalo, E., Kano, F., Murata, M., Zhang, X., Canas, B., Newman, R., Rabouille, C., Pappin, D., Freemont, P., et al. (2002). VCIP135, a novel essential factor for p97/p47-mediated membrane fusion, is required for Golgi and ER assembly in vivo. J Cell Biol *159*, 855–866.

Uchiyama, K., Totsukawa, G., Puhka, M., Kaneko, Y., Jokitalo, E., Dreveny, I., Beuron, F., Zhang, X., Freemont, P., and Kondo, H. (2006). p37 Is a p97 Adaptor Required for Golgi and ER Biogenesis in Interphase and at the End of Mitosis. Developmental Cell *11*, 803–816.

Verma, R., Oania, R.S., Kolawa, N.J., and Deshaies, R.J. (2013). Cdc48/p97 promotes degradation of aberrant nascent polypeptides bound to the ribosome. ELife *2013*.

Virshup, D.M., and Shenolikar, S. (2009). From Promiscuity to Precision: Protein Phosphatases Get a Makeover. Molecular Cell *33*, 537–545.

Wakula, P., Beullens, M., Ceulemans, H., Stalmans, W., and Bollen, M. (2003). Degeneracy and Function of the Ubiquitous RVXF Motif That Mediates Binding to Protein Phosphatase-1 *. Journal of Biological Chemistry *278*, 18817–18823.

Wang, K.Z.Q., Steer, E., Otero, P.A., Bateman, N.W., Cheng, M.H., Scott, A.L., Wu, C., Bahar, I., Shih, Y.-T., Hsueh, Y.-P., et al. (2018). PINK1 Interacts with VCP/p97 and Activates PKA to Promote NSFL1C/p47 Phosphorylation and Dendritic Arborization in Neurons. ENeuro *5*.

Wang, L., Myasnikov, A., Pan, X., and Walter, P. (2020). Structure of the AAA protein Msp1 reveals mechanism of mislocalized membrane protein extraction. ELife *9*, e54031.

Wang, Y., Satoh, A., Warren, G., and Meyer, H.H. (2004). VCIP135 acts as a deubiquitinating enzyme during p97–p47-mediated reassembly of mitotic Golgi fragments. Journal of Cell Biology *164*, 973–978.

Watts, G.D.J., Wymer, J., Kovach, M.J., Mehta, S.G., Mumm, S., Darvish, D., Pestronk, A., Whyte, M.P., and Kimonis, V.E. (2004). Inclusion body myopathy associated with

Paget disease of bone and frontotemporal dementia is caused by mutant valosin-containing protein. Nature Genetics *36*, 377–381.

Weith, M., Seiler, J., van den Boom, J., Kracht, M., Hülsmann, J., Primorac, I., del Pino Garcia, J., Kaschani, F., Kaiser, M., Musacchio, A., et al. (2018). Ubiquitin-Independent Disassembly by a p97 AAA-ATPase Complex Drives PP1 Holoenzyme Formation. Molecular Cell *72*, 766-777.e6.

White, K.I., Zhao, M., Choi, U.B., Pfuetzner, R.A., and Brunger, A.T. (2018). Structural principles of SNARE complex recognition by the AAA+ protein NSF. ELife *7*, e38888.

Wong, H.H., Kumar, P., Tay, F.P.L., Moreau, D., Liu, D.X., and Bard, F. (2015). Genome-Wide Screen Reveals Valosin-Containing Protein Requirement for Coronavirus Exit from Endosomes. J Virol *89*, 11116–11128.

Wu, X., and Rapoport, T.A. (2018). Mechanistic insights into ER-associated protein degradation. Current Opinion in Cell Biology *53*, 22–28.

Xia, D., Tang, W.K., and Ye, Y. (2016). Structure and function of the AAA+ ATPase p97/Cdc48p. Gene *583*, 64–77.

Xu, Y., Anderson, D.E., and Ye, Y. (2016). The HECT domain ubiquitin ligase HUWE1 targets unassembled soluble proteins for degradation. Cell Discovery *2*.

Ye, Y., and Rape, M. (2009). Building ubiquitin chains: E2 enzymes at work. Nat Rev Mol Cell Biol *10*, 755–764.

Ye, Y., Meyer, H.H., and Rapoport, T.A. (2001). The AAA ATPase Cdc48/p97 and its partners transport proteins from the ER into the cytosol. Nature *414*, 652–656.

Ye, Y., Meyer, H.H., and Rapoport, T.A. (2003). Function of the p97–Ufd1–Npl4 complex in retrotranslocation from the ER to the cytosol : dual recognition of nonubiquitinated polypeptide segments and polyubiquitin chains. Journal of Cell Biology *162*, 71–84.

Ye, Y., Shibata, Y., Kikkert, M., Voorden, S. van, Wiertz, E., and Rapoport, T.A. (2005). Recruitment of the p97 ATPase and ubiquitin ligases to the site of retrotranslocation at the endoplasmic reticulum membrane. PNAS *102*, 14132–14138.

Yuan, X., Simpson, P., Mckeown, C., Kondo, H., Uchiyama, K., Wallis, R., Dreveny, I., Keetch, C., Zhang, X., Robinson, C., et al. (2004). Structure, dynamics and interactions of p47, a major adaptor of the AAA ATPase, p97. EMBO J *23*, 1463–1473.

Zhang, X., and Wang, Y. (2015). Cell cycle regulation of VCIP135 deubiquitinase activity and function in p97/p47-mediated Golgi reassembly. MBoC *26*, 2242–2251.

Zhang, L., Qi, Z., Gao, Y., and Lee, E.Y.C. (2008). Identification of the Interaction Sites of Inhibitor-3 for Protein Phosphatase-1. Biochem Biophys Res Commun *377*, 710–713.

Zhang, M., Chang, H., Zhang, Y., Yu, J., Wu, L., Ji, W., Chen, J., Liu, B., Lu, J., Liu, Y., et al. (2012). Rational design of true monomeric and bright photoactivatable fluorescent proteins. Nature Methods *9*, 727–729.

Zhang, S., Guha, S., and Volkert, F.C. (1995). The Saccharomyces SHP1 gene, which encodes a regulator of phosphoprotein phosphatase 1 with differential effects on glycogen metabolism, meiotic differentiation, and mitotic cell cycle progression. Molecular and Cellular Biology *15*, 2037–2050.

Zhang, T., Mishra, P., Hay, B.A., Chan, D., and Guo, M. (2017). Valosin-containing protein (VCP/p97) inhibitors relieve Mitofusin-dependent mitochondrial defects due to VCP disease mutants. ELife *6*, e17834.

Zhang, X., Gui, L., Zhang, X., Bulfer, S.L., Sanghez, V., Wong, D.E., Lee, Y., Lehmann, L., Lee, J.S., Shih, P.-Y., et al. (2015). Altered cofactor regulation with disease-associated p97/VCP mutations. PNAS *112*, E1705–E1714.

Zhao, G., Zhou, X., Wang, L., Li, G., Schindelin, H., and Lennarz, W.J. (2007). Studies on peptide:N-glycanase-p97 interaction suggest that p97 phosphorylation modulates endoplasmic reticulum-associated degradation. Proceedings of the National Academy of Sciences *104*, 8785–8790.

Xia, D., Tang, W.K., Ye, Y. (2016). Structure and function of the AAA + ATPase p97/Cdc48p. Gene *583*, 64–77.

Abbreviations

AAA	ATPases associated with diverse cellular activities
ADP	adenosine 5‘-diphosphate
ALS	amyotrophic lateral sclerosis
ATP	adenosine 5‘-triphosphate
ATPase	adenosine 5‘-triphosphatase
ATPγS	adenosine-5'-(γ-thio)-triphosphate
Cdc48	Cell division control protein 48
ClpB	Caseinolytic peptidase B
DNA	deoxyribonucleic acid
DTT	dithiothreitol
DUB	deubiquitinating enzyme
EDTA	ethylenediaminetetraacetic acid
ER	Endoplasmic Reticulum
ERAD	ER-associated degradation
FAF1	FAS-associated factor 1
GFP	green fluorescent protein
GST	Glutathione S-transferase
HeLa	Henrietta Lacks human cervical carcinoma cell line
HEPES	4-(2-hydroxyethyl)-1-piperazineethanesulfonic acid
IBMPFD	inclusion body myopathy associated with Paget’s disease of the bone and frontotemporal dementia
IFT	intraflagellar transport complex

IP	immunoprecipitation
Ipl1	Increase in Ploidy 1
I3	inhibitor-3
KNL1	kinetochore null protein 1
MSP1	Multisystem proteinopathy 1
MWCO	molecular weight cut-off
Mypt1	myosin phosphatase-targeting subunit 1
Nf-ƙB	Nuclear factor kappa B
NIPP1	Nuclear Inhibitor of PP1
Npl4	nuclear protein localization protein 4
NSF	N-ethylmaleimide sensitive fusion protein
NuMA	nuclear mitotic apparatus protein
PAGE	polyacrylamide gel electrophoresis
pBpA	p-benzoyl-L-phenylalanine
PCR	polymerase chain reaction
PIP	PP1 interacting protein
PNGase	Peptide-N(4)-(N-acetyl-beta-glucosaminyl) asparagine amidase
PP1	Proteine phosphatase 1
PUB	peptide N-glycosidase / ubiquitin-associated
PUL	PLAA, Ufd3 and Lub1
RING	Really Interesting New Gene
RQC	ribosomal quality control
SCF	Skp1, cullin and F box

SDS	sodium dodecyl sulfate
SDS22	suppressor of Dis2 mutant 2
SEP	Shp1, eyes closed and p47
Shp1	suppressor of high-copy PP1
SNARE	soluble NSF attachment protein receptor
SPI	SDS22 + PP1 + I3
TE	Tris EDTA
Tris	Tris(hydroxymethyl)-aminomethan
Ub	ubiquitin
UBA	ubiquitin-associated
UBX	ubiquitin-regulatory X
Ufd1	ubiquitin fusion degradation protein 1
UPS	ubiquitin-proteasome system
VAT	vesicle amine transport 1
VCP	valosin containing protein
VIM	VCP-interacting motif
VPS4	Vacuolar protein sorting-associated protein 4
YFP	yellow fluorescent protein
Ypi1	Yeast phosphatase inhibitor 1

Acknowledgements

First, I want to thank Hemmo for the opportunity to join his lab and work on this interesting project, as well as his advice, numerous discussions and mentorship throughout the project.

I thank Peter Bayer for helpful input at thesis advisory committee meetings.

Special thanks go to Johannes van den Boom for numerous advice and troubleshooting.

I thank Jonas Seiler und Matthias Weith, who also worked on the SPI complex and laid the groundwork upon which this thesis expanded.

A big thank you to all current and former members of the AG Meyer for the excellent atmosphere, fun and comradery both in and outside the lab. You are all indeed very cool people.

Special thanks go to Sabine Effenberger, Miriam Schmidt, Christina Kamp-Meltzer and Cristina Hartmann-Fatu for assistance in technical and organizational matters, without which lab work would not be possible.

I also thank all members of the ZMB who have helped me over the years by lending reagents or advice.

I thank the graduate school of the CRC1093 for funding and the opportunity to expand my scientific horizon.

Finally, I have to thank my family, especially my parents, for their invaluable support and assistance throughout all the years that have helped me reach this point.

Curriculum Vitae

Der Lebenslauf ist in der Online-Version aus Gründen des Datenschutzes nicht enthalten.

Der Lebenslauf ist in der Online-Version aus Gründen des Datenschutzes nicht enthalten.

Erklärungen

Erklärung:

Hiermit erkläre ich, gem. § 7Abs. (2) d) + f) der Promotionsordnung der Fakultät für Biologie zur Erlangung des Dr. rer. nat., dass ich die vorliegende Dissertation selbständig verfasst und mich keiner anderen als der angegebenen Hilfsmittel bedient, bei der Abfassung der Dissertation nur die angegebenen Hilfsmittel benutzt und alle wörtlich oder inhaltlich übernommenen Stellen als solche gekennzeichnet habe.

Essen, den _____ _____

Unterschrift des/r Doktoranden/in

Erklärung:

Hiermit erkläre ich, gem. § 7Abs. (2) e) + g) der Promotionsordnung der Fakultät für Biologie zur Erlangung des Dr. rer. nat., dass ich keine anderen Promotionen bzw. Promotionsversuche in der Vergangenheit durchgeführt habe und dass diese Arbeit von keiner anderen Fakultät/Fachbereich abgelehnt worden ist.

Essen, den _____ _____

Unterschrift des Doktoranden

Erklärung:

Hiermit erkläre ich, gem. § 6 Abs. (2) g) der Promotionsordnung der Fakultät für Biologie zur Erlangung der Dr. rer. nat., dass ich das Arbeitsgebiet, dem das Thema „Molecular function of SEP domain adapters in VCP/p97 mediated protein unfolding“ zuzuordnen ist, in Forschung und Lehre vertrete und den Antrag von Matthias Kracht befürworte und die Betreuung auch im Falle eines Weggangs, wenn nicht wichtige Gründe dem entgegenstehen, weiterführen werde.

Essen, den _____ _____

Unterschrift eines Mitglieds der Universität Duisburg-Essen